Measurements of neurotransmitter release in animal models of the central nervous system using fast scan cyclic voltammetry

By

© 2017

Rachel C. Ginther

B.A., Saint Louis University, 2012

Submitted to the graduate degree program in Chemistry and the Graduate Faculty of the University of Kansas in partial fulfillment of the requirements for the degree of Doctor of Philosophy.

_____

Chair: Michael Johnson, PhD

_____

Susan Lunte, PhD

_____

Robert Dunn, PhD

_____

Ward Thompson, PhD

_____

David Jarmolowicz, PhD

_____

Michael Wang, PhD

Date Defended: 25 August 2017

The dissertation committee for Rachel Ginther certifies that this is the approved version of the following dissertation:

Measurements of neurotransmitter release in animal models of the central nervous system using fast scan cyclic voltammetry

_____

Chair: Michael Johnson, PhD

Date Approved: 25 August 2017

Abstract

This dissertation is a compilation of the work we have done in the past five years using fast-scan cyclic voltammetry in model organisms to solve biological problems. In this work, we use fast-scan cyclic voltammetry to measure neurotransmitter release in rodent models of neurodegeneration and neurotoxicity. Later, we develop this technique for use in zebrafish whole mount retinas.

In Chapter One, we will introduce fast-scan cyclic voltammetry and the underlying electrochemical concepts. We will also introduce the various biological problems investigated in this work and the model organisms used to investigate these problems.

In Chapter Two, we will discuss fast-scan cyclic voltammetry measurements of serotonin release in Huntington's disease model mice. We have demonstrated that serotonin release is impaired in multiple regions of the brain and across multiple mouse models.

In Chapter Three, we will discuss fast-scan cyclic voltammetric measurements of both dopamine and serotonin in chemotherapy-treated rats. Here, we have treated rats with both carboplatin and 5-fluorouracil in order to investigate the effect of chemotherapy on neurotransmitter release. Additionally, we will discuss our collaboration with Dr. David Jarmolowicz, in which his lab measured cognitive behavioral changes in rats treated with chemotherapy. We have also investigated the novel drug, KU-32, developed by Dr. Brian Blagg's group, as a potential therapy for chemotherapy-induced cognitive changes.

In Chapter Four, we will discuss our work developing a method to measure light-stimulated neurotransmitter release in adult zebrafish whole mount retinas. Here, we have shown

through pharmacological studies that dopamine can be measured using fast-scan cyclic voltammetry in the retina.

Finally, in Chapter Five, we will present our conclusions and future directions for this work.

Acknowledgements

This work would not be possible without the help of my advisor, Dr. Michael Johnson, and all of our group members, especially Dr. Sam Kaplan, Dr. Mimi Shin, and Thomas Field. The behavioral neuroscience experiments in this work are the product of collaboration with Dr. David Jarmolowicz's lab. Additionally, Dr. Brian Blagg's lab provided a novel drug they synthesized, KU-32, for use in our experiments.

To my parents, my parents-in-law, and the rest of my family: thank you for all of your support and love; I could not have done this without you.

To Nick: thank you for putting up with being married to a graduate student.

"That's why they call it graduate school: you're supposed to graduate."

- *Dr. Brian Laird*

CONTENTS

1 INTRODUCTION

1.1 INTRODUCTION

For this work, we obtained measurements of neurotransmitter release and uptake using fast-scan cyclic voltammetry at carbon fiber microelectrodes. This technique has several advantages. The 7 μm diameter of the carbon fiber electrodes allows for high spatial resolution and also minimizes tissue damage. Additionally, the fast scan rate combined with background subtraction provides sub-second temporal resolution. Also, this technique gives limits of detection in the nM range, which is suitable for the concentrations of neurotransmitters released in the brain. Finally, fast-scan cyclic voltammetry has a good specificity, which allows for identification of the analyte of interest without a separation step.

1.2 ELECTROCHEMICAL CELLS

This work relies on fast-scan cyclic voltammetry (FSCV), an electrochemical technique, to quantify changes in neurotransmitter concentrations in biological tissues. Therefore, it is important to discuss the fundamentals of electrochemical analysis. The foundation of electrochemical techniques lies in electrochemical cells. A galvanic cell contains a spontaneously-occurring reaction at electrodes that generates a current when connected by a salt bridge. On the other hand, an electrolytic cell requires an external power source and can push nonspontaneous reactions to occur at electrodes. Figure 1.2.1 shows a galvanic cell .[1]

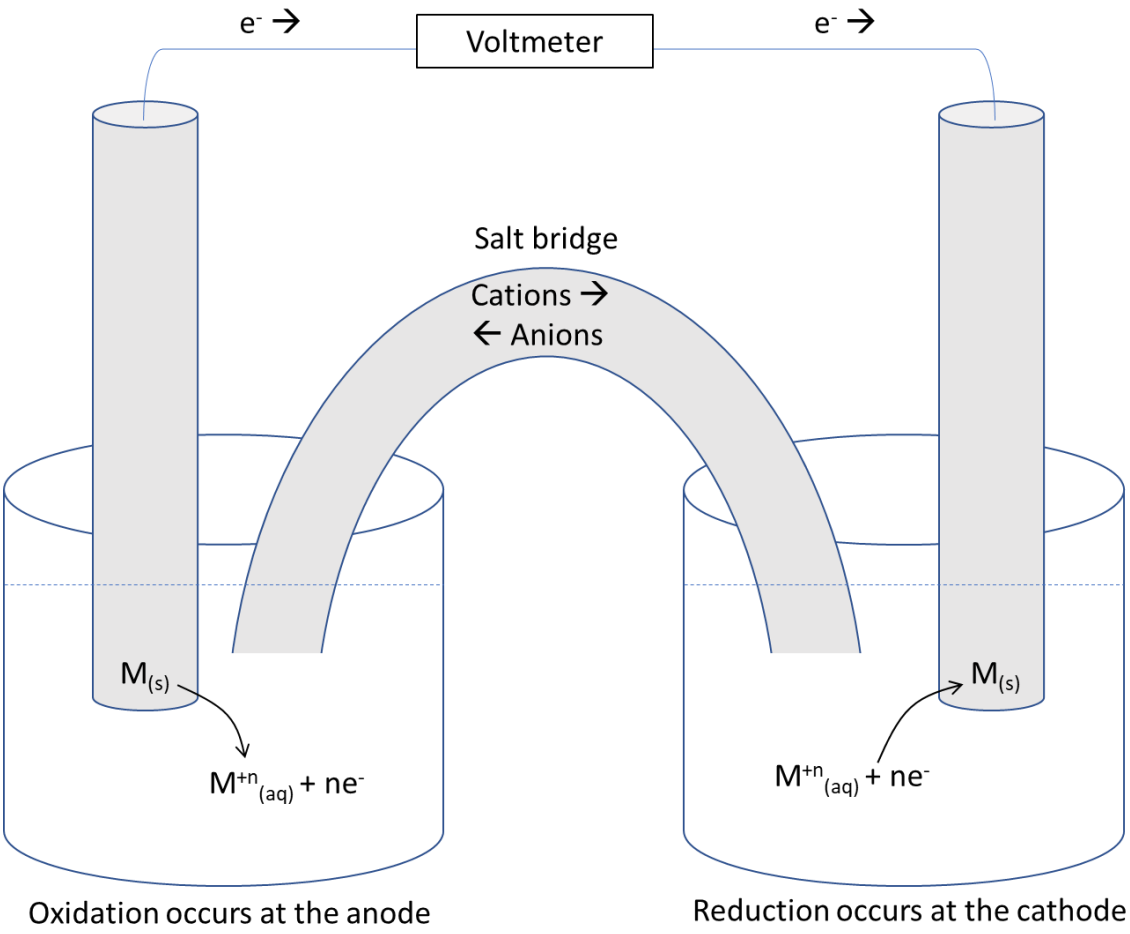

Figure 1.2.1. Schematic diagram of a Galvanic cell.

In this work, a two-electrode cell is used to make electrochemical measurements. Two-electrode cells typically consist of a working electrode and reference electrode, while a three-electrode cell includes a counter electrode in addition to the other two. Here, we will discuss the components of the two-electrode cell used.

The working electrode is the electrode at which the reaction of interest occurs; in this work, a carbon fiber microelectrode is used. The reference electrode is an electrode whose behavior approaches that of an ideal nonpolarizable electrode. Figure 1.2.2 shows current potential curves for an ideal polarizable electrode (left) and an ideal nonpolarizable electrode

(right).[1] Ideal nonpolarizable electrodes make good reference electrodes because their potential remains constant regardless of changes in current.[1] Although actual electrodes never behave exactly as ideal ones, in this work, an Ag/AgCl electrode was used as a reference, and approximates an ideal nonpolarizable electrode under the experimental conditions.

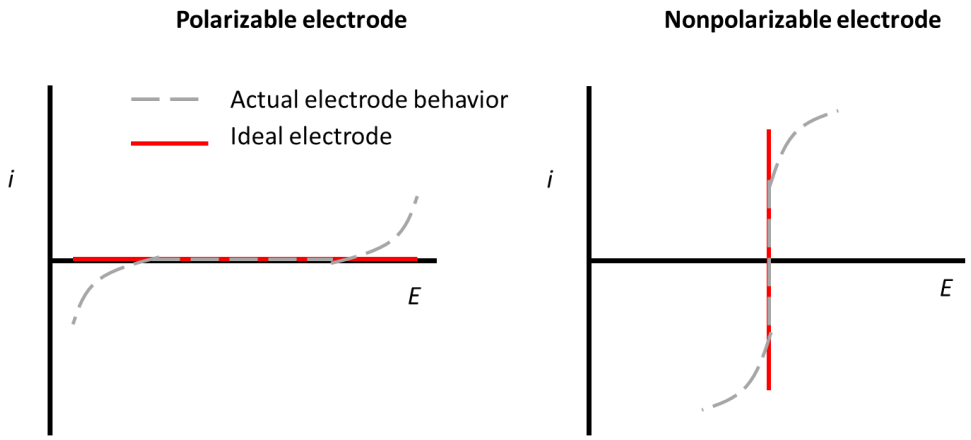

Figure 1.2.2. Behavior of actual and ideal polarizable (left) and nonpolarizable (right) electrodes.[1]

Under conditions in which measurements are obtained in highly resistive solutions or when large currents are measured, a three-electrode cell may be required, in which current passes between the counter and working electrodes. In this type of cell, a counter electrode is required to correct for IR drop, which is the decrease in applied potential at the electrode surface.[2] In this work, a two-electrode cell is used. Due to the use of carbon fiber microelectrodes, currents measured are on the order of nanoamps; thus, the currents at the working electrodes are sufficiently low to avoid a significant ohmic drop, and a counter electrode is not necessary.[2] Figure 1.2.3 shows a schematic of a two-electrode cell.

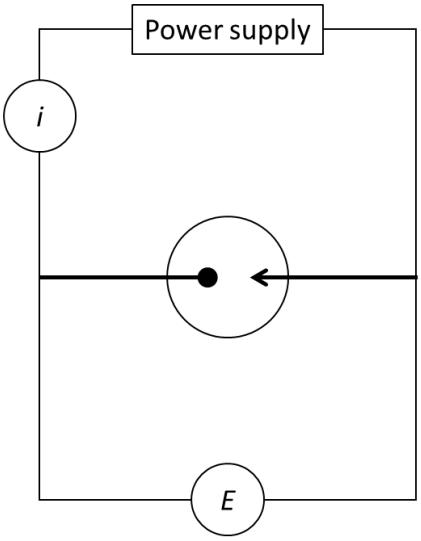

Figure 1.2.3. A schematic showing a two-electrode cell.

1.2.1 Faradaic current and electrode reactions

Faradaic current is electron flow due to an oxidation or reduction reaction. For a Faradaic process, the amount of current will be directly proportional to the charge transfer in an oxidation or reduction reaction.[2] For electroanalytical chemistry, this is important since it means that an electroactive analyte can be quantified by the oxidation or reduction current generated when a potential is applied. For a redox reaction producing faradaic current, the following equations are relevant:

$$Q = nFN$$

$$\frac{dQ}{dt} = i = nF\frac{dN}{dt}$$

Where Q = charge, n = moles of analyte, F is faraday's constant, N is the number of electrons in the redox reaction, i is current, and t is time. Thus, faradaic current is equal to charge transfer over time and is proportional to the moles of analyte.[3] Figure 1.2.4 shows a schematic of a Faradaic process: the oxidation of A to A^+ at an electrode surface. As the potential of the

electrode becomes more positive, the energy level of the electrons at the electrode surface becomes lower than the species A's highest occupied molecular orbital. When this occurs, electron transfer occurs from the molecular orbital to the electrode surface, and species A is oxidized to A^+.[1]

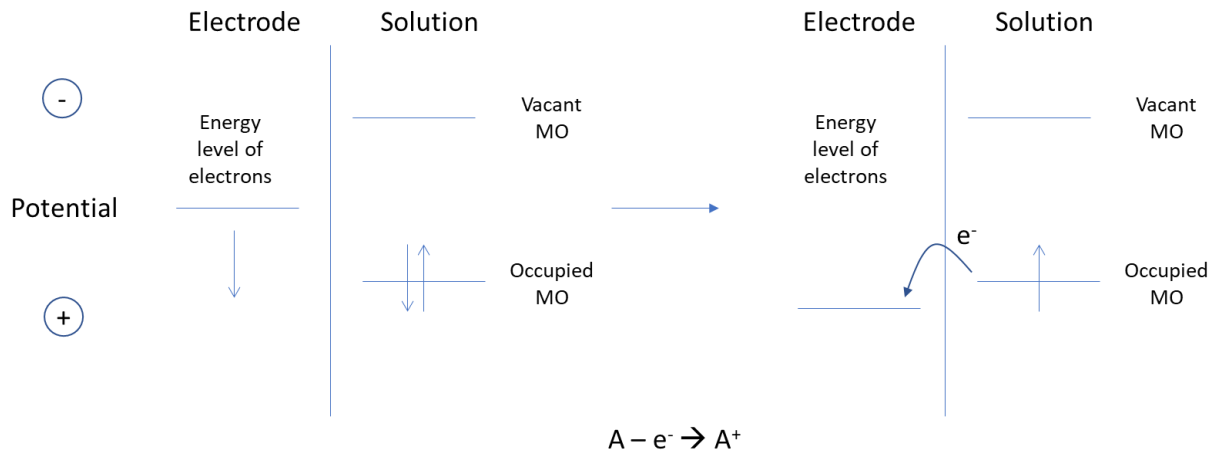

Figure 1.2.4. Oxidation of A to A^+.

1.2.2 Capacitance at the electrode-solution interface

A capacitor is any two conductive materials in proximity to each other, with a separation such that charges cannot cross, and across which charge can be stored. Thus, the electrode-solution interface can be thought of as a capacitor, of sorts, because charges cannot cross. Capacitance is given by:

$$C = \frac{q}{E}$$

Where C is capacitance, q is the charge stored, and E is the potential across the capacitor.[1]

Figure 1.2.5 shows (A) a capacitor in a circuit, and (B) the interface of a negatively charged electrode in solution as a capacitor. Capacitance is important in the context of our measurements

using fast-scan cyclic voltammetry because of the significant capacitive charging current that occurs at high scan rates.

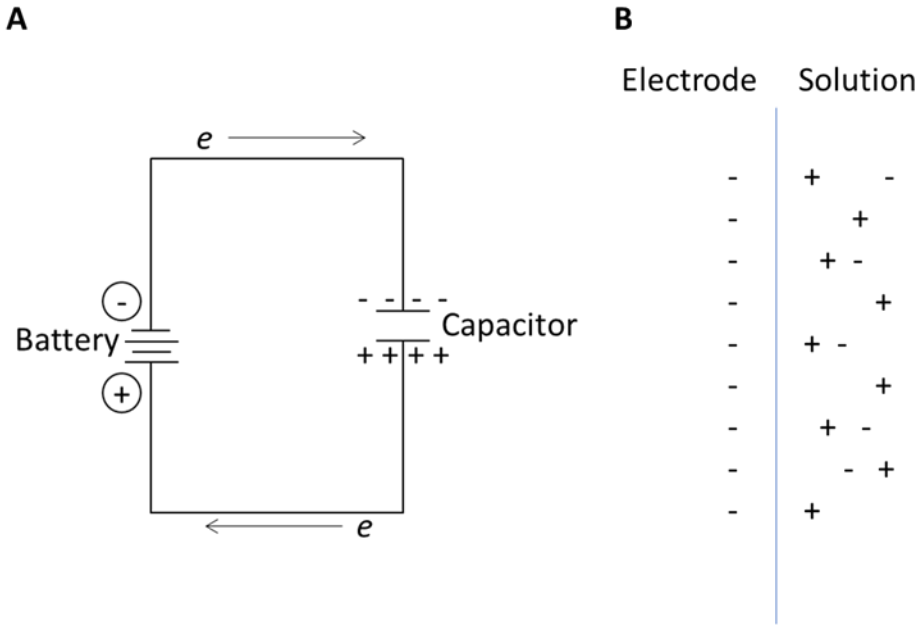

Figure 1.2.5. (A) A capacitor as part of a circuit. (B) An electrode with a negatively charged surface as a capacitor in solution.

An electric double-layer forms at electrode surfaces due to charge separation across the solution-electrode interface. Figure 1.2.6 shows a schematic of the electric double-layer. Here, anions are specifically adsorbed to the surface of the electrode. Represented by x_1 is the locus of electrical centers of specifically adsorbed ions. Due to the specific adsorption of anions here, solvated cations can only approach the electrode surface to the distance represented by x_2. The solvated cations here are nonspecifically adsorbed.[1]

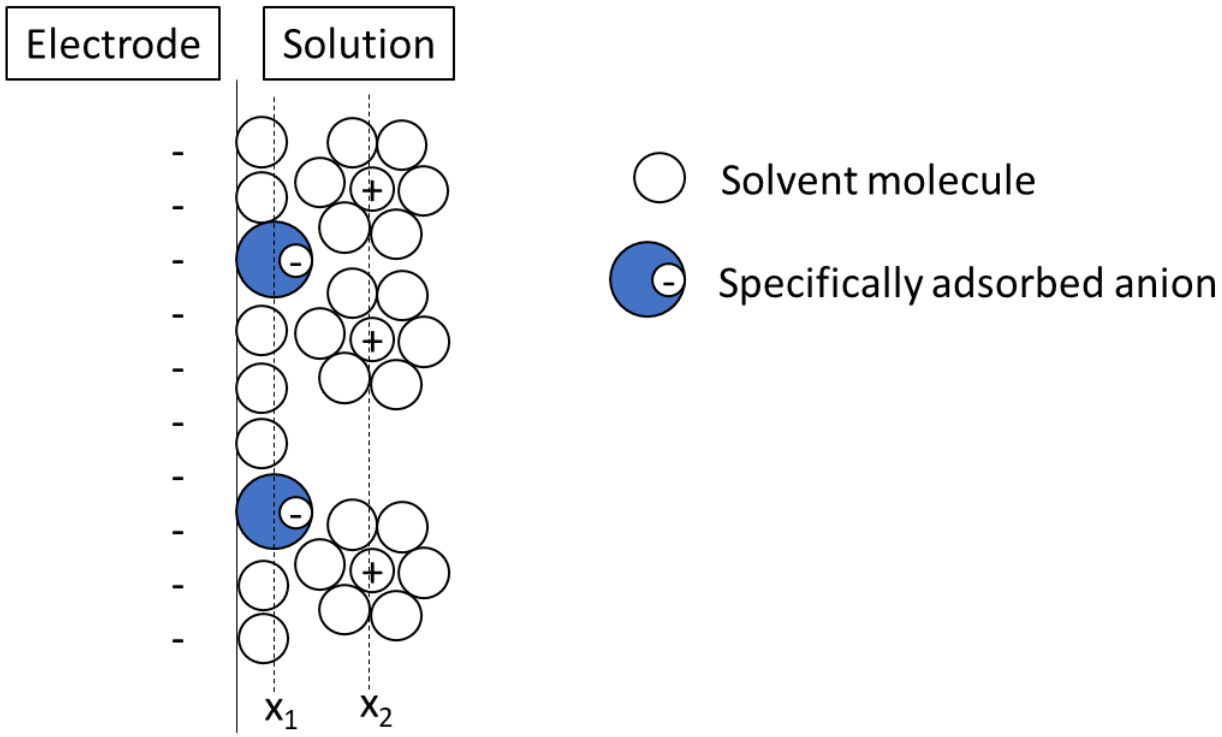

Figure 1.2.6. The electric double-layer.

1.3 VOLTAMMETRY

In this work, voltammetry is used to measure transient changes in neurotransmitter concentrations in biological tissues. Voltammetry is a group of electrochemical techniques in which a known potential is applied at a working electrode, and the resulting current from any reactions occurring at the electrode is measured.[2] These techniques include square wave voltammetry and various potential step methods. This work makes use of cyclic voltammetry, a linear sweep method in which the potential is increased from a given holding potential at a selected scan rate. In these experiments, potential E is a function of the scan rate v and time, t:

$$E = vt$$

After the switching potential is reached, the scan rate switches from *v* to -*v*, and the potential returns to the holding potential until the waveform is scanned again.[4] Figure 1.3.1 shows a typical waveform used for cyclic voltammetry. In cyclic voltammetry at macroelectrodes, scan rates are typically on the order of 100-1000 mV.

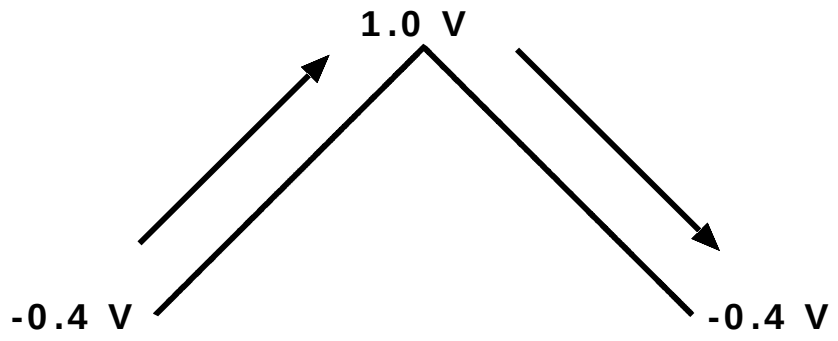

Figure 1.3.1. A typical waveform used for cyclic voltammetry.

As the potential is scanned up from negative to positive, oxidation of the analyte of interest can occur at the electrode surface, resulting in faradaic current. The oxidation and reduction currents can be plotted vs. potential in order to obtain a cyclic voltammogram, which serves as a signature of a given analyte. What happens on the reverse scan is determined by the type of reaction: reversible, quasi-reversible, irreversible, or chemically irreversible. In a reversible reaction, the difference between oxidation and reduction potentials is less than 0.058 V/n, where *n* is the number of electrons transferred; a reversible reaction will obey the Nernst equation:

$$E = E^o + \frac{RT}{nF} * \ln(\frac{[ox]}{[red]})$$

Where E is applied potential, E^0 is the formal reduction potential of the analyte, R is the universal gas constant, n is the number of electrons transferred in the reaction, and F is Faraday's

constant. The Nernst equation describes the changes in concentrations of species due to oxidation and reduction at the electrode surface as a function of applied potential, where E^o is the formal reduction potential of the analyte, R is the universal gas constant, n is the number of electrons per reaction, and F is the faraday constant.[1]

For a quasi-reversible reaction, the separation between oxidation and reduction peaks will exceed 0.058 V/*n*, and irreversible reactions will have a peak separation of far greater than 0.058 V/*n*. In the case of a chemically irreversible reaction, a molecule oxidized at the electrode surface will undergo a chemical change preventing a reduction reaction on the reverse scan.[1] In this work, significant non-faradaic charging currents are generated at the working electrode. Figure 1.3.2A shows a typical potential-versus-time plot for a linear sweep experiment, where potential is ramped up over time. As potential is ramped up, resulting non-faradaic charging current reaches a steady state.[1] Here, the charging current is given by the scan rate and capacitance of the double-layer. Figure 1.3.2B shows plots for a triangular waveform, where potential is ramped up to a switching potential, and then back down. In this case, the steady state current switches its sign as potential is ramped back down, as the scan rate switches from *v* to -*v*.[1]

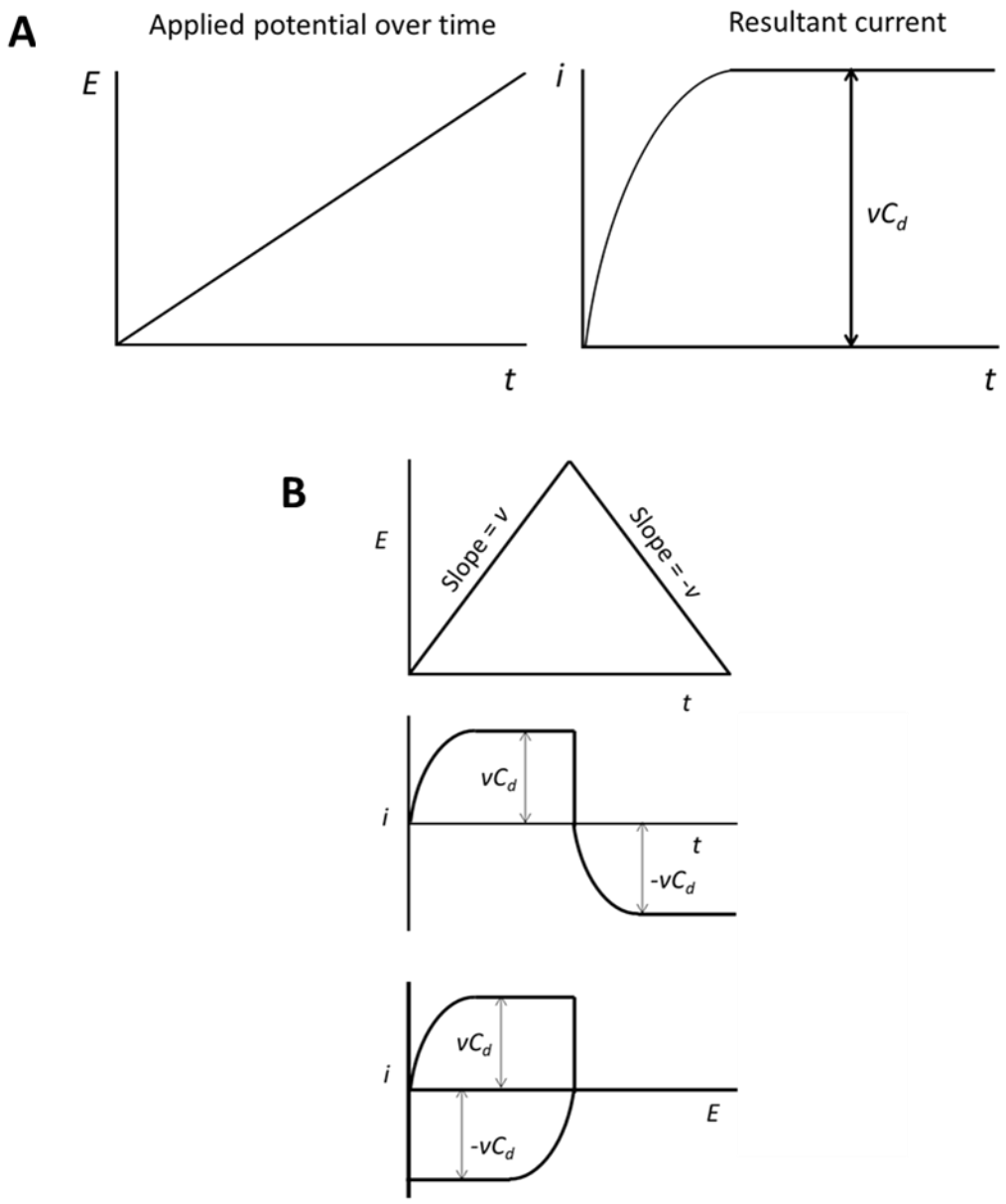

Figure 1.3.2. (A) Resultant charging current in a potential sweep experiment. (B) Applied potential (top), resulting charging current versus time (middle), and resulting charging current versus potential (bottom) in a cyclic voltammetry experiment. Figure adapted from Bard and Faulkner, with permission. ©John Wiley and Sons (2000).

1.4 FAST-SCAN CYCLIC VOLTAMMETRY

1.4.1 Introduction to fast-scan cyclic voltammetry

This work makes use of techniques originally developed here, at the University of Kansas, by Ralph N. Adams. In 1958, Adams first published on his invention of carbon paste electrodes,[5] which were a major innovation over the mercury electrodes that were dominant in electroanalytical chemistry at the time.[6] Then, in 1967, Adams published on oxidation reactions of catecholamines,[7] and followed this six years later with in vivo voltammetric measurements using carbon paste electrodes.[8] Adams's work laid the foundation for the development of voltammetry as a technique to measure catecholamines in biological tissues. In this work, cyclic voltammetry is used in the central nervous system to measure neurotransmitter release. As discussed in section 1.3, cyclic voltammetry is a linear sweep method in which a potential is ramped up to some switching potential, and then back down to the holding potential at some scan rate. In fast-scan cyclic voltammetry, scan rates of up to 10^5 V/s have been used.[9] The fast scan rate allows for increased sensitivity and the ability to detect rapid changes in analyte concentration.[9] As discussed in section 1.3, experiments involving a linear potential sweep generate charging currents proportional to the potential scan rate. In this work, scan rates range from 300 V/s to 800 V/s; therefore, large charging currents are generated, and it is necessary to use background subtraction to obtain useful data. Figure 1.4.1 shows an example of a background-subtracted cyclic voltammogram for dopamine. In this process, multiple cyclic voltammograms are averaged over time. This averaged background cyclic voltammogram is then subtracted from the other cyclic voltammograms throughout a given file obtained, in order to yield a background-subtracted cyclic voltammogram. This does create a limitation: fast-scan cyclic voltammetry cannot detect absolute concentrations; it can only detect changes in

concentration. However, since we are interested in measuring neurotransmitter release in response to stimuli and not endogenous concentrations, this limitation falls outside the scope of this work.

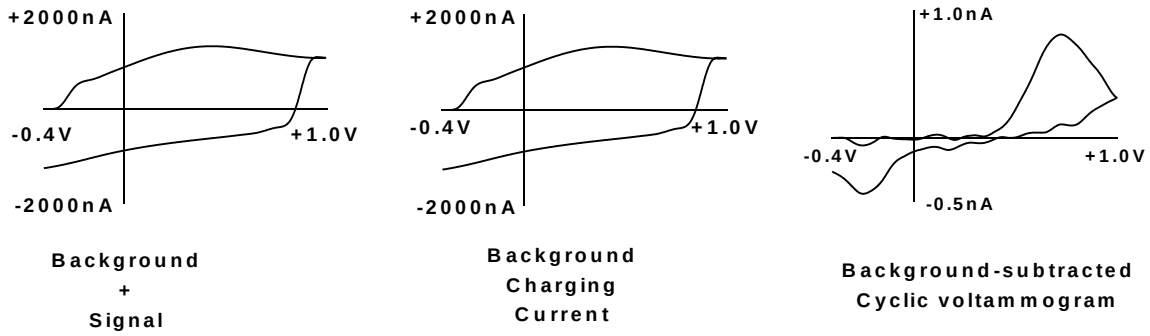

Figure 1.4.1. Fast-scan cyclic voltammetry is a background-subtracted technique.

1.4.2 Carbon fiber microelectrodes

In this work, carbon fiber microelectrodes were used with fast-scan cyclic voltammetry to obtain neurotransmitter release measurements in biological tissues. When used with fast-scan cyclic voltammetry, the small size of carbon fiber microelectrodes allows low limits of detection, high temporal resolution, and high spatial resolution.[9] Electrode fabrication will be discussed in greater detail in the Methods sections of later chapters, but a brief introduction will be given here. The electrodes were made in-house, consisting of 7 µM diameter carbon fiber, cut to 30 µM in length, and encased in a glass sheath. Figure 1.4.2 shows a scanning-electron microscopy image of a carbon fiber microelectrode.

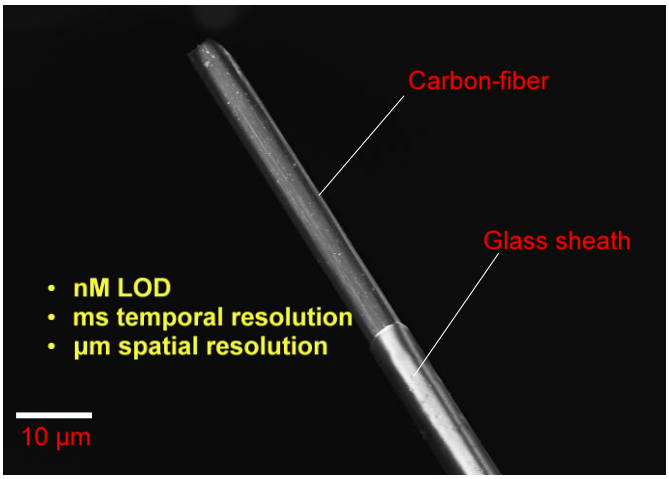

Figure 1.4.2. Scanning electron microscope image of a carbon fiber microelectrode tip.

1.4.3 Voltammetry of Dopamine

In this work, dopamine is measured at carbon fiber microelectrodes using fast-scan cyclic voltammetry. This was done using a waveform scanning up from a holding potential of -0.4 V, up to a switching potential of 1.0 V, and back down to -0.4 V at 300 V/s. As the potential is scanned from negative to positive, in a two-electron oxidation, dopamine is converted to dopamine-*o*-quinone at about 0.6 V, and an oxidation peak appears on the cyclic voltammogram. As the potential is scanned back down, dopamine-*o*-quinone is reduced back to dopamine at about -0.1 V, and a reduction peak appears on the cyclic voltammogram. Figure 1.4.3 shows a dopamine waveform along with a characteristic dopamine cyclic voltammogram and the redox reaction of dopamine to dopamine-*o*-quinone.

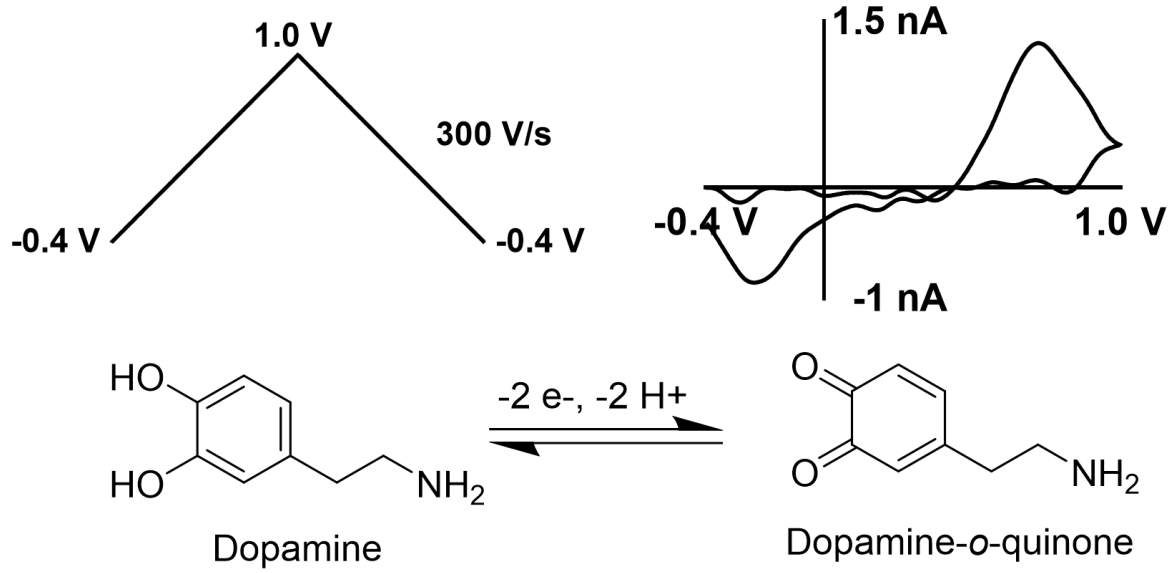

Figure 1.4.3. Dopamine oxidation to dopamine-ortho-quinone and reduction back to dopamine at the electrode surface and the resulting cyclic voltammogram.

1.4.4 Voltammetry of Serotonin

The other neurotransmitter discussed at length in this work is serotonin. A serotonin-optimized waveform[10] was used to make serotonin measurements. This waveform consists of a sawtooth pattern in which potential is increased from 0.2 V up to 1.0 V, down to -0.1 V and back up to a holding potential of 0.2 V at 800 V/s was used. On the positive scan, serotonin is oxidized in a two-electron oxidation to serotonin-*p*-quinone imine around 0.8 V. On the reverse scan, serotonin-*p*-quinone imine is reduced back to serotonin around 0.0 V. This waveform was found by Hashemi et al. to be more sensitive to serotonin than dopamine by 50-fold because dopamine-*o*-quinone, the oxidation product of dopamine, is not reduced back to dopamine until -0.1 V.[10] Further considerations for measuring serotonin in brain slices will be discussed in

Chapters 2 and 3 of this work. Figure 1.4.4 shows the serotonin waveform that was used, the serotonin redox reaction, and a characteristic serotonin cyclic voltammogram.

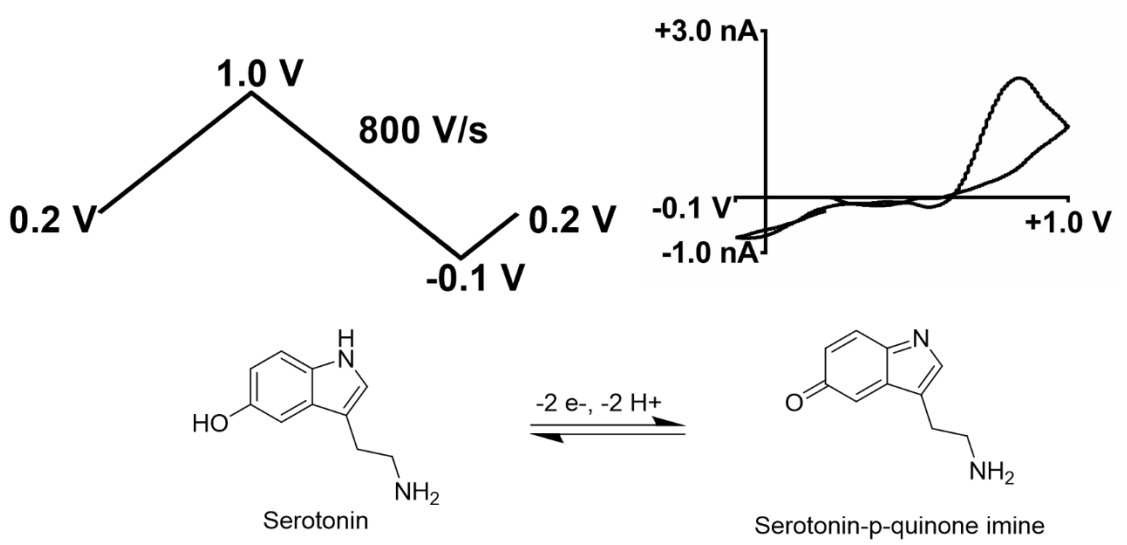

Figure 1.4.4. Serotonin waveform, cyclic voltammogram, and oxidation to serotonin-*p*-quinone imine.

1.4.5 Color plots

Raw data were collected in the form of color plots, which allow for visualization of multiple cyclic voltammograms over time. Figure 1.4.5 shows a representative color plot collected in a flow cell. Here, time is plotted on the x-axis. Potential is plotted on the y-axis, and current is represented by false color, with the green color representing positive current, yellow representing currents close to zero, and dark blue representing negative current. Cyclic voltammograms are unfolded and stacked over time to obtain these plots. Taking a horizontal slice of the color plot, the current versus time plot can be viewed to determine current changes over time, while a vertical slice gives an extracted cyclic voltammogram collected at that specific time. The background can be subtracted from any time point to obtain a background-subtracted cyclic voltammogram.

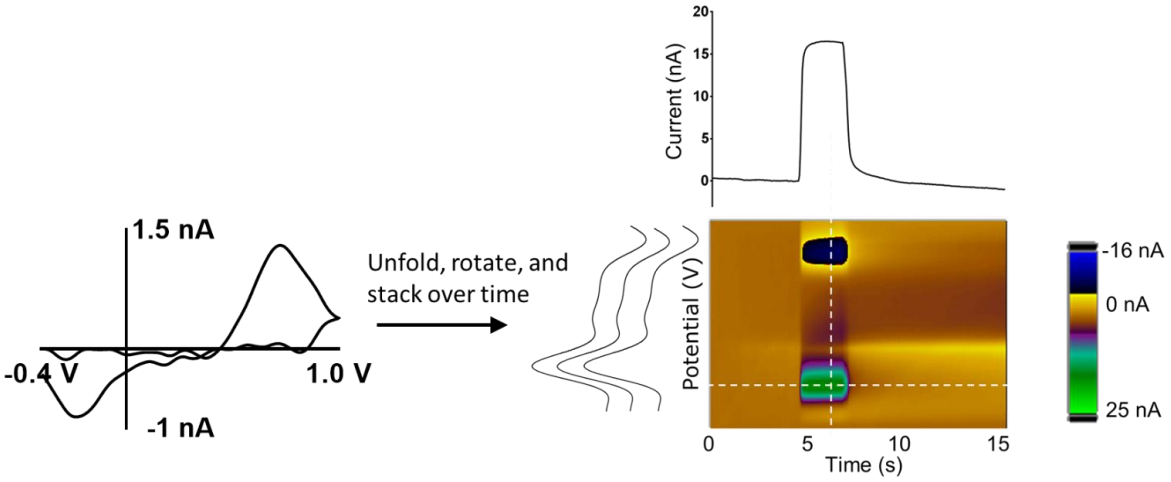

Figure 1.4.5. Representative color plot collected during flow cell analysis of dopamine. Cyclic voltammograms are unfolded, rotated such that current peaks are on the *z*-axis represented in false color, and stacked over time.

1.5 NEUROTRANSMISSION

The central nervous system is composed of two parts: (1) the brain, and (2) the eye. The central nervous system is distinct from the peripheral nervous system, which consists of other nerves throughout the body.[11] The cells in each of the components of the nervous system, however, communicate in much the same way via action potentials.[12-15]

Neurons are made up of three major parts: (1) the cell body, (2) the axon, and (3) the dendrites,[16] as shown in Figure 1.5.1.

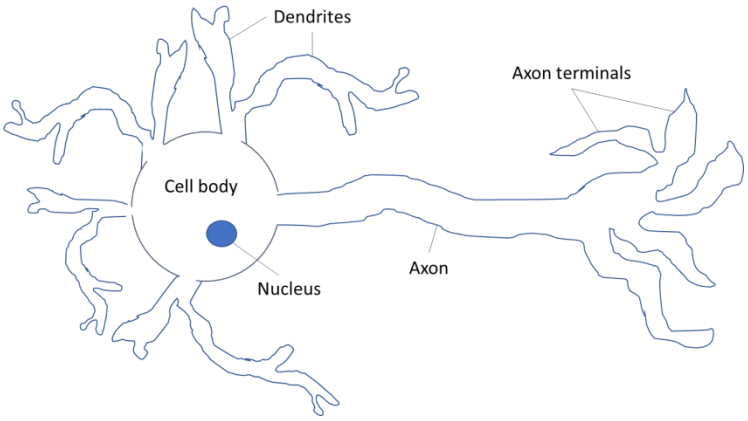

Figure 1.5.1. A schematic showing the main parts of a neuron.

Typically, a neuron receives input at the dendrites.[17-18] If a neuron's membrane potential becomes sufficiently depolarized, an action potential takes place,[15] where an electrical current is propagated down the axon, and neurotransmission can occur at the terminals.[19-20] When a neuron is in its resting state, its membrane potential rests at -70 mV, and voltage-gated channels remain closed.[21-22] When the membrane potential is sufficiently depolarized to a threshold of -55 mV, voltage-gated channels open, and sodium enters the axon, which further increases the cell membrane potential.[23-24] As the available sodium channels continue to open, the membrane potential increases to +40 mV with the rapid influx of sodium ions.[12] The membrane potential reaches a maximum when the sodium channels close and potassium channels open.[24] Then, an efflux of potassium from the cell occurs, hyperpolarizing the cell membrane before eventually returning to its resting voltage of -70 mV through active transport via sodium/potassium pumps.[12, 23] This cycle of membrane depolarization and resulting electrical impulses propagates down an axon, ultimately triggering exocytotic release of neurotransmitters into synapses.[25] Release of neurotransmitters into the synaptic cleft (i.e. space where neurons contact each other) allows for intercellular communication.[20, 25-26]

1.6 DOPAMINE

Dopamine is a monoamine neurotransmitter that has been implicated in many brain processes, including reward signaling,[27] addiction,[28] and motor control.[29] Moreover, dopamine dysfunction has been observed in a variety of neurodegenerative disease states, including Alzheimer's disease,[30] Parkinson's disease,[31-32] and Huntington's disease.[33-42]

1.6.1 Dopamine in the striatum

The striatum is part of the basal ganglia, which is a group of sub-cortical nuclei located in the forebrain. Other components of the basal ganglia include the globus pallidus, entopeduncular nucleus, subthalamic nucleus, substantia nigra pars compacta, substantia nigra pars reticulata, and nucleus accumbens.[43] The striatum contains both the caudate putamen and nucleus accumbens, both of which are heavily innervated with dopamine.[43] The two primary pathways from which the striatum receives dopaminergic input are the mesolimbic pathway, via the ventral tegmental area, and the nigrostriatal pathway via the substantia nigra pars compacta.[44] Figure 1.6.1 shows a schematic diagram of the dopaminergic pathways in the adult mouse brain.[45] The ventral striatum has been implicated in reward and motor function,[47] while the dorsal striatum has been shown to have some role in learning. [46] GABAergic neurons make up 90-95% of cell bodies in the striatum.[48] These cells are called "spiny" because of their dendritic projections that are covered in spines.[48] Alterations in the striatum have been associated with many disease states and neuropsychiatric conditions, including schizophrenia,[49-51] alcohol abuse disorders,[52] eating disorders,[53] anxiety,[54] major depression,[55] Parkinson's disease,[56] and Huntington's disease.[33]

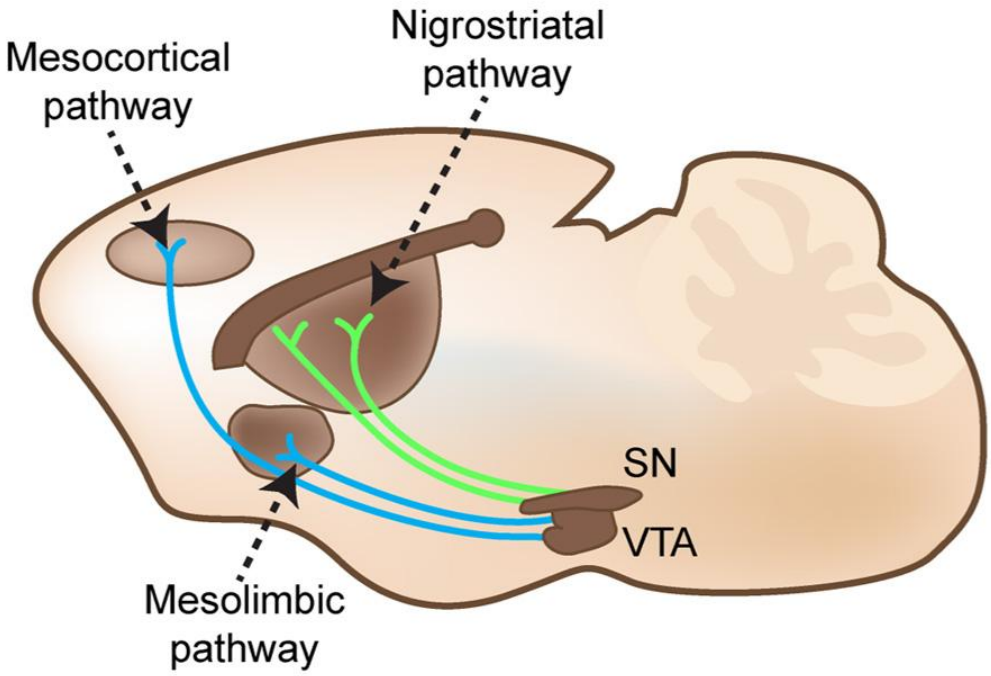

Figure 1.6.1. Dopaminergic pathways in the adult mouse brain. Reproduced from Money KM and Stanwood GD (2013), Open Acess.[45]

1.6.2 Dopamine in retina

For a more detailed description of the retinal architecture and dopamine function in the retina, see Chapter 4. Briefly, dopamine in the retina is primarily located in A2 amacrine cells. These cells integrate and modulate visual messages to ganglion cells.[57] Dopamine function has been found to play a potential role in several retinal diseases, including diabetic retinopathy,[58-59] Parkinsonian retinopathy,[60] myopia,[61-62] and age-related macular degeneration.[63-64]

1.6.3 Dopamine synthesis, release, and uptake

Throughout this work, neurotransmitter release is evoked via electrical or light stimulus, and neurotransmitter release is manipulated via pharmacology. Therefore, it is important to discuss the synthesis, release, and uptake of dopamine at synapses. Figure 1.6.2 shows this process.

Dopamine is synthesized from tyrosine;[65] the rate-limiting step is the conversion of tyrosine to L-DOPA by tyrosine hydroxylase.[66] L-DOPA is then converted to dopamine by DOPA decarboxylase.[67-69] Vesicular monoamine transporter then packages dopamine into vesicles,[70] which can be released into the synapse by exocytosis, where the vesicle fuses with the cell membrane and releases its contents into the extracellular space.[25] Upon release, dopamine can be taken back into the cell by dopamine transporter,[31, 70] bind to autoreceptors on the same neuron from which it was released,[71] diffuse across the synaptic cleft and bind receptors on a different neuron, or diffuse out of the synaptic cleft and act on distance receptors.[20, 72]

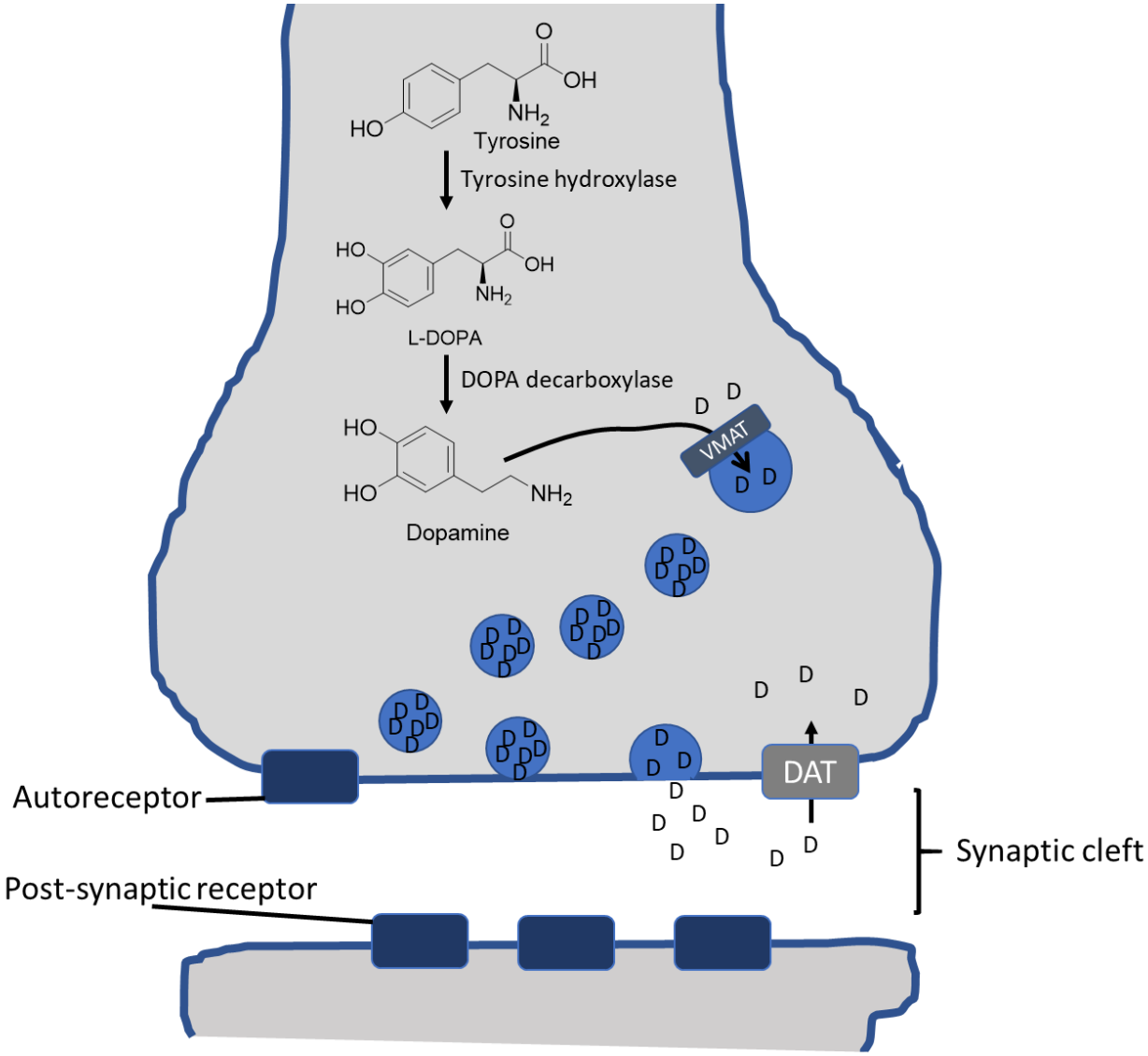

Figure 1.6.2. A schematic diagram showing the synthesis, release, and uptake of dopamine.

1.7 SEROTONIN

Serotonin is a monoamine neurotransmitter involved in mood,[73-74] motor function,[75] memory,[76] and learning.[77] Figure 1.7.1 shows a diagram of serotonin innervation. Serotonergic innervation originates in the raphe nuclei, located in the brainstem.[78] These nuclei consist of the rostral nuclei, which is composed of the caudal linear nuclei, dorsal raphe nuclei, and median

raphe nuclei, and the caudal nuclei, which is composed of the nucleus raphe magnus, the raphe obscurus nucleus, the raphe pallidus nucleus, and the lateral medullary reticular formation.[73] The rostral nuclei project into cortical and subcortical structures, while the caudal nuclei project into the brainstem.[79]

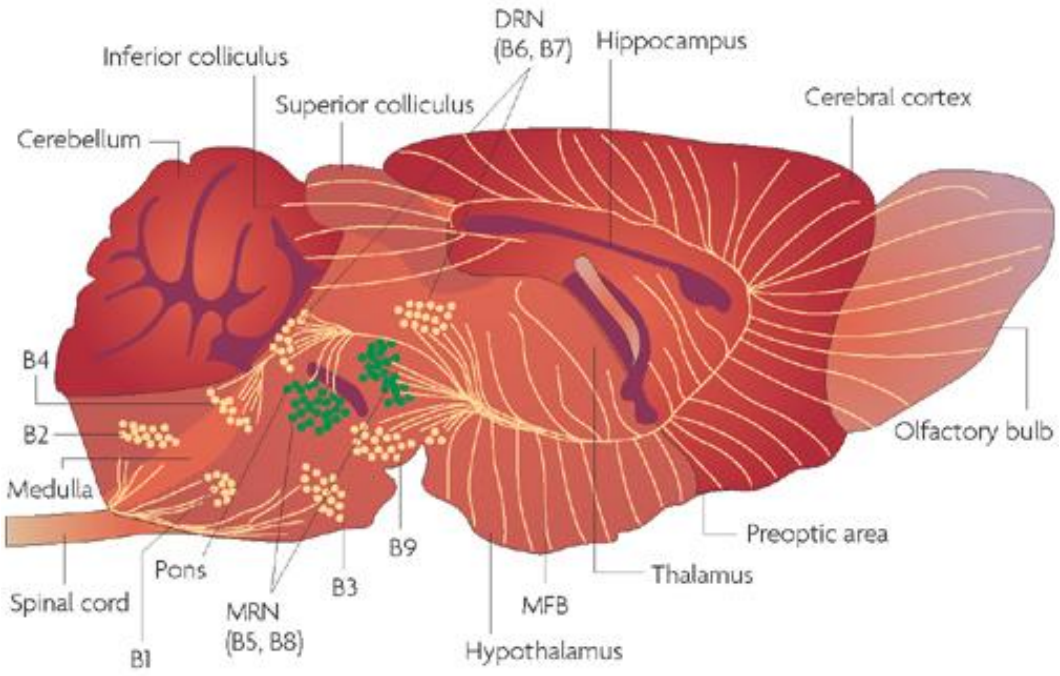

Figure 1.7.1. Serotonergic innervation originates in the raphe nuclei. The rostral nuclei and projects into cortical and subcortical structures, while the caudal nuclei projects into the brainstem. B1-B3 are the caudal nuclei and project to the spinal cord and peripheral nervous system. The rostral nuclei are the dorsal raphe (B6 and B7) and the median raphe (B5 and B8), which project into the cortical and subcortical structures. Figure reproduced from Murphy and Lesch, with permission. ©Nature Publishing Group (2008).[80]

The substantia nigra pars reticulata receives input from the dorsal raphe nucleus, where serotonin is synthesized. The dorsal raphe nucleus contains about 50% serotonergic neurons, and has the highest concentration of serotonergic neurons in the brain.[78] The substantia nigra pars

reticulata has been found to be involved in motor control and movement disorders,[42, 81-85] while the dorsal raphe nucleus appears to be important in depression and neuroplasticity.[86-87] In this work, we measured serotonin release in both the substantia nigra pars reticulata and dorsal raphe nucleus of rodent models.

1.8 ANIMAL MODELS

Animals have been used to great success in research to shed light on human behavior,[88-89] physiology,[90-93] and disease.[94-99] This work relies on the use of rats, mice, and zebrafish to model neurological function. This introduction provides only a brief overview; additional details of each model organism used are provided in the individual chapters.

1.8.1 Historical perspectives of model organisms in research

Animals have been used for research for over 2400 years—at least since ancient Greece. In the 6th century BCE, Alcmaeon of Croton used dogs to determine that the brain was the seat of intelligence. By the 4th century BCE, Aristotle used chicks as a model for embryogenesis. Around a century later, Erasistratus determined that the heart functioned as a pump using animal models. In the 12th century, Avenzoar practiced surgical techniques on animals, such as tracheotomies, and in the 17th century, William Harvey was able to use animal models to describe in detail the workings of the cardiovascular system.[100]

Within the past century, animal research has taken off to an even greater extent. With the advent of genetic manipulation, a new world of research possibilities in animal models was opened; the first transgenic mouse was developed in 1976.[101] Figure 1.8.1 shows the rapid increase in publication of papers using animal models since the 1970s. Today, the genomes of mice,[102] rats,[103] and zebrafish[104] have all been fully sequenced. In this work, each of these model

organisms is used to shed light on neurotransmitter release. There are several considerations for choosing a model organism, including cost, ease of use, duration of life cycle, and relevance to humans. Oftentimes, this is a balancing act; invertebrates such as drosophila and Caenorhabditis elegans are extremely inexpensive and high-throughput, but are not as similar to humans as vertebrate models.[105]

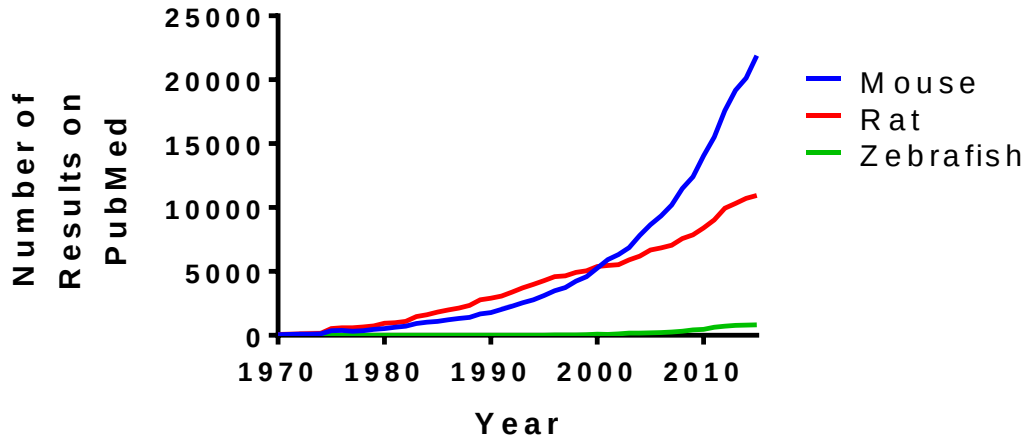

Figure 1.8.1. The use of animal models, especially mice, has skyrocketed since the 1970s.

1.8.2 Rodent model organisms

In this work, rats are used to study the effect of chemotherapy treatment on the brain. In Chapter 3, this will be discussed in further detail; briefly, rats were treated with chemotherapeutic agents via i.v. tail vein injections. Our collaborator, Dr. David Jarmolowicz, and his lab measured cognitive changes in rats receiving chemotherapy. At the end of a full course of chemotherapeutic treatments, our lab performed neurochemical analysis in the form of FSCV in brain slices. Rats (*rattus norvegicus*) have several advantages as model organisms. Due to their relatively large size, administration of chemotherapy via i.v. tail vein injection is easier in

comparison to mice. Rats have also been developed further as a model for studying cognition compared to mice.[88]

Mice (*mus musculus*) are also used in this work to study changes in the brain in Huntington's disease. Specifically, mutant mice carrying a truncated version of the human Huntington gene were used. FSCV measurements were made in brain slices of these mutant Huntington's disease model mice. The major advantage to using mice is that they have proven to be easier to genetically manipulate; thus, several strains of transgenic Huntington's disease model mice are readily available.[106] Mice have the added benefit of being relatively inexpensive to purchase and house, compared to rats. Our work using mice in our study of Huntington's disease is discussed in greater depth in Chapter 2.

1.8.3 Zebrafish

In this work, we develop a method for using FSCV to measure dopamine release in zebrafish whole mount retina. Zebrafish (*danio rerio*) present some unique advantages for use as a model organism, and yet, they are a relatively young animal model in research. Zebrafish were initially used as a model organism in the 1960s.[107] Their relatively large, external embryos and fast life cycle make them an ideal model organism for studying development.[108-109] The genome of zebrafish has been fully sequenced; thus, they are easily genetically manipulatable. As vertebrates, zebrafish have the added benefit of being relatively genetically similar to humans compared to invertebrate models such as fruit flies and c. elegans.[108] Specifically, the functional architecture retina is well-conserved across vertebrates.[110] In Chapter 4, our work developing a method to use zebrafish to study the retina is discussed further.

1.9 USING FAST-SCAN CYCLIC VOLTAMMETRY TO MEASURE NEUROTRANSMITTER RELEASE IN ANIMAL MODELS

One commonality throughout this work is the instrumentation used to measure neurotransmitter release in animal models. Figure 1.9.1 shows a block diagram of a typical instrumental setup for fast-scan cyclic voltammetry measurements of neurotransmitter release. On the computer, waveforms and stimulation patterns are input into the software. Through a breakout box and National Instruments cards, the digital signal from the software is converted to an analog signal and sent to the potentiostat and stimulating electrodes or LED setup. The potentiostat sends a waveform to the working electrode and receives current information from the working electrode, which it sends back to the computer.

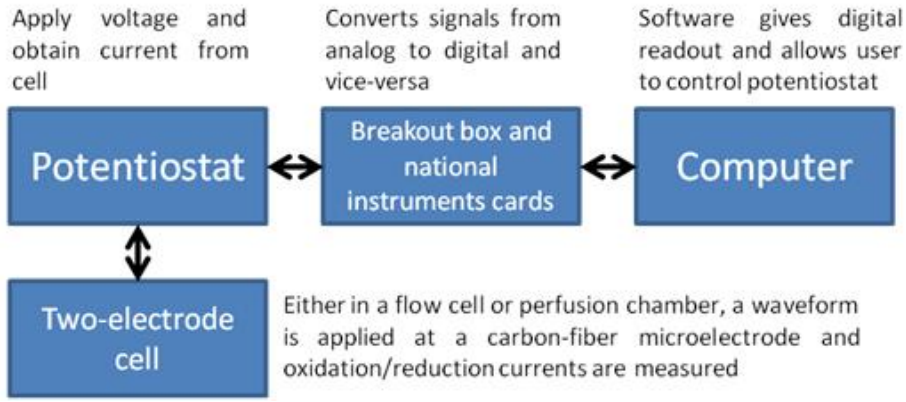

Figure 1.9.1. Schematic showing a typical electrochemical setup for a fast-scan cyclic voltammetry experiment.

1.9.1 Experimental setup

In this work, brain slices and whole mount retinas are placed in a perfusion chamber, a schematic of which is shown in Figure 1.9.2. Artificial cerebrospinal fluid (aCSF) is perfused over the tissue in order to keep it functional throughout the course of the experiment. Artificial cerebrospinal fluid enters the chamber by gravity and is removed through vacuum suction. There

is a reservoir where an Ag/AgCl reference electrode is placed. A microscope or stereoscope objective allows for visualization of the tissue and electrodes. Stimulating electrodes, fiber optic-coupled LEDs for light stimulation, and carbon fiber microelectrodes can all be placed in the tissue using micromanipulators.

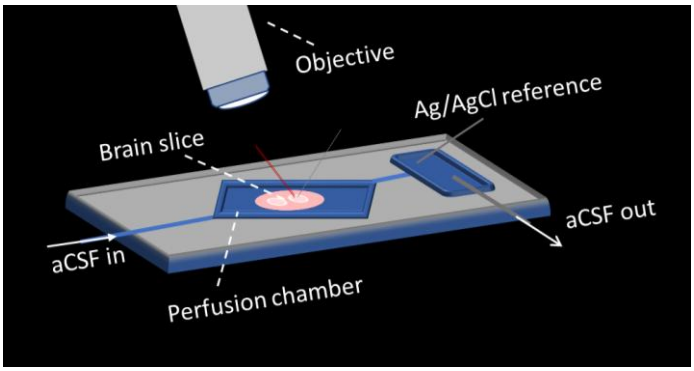

Figure 1.9.2. Perfusion chamber.

1.9.2 Fast-scan cyclic voltammetric measurements *ex vivo*

Figure 1.9.3 (A) shows placement of stimulating electrodes and a carbon fiber microelectrode in a striatal brain slice obtained from a rat. As shown here, the working electrode is placed 100 µm deep in the striatal tissue directly between the two stimulating electrodes. Dopamine release is evoked electrically using the stimulating electrodes and measured at the working electrode. Electrical stimulation is necessary as the background subtraction required to obtain useful data using FSCV renders the technique incapable of detecting endogenous concentrations; rather, only changes in concentration can be quantified with FSCV. Serotonin release measurements were recorded similarly; the main differences were the waveform and stimulation paradigm, as well as the region of the brain. Later, retinal dopamine release measurements were collected using light stimulation; Figure 1.9.3 (B) shows a working electrode

placed in adult zebrafish whole mount retina. To obtain concentration data, electrodes are calibrated against a known concentration of the analyte of interest.

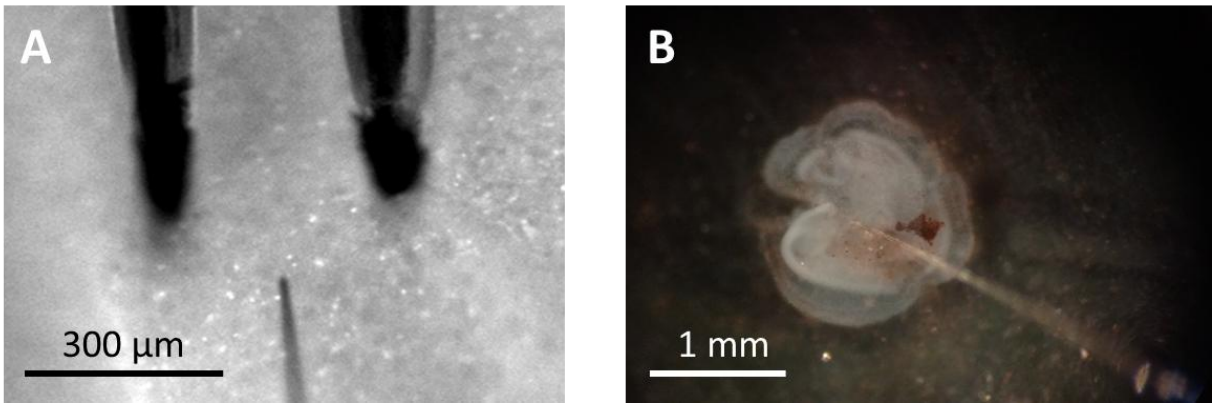

Figure 1.9.3. (A) A carbon fiber microelectrode placed at a depth of 100 µm in rat striatal tissue, directly between stimulating electrodes. (B) A carbon fiber microelectrode placed at a depth of 100 µm in adult zebrafish whole mount retina.

1.10 SUMMARY OF FUTURE CHAPTERS

In this work, fast-scan cyclic voltammetry at carbon fiber microelectrodes is used to measure neurotransmitter release in animal models. In Chapter 2, work is described in which serotonin release evoked by electrical stimulation was measured in Huntington's disease model mice. Chapter 3 describes our work in which serotonin and dopamine release were measured in rats treated with chemotherapeutic agents. Chapter 4 describes the development and application of methods in which we measured dopamine release, evoked by stimulation with light, in whole mount zebrafish retinas. In the final chapter, conclusions and future directions are offered.

1.11 REFERENCES

1. Bard, A. J.; Faulkner, L. R.; Leddy, J.; Zoski, C. G., *Electrochemical methods: fundamentals and applications*. wiley New York: 1980; Vol. 2.

2. Kissinger, P.; Heineman, W. R., *Laboratory Techniques in Electroanalytical Chemistry, revised and expanded*. CRC press: 1996.

3. Ehl, R. G.; Ihde, A. J., Faraday's electrochemical laws and the determination of equivalent weights. *Journal of Chemical Education* **1954,** *31* (5), 226.

4. Kissinger, P. T.; Heineman, W. R., Cyclic voltammetry. *Journal of Chemical Education* **1983,** *60* (9), 702.

5. Voorhies, J. D.; Adams, R. N., Voltammetry Solid Electrodes. Anodic Polarography of Sulfa Drugs. *Analytical Chemistry* **1958,** *30* (3), 346-350.

6. Kissinger, P. T., Lessons from the Work of Professor Ralph N. Adams. *Electroanalysis* **1999,** *11* (5), 292-294.

7. Hawley, M. D.; Tatawawadi, S. V.; Piekarski, S.; Adams, R. N., Electrochemical Studies of the Oxidation Pathways of Catecholamines. *Journal of the American Chemical Society* **1967,** *89* (2), 447-450.

8. Kissinger, P. T.; Hart, J. B.; Adams, R. N., Voltammetry in brain tissue--a new neurophysiological measurement. *Brain Res* **1973,** *55* (1), 209-13.

9. Wightman, R. M., Voltammetry with microscopic electrodes in new domains. *Science* **1988,** *240* (4851), 415-20.

10. Hashemi, P.; Dankoski, E. C.; Petrovic, J.; Keithley, R. B.; Wightman, R. M., Voltammetric detection of 5-hydroxytryptamine release in the rat brain. *Anal Chem* **2009,** *81* (22), 9462-71.

11. Coriat, I. H., A review of some recent literature on the chemistry of the central nervous system. *The Journal of comparative neurology and psychology 15* (2), 148-159.

12. Shanes, A. M., Electrochemical aspects of physiological and pharmacological action in excitable cells. II. The action potential and excitation. *Pharmacological reviews* **1958,** *10* (2), 165-273.

13. Erlanger, J.; Bishop, G. H.; Gasser, H. S., The action potential waves transmitted between the sciatic nerve and its spinal roots. *The American journal of physiology* **1926,** *78* (3), 574-591.

14. Erlanger, J.; Bishop, G. H.; Gasser, H. S., On conduction of the action potential wave through the dorsal root ganglion. *Proceedings of the Society for Experimental Biology and Medicine* **1926,** *23* (5), 372-373.

15. Amberson, W. R.; Downing, A. C., On the form of the action potential wave in nerve. *The Journal of physiology* **1929,** *68* (1), 19-38.

16. Verworn, M., The neuron in anatomy and physiology. *Deutsche medizinische Wochenschrift* **1900,** *26*, 605-611.

17. Collin, R., Mitochondria of the axon, dendrites and ganglionic body cells of the retina. *Comptes rendus des séances de la Société de biologie et de ses filiales* **1913,** *74*, 1358-1360.

18. Watkins, A. O., The formation of dendrites. *Philosophical magazine (Abingdon, England)* **1900,** *49* (296-01), 415-416.

19. Fuxe, K., EVIDENCE FOR EXISTENCE OF MONOAMINE NEURONS IN CENTRAL NERVOUS SYSTEM .4. DISTRIBUTION OF MONOAMINE TERMINALS IN CENTRAL NERVOUS SYSTEM. *Acta physiologica Scandinavica* **1965,** *S 64*, 37-+.

20. Decima, E. E., An Effect of Postsynaptic Neurons upon Presynaptic Terminals. *Proceedings of the National Academy of Sciences of the United States of America* **1969,** *63* (1), 58-64.

21. Curtis, H. J.; Cole, K. S., Membrane resting and action potentials from the squid giant axon. *Journal of cellular and comparative physiology 19* (2), 135-144.

22. Woodbury, J. W.; Woodbury, L. A. In *MEMBRANE RESTING AND ACTION POTENTIALS FROM EXCITABLE TISSUES*, 1950; pp 139-140.

23. Mummert, H.; Gradmann, D., Action potentials in Acetabularia: measurement and simulation of voltage-gated fluxes. *The Journal of membrane biology* **1991,** *124* (3), 265-273.

24. Chiu, S. Y., Functions and distribution of voltage-gated sodium and potassium channels in mammalian Schwann cells. *Glia* **1991,** *4* (6), 541-558.

25. De Camilli, P.; Jahn, R., Pathways to regulated exocytosis in neurons. *Annual review of physiology* **1990,** *52* (1), 625-645.

26. Pappas, G. D.; Purpura, D. P., Distribution of colloidal particles in extracellular space and synaptic cleft substance of mammalian cerebral cortex. *Nature (London)* **1966,** *210* (5043), 1391-1392.

27. Wise, R. A.; Rompre, P. P., BRAIN DOPAMINE AND REWARD. *Annu. Rev. Psychol.* **1989,** *40*, 191-225.

28. Volkow, N. D.; Wang, G. J.; Fowler, J. S.; Tomasi, D.; Telang, F., Addiction: beyond dopamine reward circuitry. *Proc Natl Acad Sci U S A* **2011,** *108* (37), 15037-42.

29. Wooten, G. F.; Trugman, J. M., THE DOPAMINE MOTOR SYSTEM. *Mov. Disord.* **1989,** *4*, S38-S47.

30. Mateo, I.; Infante, J.; Rodriguez, E.; Berciano, J.; Combarros, O.; Llorca, J., Interaction between dopamine beta-hydroxylase and interleukin genes increases Alzheimer's disease risk. *Journal of Neurology Neurosurgery and Psychiatry* **2006,** *77* (2), 278-279.

31. Pimoule, C.; Schoemaker, H.; Javoyagid, F.; Scatton, B.; Agid, Y., Decrease in [3H]cocaine binding to the dopamine transporter in Parkinson's disease. *European journal of pharmacology* **1983,** *95* (1-2), 145-146.

32. Edwards, R.; Fon, E.; Merickel, A.; Finn, P.; Krantz, D.; Liu, Y., Vesicular monoamine transport, dopamine toxicity and Parkinson's disease. *Faseb J.* **1997,** *11* (9), A869-A869.

33. Vetter, J. M.; Jehle, T.; Heinemeyer, J.; Franz, P.; Behrens, P. F.; Jackisch, R.; Landwehrmeyer, G. B.; Feuerstein, T. J., Mice transgenic for exon 1 of Huntington's disease: properties of cholinergic and dopaminergic pre-synaptic function in the striatum. *Journal of Neurochemistry* **2003,** *85* (4), 1054-1063.

34. Johnson, M. A.; Rajan, V.; Miller, C. E.; Wightman, R. M., Dopamine release is severely compromised in the R6/2 mouse model of Huntington's disease. *J Neurochem* **2006,** *97* (3), 737-46.

35. Kraft, J. C.; Osterhaus, G. L.; Ortiz, A. N.; Garris, P. A.; Johnson, M. A., In vivo dopamine release and uptake impairments in rats treated with 3-nitropropionic acid. *Neuroscience* **2009,** *161* (3), 940-9.

36. Ortiz, A. N.; Kurth, B. J.; Osterhaus, G. L.; Johnson, M. A., Dysregulation of intracellular dopamine stores revealed in the R6/2 mouse striatum. *J Neurochem* **2010,** *112* (3), 755-61.

37. Callahan, J. W.; Abercrombie, E. D., In vivo Dopamine Efflux is Decreased in Striatum of both Fragment (R6/2) and Full-Length (YAC128) Transgenic Mouse Models of Huntington's Disease. *Front Syst Neurosci* **2011,** *5*, 61.

38. Ortiz, A. N.; Kurth, B. J.; Osterhaus, G. L.; Johnson, M. A., Impaired dopamine release and uptake in R6/1 Huntington's disease model mice. *Neurosci Lett* **2011,** *492* (1), 11-4.

39. Ortiz, A. N.; Osterhaus, G. L.; Lauderdale, K.; Mahoney, L.; Fowler, S. C.; von Horsten, S.; Riess, O.; Johnson, M. A., Motor function and dopamine release measurements in transgenic Huntington's disease model rats. *Brain Res* **2012,** *1450*, 148-56.

40. Maina, F. K.; Khalid, M.; Apawu, A. K.; Mathews, T. A., Presynaptic dopamine dynamics in striatal brain slices with fast-scan cyclic voltammetry. *J Vis Exp* **2012,** (59).

41. Mittal, S. K.; Eddy, C., The role of dopamine and glutamate modulation in Huntington disease. *Behav Neurol* **2013,** *26* (4), 255-63.

42. Jahanshahi, A.; Vlamings, R.; van Roon-Mom, W. M. C.; Faull, R. L. M.; Waldvogel, H. J.; Janssen, M. L. F.; Yakkioui, Y.; Zeef, D. H.; Kocabicak, E.; Steinbusch, H. W. M.; Temel, Y., Changes in brainstem serotonergic and dopaminergic cell populations in experimental and clinical Huntington's disease. *Neuroscience* **2013,** *238*, 71-81.

43. Joel, D.; Weiner, I., The connections of the dopaminergic system with the striatum in rats and primates: an analysis with respect to the functional and compartmental organization of the striatum. *Neuroscience* **2000,** *96* (3), 451-74.

44. Smith, Y.; Shink, E.; Sidibe, M., Neuronal circuitry and synaptic connectivity of the basal ganglia. *Neurosurgery clinics of North America* **1998,** *9* (2), 203-22.

45. Money, K.; Stanwood, G., Developmental origins of brain disorders: roles for dopamine. *Frontiers in Cellular Neuroscience* **2013,** *7* (260).

46. Palmiter, R. D., Dopamine signaling in the dorsal striatum is essential for motivated behaviors: lessons from dopamine-deficient mice. *Annals of the New York Academy of Sciences* **2008,** *1129*, 35-46.

47. Jocham, G.; Klein, T. A.; Ullsperger, M., Dopamine-mediated reinforcement learning signals in the striatum and ventromedial prefrontal cortex underlie value-based choices. *The Journal of neuroscience : the official journal of the Society for Neuroscience* **2011,** *31* (5), 1606-13.

48. Wilson, C. J.; Groves, P. M., Fine structure and synaptic connections of the common spiny neuron of the rat neostriatum: a study employing intracellular inject of horseradish peroxidase. *J Comp Neurol* **1980,** *194* (3), 599-615.

49. Joyce, J. N.; Lexow, N.; Bird, E.; Winokur, A., ORGANIZATION OF DOPAMINE D1 AND D2 RECEPTORS IN HUMAN STRIATUM - RECEPTOR AUTORADIOGRAPHIC STUDIES IN HUNTINGTONS-DISEASE AND SCHIZOPHRENIA. *Synapse* **1988,** *2* (5), 546-557.

50. Holt, D. J.; Herman, M. M.; Hyde, T. M.; Kleinman, J. E.; Sinton, C. M.; German, D. C.; Hersh, L. B.; Graybiel, A. M.; Saper, C. B., Evidence for a deficit in cholinergic interneurons in the striatum in schizophrenia. *Neuroscience* **1999,** *94* (1), 21-31.

51. Holt, D. J.; Bachus, S. E.; Hyde, T. M.; Wittie, M.; Herman, M. M.; Vangel, M.; Saper, C. B.; Kleinman, J. E., Reduced density of cholinergic interneurons in the ventral striatum in schizophrenia: An in situ hybridization study. *Biological Psychiatry* **2005,** *58* (5), 408-416.

52. Ron, D., Plasticity in the dorsal striatum underlies alcohol abuse disorders. *Journal of Molecular Neuroscience* **2012,** *48*, S97-S98.

53. Baldermann, J. C.; Kohl, S.; Visser-Vandewalle, V.; Klehr, M.; Huys, D.; Kuhn, J., Deep Brain Stimulation of the Ventral Capsule/Ventral Striatum Reproducibly Improves Symptoms of Body Dysmorphic Disorder. *Brain Stimulation* **2016,** *9* (6), 957-959.

54. Gunaydin, L.; Nelson, A.; Kreitzer, A., Fronto-Striatal Modulation of Anxiety-Like Behaviors. *Biological Psychiatry* **2017,** *81* (10), S203-S203.

55. Okada, G.; Okamoto, Y.; Takamura, M.; Toki, S.; Yamamoto, T.; Yamawaki, S., Functional Connectivity of Striatum and SSRI Treatment in Major Depressive Disorder. *Neuropsychopharmacology* **2015,** *40*, S315-S315.

56. Kim, T. J.; Kim, T. J.; Lee, H.; Kim, Y. E.; Jeon, B. S., A case of Parkin disease (PARK2) with schizophrenia: Evidence of regional selectivity. *Clinical Neurology and Neurosurgery* **2014,** *126*, 35-37.

57. Kolb, H., Roles of Amacrine Cells. . In *Webvision: The Organization of the Retina and Visual System [Internet]*. Kolb, H.; Fernandez, E.; Nelson, R., Eds. University of Utah Health Sciences Center: Salt Lake City, UT, 2005 [Updated 2007 Apr 30].

58. Tian, T.; Li, Z.; Lu, H., Common pathophysiology affecting diabetic retinopathy and Parkinson's disease. *Medical hypotheses* **2015,** *85* (4), 397-8.

59. Aung, M. H.; Park, H. N.; Han, M. K.; Obertone, T. S.; Abey, J.; Aseem, F.; Thule, P. M.; Iuvone, P. M.; Pardue, M. T., Dopamine deficiency contributes to early visual dysfunction in a rodent model of type 1 diabetes. *The Journal of neuroscience : the official journal of the Society for Neuroscience* **2014,** *34* (3), 726-36.

60. Harnois, C.; Di Paolo, T., Decreased dopamine in the retinas of patients with Parkinson's disease. *Investigative ophthalmology & visual science* **1990,** *31* (11), 2473-5.

61. Zhang, N.; Favazza, T. L.; Baglieri, A. M.; Benador, I. Y.; Noonan, E. R.; Fulton, A. B.; Hansen, R. M.; Iuvone, P. M.; Akula, J. D., The rat with oxygen-induced retinopathy is myopic with low retinal dopamine. *Investigative ophthalmology & visual science* **2013,** *54* (13), 8275-84.

62. Feldkaemper, M.; Schaeffel, F., An updated view on the role of dopamine in myopia. *Experimental eye research* **2013,** *114*, 106-19.

63. Smith, C. P.; Sharma, S.; Steinle, J. J., Age-related changes in sympathetic neurotransmission in rat retina and choroid. *Experimental eye research* **2007,** *84* (1), 75-81.

64. Shibagaki, K.; Okamoto, K.; Katsuta, O.; Nakamura, M., Beneficial protective effect of pramipexole on light-induced retinal damage in mice. *Experimental eye research* **2015,** *139*, 64-72.

65. Scally, M. C.; Ulus, I.; Wurtman, R. J., Brain tyrosine level controls striatal dopamine synthesis in haloperidol-treated rats. *Journal of neural transmission* **1977,** *41* (1), 1-6.

66. Cheramy, A.; Besson, M. J.; Mussachio, J. M. In *EFFECTS OF PSYCHOTROPIC DRUGS ON DOPAMINE (DA) SYNTHESIS AND TYROSINE HYDROXYLASE ACTIVITY IN STRIATUM OF RAT*, 1971; pp 205-+.

67. Wahbe, F.; Hagege, J.; Loreau, N.; Ardaillou, R., Endogenous dopamine synthesis and dopa-decarboxylase activity in rat renal cortex. *Molecular and cellular endocrinology* **1982,** *27* (1), 45-54.

68. Dawson, R.; Phillips, M. I., Dopamine synthesis and release in LLC-PK1 cells. *European journal of pharmacology* **1990,** *189* (6), 423-426.

69. Bernard, C.; Chireux, M.; Barraille, P.; Thai, A. L.; Vidal, S., Regulation of neurotransmitter synthesis: from neuron to gene. *Journal de physiologie* **1991,** *85* (2), 97-104.

70. Rost; egrave; ne, W.; Boja, J. W.; Scherman, D.; Carroll, F. I.; Kuhar, M. J., Dopamine transport: pharmacological distinction between the synaptic membrane and the vesicular transporter in rat striatum. *European journal of pharmacology* **1992,** *218* (1), 175-177.

71. Chiodo, L. A.; Antelman, S. M., Repeated tricyclics induce a progressive dopamine autoreceptor subsensitivity independent of daily drug treatment. *Nature (London)* **1980,** *287* (5781), 451-454.

72. Zivkovic, B.; Guidotti, A.; Costa, E., The regulation of the kinetic state of striatal tyrosine hydroxylase and the role of postsynaptic dopamine receptors. *Brain research* **1975,** *92* (3), 516-521.

73. Molliver, M. E., Serotonergic neuronal systems: what their anatomic organization tells us about function. *Journal of clinical psychopharmacology* **1987,** *7* (6 Suppl), 3s-23s.

74. Golden, R. N.; Gilmore, J. H., SEROTONIN AND MOOD DISORDERS. *Psychiatr. Ann.* **1990,** *20* (10), 580-&.

75. Pang, T. Y.; Du, X.; Zajac, M. S.; Howard, M. L.; Hannan, A. J., Altered serotonin receptor expression is associated with depression-related behavior in the R6/1 transgenic mouse model of Huntington's disease. *Hum Mol Genet* **2009,** *18* (4), 753-66.

76. Cowen, P.; Sherwood, A. C., The role of serotonin in cognitive function: evidence from recent studies and implications for understanding depression. *Journal of Psychopharmacology* **2013,** *27* (7), 575-583.

77. Altman, H. J.; Normile, H. J., SEROTONIN, LEARNING, MEMORY, AND ALZHEIMERS-DISEASE. *Neurobiol. Aging* **1990,** *11* (3), 341-341.

78. Frazer, A.; Hensler, J., Serotonin. In *Basic Neurochemistry: Molecular, Cellular and Medical Aspects.* , 6th ed.; Siegel, G.; Agranoff, B.; Albers, R., Eds. Lippincott-Raven: Philadelphia, 1999.

79. Tork, I., Anatomy of the serotonergic system. *Annals of the New York Academy of Sciences* **1990,** *600*, 9-34; discussion 34-5.

80. Murphy, D. L.; Lesch, K.-P., Targeting the murine serotonin transporter: insights into human neurobiology. *Nat Rev Neurosci* **2008,** *9* (2), 85-96.

81. Castro, M. E.; Pascual, J.; Romon, T.; Berciano, J.; Figols, J.; Pazos, A., 5-HT1B receptor binding in degenerative movement disorders. *Brain Res* **1998,** *790* (1-2), 323-8.

82. Threlfell, S.; Greenfield, S. A.; Cragg, S. J., 5-HT(1B) receptor regulation of serotonin (5-HT) release by endogenous 5-HT in the substantia nigra. *Neuroscience* **2010,** *165* (1), 212-20.

83. Lehericy, S.; Bardinet, E.; Poupon, C.; Vidailhet, M.; Francois, C., 7 Tesla magnetic resonance imaging: a closer look at substantia nigra anatomy in Parkinson's disease. *Movement disorders : official journal of the Movement Disorder Society* **2014,** *29* (13), 1574-81.

84. Broadstock, M.; Austin, P. J.; Betts, M. J.; Duty, S., Antiparkinsonian potential of targeting group III metabotropic glutamate receptor subtypes in the rodent substantia nigra pars reticulata. *British journal of pharmacology* **2012,** *165* (4b), 1034-45.

85. Lobb, C. J.; Jaeger, D., Bursting activity of substantia nigra pars reticulata neurons in mouse parkinsonism in awake and anesthetized states. *Neurobiol Dis* **2015,** *75*, 177-85.

86. Michelsen, K. A.; Prickaerts, J.; Steinbusch, H. W., The dorsal raphe nucleus and serotonin: implications for neuroplasticity linked to major depression and Alzheimer's disease. *Progress in brain research* **2008,** *172*, 233-64.

87. Hendricksen, M.; Thomas, A. J.; Ferrier, I. N.; Ince, P.; O'Brien, J. T., Neuropathological study of the dorsal raphe nuclei in late-life depression and Alzheimer's disease with and without depression. *The American journal of psychiatry* **2004,** *161* (6), 1096-102.

88. Mulvanny, P., Behavioral Neuroscience: An Introduction. *The American journal of psychology 94* (2), 363-365.

89. van der Staay, F. J.; Arndt, S. S.; Nordquist, R. E., Evaluation of animal models of neurobehavioral disorders. *Behavioral and brain functions* **2009,** *5* (1), 11.

90. Wightman, R. M.; Amatore, C.; Engstrom, R. C.; Hale, P. D.; Kristensen, E. W.; Kuhr, W. G.; May, L. J., Real-time characterization of dopamine overflow and uptake in the rat striatum. *Neuroscience* **1988,** *25* (2), 513-23.

91. Witkovsky, P.; Nicholson, C.; Rice, M. E.; Bohmaker, K.; Meller, E., Extracellular dopamine concentration in the retina of the clawed frog, Xenopus laevis. *Proceedings of the National Academy of Sciences of the United States of America* **1993,** *90* (12), 5667-71.

92. Yazulla, S.; Studholme, K. M., Neurochemical anatomy of the zebrafish retina as determined by immunocytochemistry. *Journal of neurocytology* **2001,** *30* (7), 551-92.

93. Shin, J. T.; Fishman, M. C., From Zebrafish to human: modular medical models. *Annu Rev Genomics Hum Genet* **2002,** *3,* 311-40.

94. Sarkisian, M. R., Overview of the Current Animal Models for Human Seizure and Epileptic Disorders. *Epilepsy & behavior* **2001,** *2* (3), 201-216.

95. Schneider, A.; Whitcomb, D. C.; Singer, M. V., Animal models in alcoholic pancreatitis--what can we learn? *Pancreatology : official journal of the International Association of Pancreatology (IAP) ... [et al.]* **2002,** *2* (3), 189-203.

96. Maragakis, N. J.; Rothstein, J. D., Glutamate transporters: animal models to neurologic disease. *Neurobiol Dis* **2004,** *15* (3), 461-73.

97. McBride, J. L.; Behrstock, S. P.; Chen, E. Y.; Jakel, R. J.; Siegel, I.; Svendsen, C. N.; Kordower, J. H., Human neural stem cell transplants improve motor function in a rat model of Huntington's disease. *J Comp Neurol* **2004,** *475* (2), 211-9.

98. Nestler, E. J.; Carlezon, W. A., Jr., The mesolimbic dopamine reward circuit in depression. *Biol Psychiatry* **2006,** *59* (12), 1151-9.

99. Lieschke, G. J.; Currie, P. D., Animal models of human disease: zebrafish swim into view. *Nat Rev Genet* **2007,** *8* (5), 353-67.

100. Ericsson, A. C.; Crim, M. J.; Franklin, C. L., A brief history of animal modeling. *Missouri medicine* **2013,** *110* (3), 201-5.

101. Jaenisch, R.; Dausman, J.; Cox, V.; Fan, H., Infection of developing mouse embryos with murine leukemia virus: tissue specificity and genetic transmission of the virus. *Hamatologie und Bluttransfusion* **1976,** *19*, 341-56.

102. Waterston, R. H.; Lindblad-Toh, K.; Birney, E.; Rogers, J.; Abril, J. F.; Agarwal, P.; Agarwala, R.; Ainscough, R.; Alexandersson, M.; An, P.; Antonarakis, S. E.; Attwood, J.; Baertsch, R.; Bailey, J.; Barlow, K.; Beck, S.; Berry, E.; Birren, B.; Bloom, T.; Bork, P.; Botcherby, M.; Bray, N.; Brent, M. R.; Brown, D. G.; Brown, S. D.; Bult, C.; Burton, J.; Butler, J.; Campbell, R. D.; Carninci, P.; Cawley, S.; Chiaromonte, F.; Chinwalla, A. T.; Church, D. M.; Clamp, M.; Clee, C.; Collins, F. S.; Cook, L. L.; Copley, R. R.; Coulson, A.; Couronne, O.; Cuff, J.; Curwen, V.; Cutts, T.; Daly, M.; David, R.; Davies, J.; Delehaunty, K. D.; Deri, J.; Dermitzakis, E. T.; Dewey, C.; Dickens, N. J.; Diekhans, M.; Dodge, S.; Dubchak, I.; Dunn, D. M.; Eddy, S. R.; Elnitski, L.; Emes, R. D.; Eswara, P.; Eyras, E.; Felsenfeld, A.; Fewell, G. A.;

Flicek, P.; Foley, K.; Frankel, W. N.; Fulton, L. A.; Fulton, R. S.; Furey, T. S.; Gage, D.; Gibbs, R. A.; Glusman, G.; Gnerre, S.; Goldman, N.; Goodstadt, L.; Grafham, D.; Graves, T. A.; Green, E. D.; Gregory, S.; Guigo, R.; Guyer, M.; Hardison, R. C.; Haussler, D.; Hayashizaki, Y.; Hillier, L. W.; Hinrichs, A.; Hlavina, W.; Holzer, T.; Hsu, F.; Hua, A.; Hubbard, T.; Hunt, A.; Jackson, I.; Jaffe, D. B.; Johnson, L. S.; Jones, M.; Jones, T. A.; Joy, A.; Kamal, M.; Karlsson, E. K.; Karolchik, D.; Kasprzyk, A.; Kawai, J.; Keibler, E.; Kells, C.; Kent, W. J.; Kirby, A.; Kolbe, D. L.; Korf, I.; Kucherlapati, R. S.; Kulbokas, E. J.; Kulp, D.; Landers, T.; Leger, J. P.; Leonard, S.; Letunic, I.; Levine, R.; Li, J.; Li, M.; Lloyd, C.; Lucas, S.; Ma, B.; Maglott, D. R.; Mardis, E. R.; Matthews, L.; Mauceli, E.; Mayer, J. H.; McCarthy, M.; McCombie, W. R.; McLaren, S.; McLay, K.; McPherson, J. D.; Meldrim, J.; Meredith, B.; Mesirov, J. P.; Miller, W.; Miner, T. L.; Mongin, E.; Montgomery, K. T.; Morgan, M.; Mott, R.; Mullikin, J. C.; Muzny, D. M.; Nash, W. E.; Nelson, J. O.; Nhan, M. N.; Nicol, R.; Ning, Z.; Nusbaum, C.; O'Connor, M. J.; Okazaki, Y.; Oliver, K.; Overton-Larty, E.; Pachter, L.; Parra, G.; Pepin, K. H.; Peterson, J.; Pevzner, P.; Plumb, R.; Pohl, C. S.; Poliakov, A.; Ponce, T. C.; Ponting, C. P.; Potter, S.; Quail, M.; Reymond, A.; Roe, B. A.; Roskin, K. M.; Rubin, E. M.; Rust, A. G.; Santos, R.; Sapojnikov, V.; Schultz, B.; Schultz, J.; Schwartz, M. S.; Schwartz, S.; Scott, C.; Seaman, S.; Searle, S.; Sharpe, T.; Sheridan, A.; Shownkeen, R.; Sims, S.; Singer, J. B.; Slater, G.; Smit, A.; Smith, D. R.; Spencer, B.; Stabenau, A.; Stange-Thomann, N.; Sugnet, C.; Suyama, M.; Tesler, G.; Thompson, J.; Torrents, D.; Trevaskis, E.; Tromp, J.; Ucla, C.; Ureta-Vidal, A.; Vinson, J. P.; Von Niederhausern, A. C.; Wade, C. M.; Wall, M.; Weber, R. J.; Weiss, R. B.; Wendl, M. C.; West, A. P.; Wetterstrand, K.; Wheeler, R.; Whelan, S.; Wierzbowski, J.; Willey, D.; Williams, S.; Wilson, R. K.; Winter, E.; Worley, K. C.; Wyman, D.; Yang, S.; Yang, S. P.; Zdobnov, E. M.;

Zody, M. C.; Lander, E. S., Initial sequencing and comparative analysis of the mouse genome. *Nature* **2002,** *420* (6915), 520-62.

103. Gibbs, R. A.; Weinstock, G. M.; Metzker, M. L.; Muzny, D. M.; Sodergren, E. J.; Scherer, S.; Scott, G.; Steffen, D.; Worley, K. C.; Burch, P. E.; Okwuonu, G.; Hines, S.; Lewis, L.; DeRamo, C.; Delgado, O.; Dugan-Rocha, S.; Miner, G.; Morgan, M.; Hawes, A.; Gill, R.; Celera; Holt, R. A.; Adams, M. D.; Amanatides, P. G.; Baden-Tillson, H.; Barnstead, M.; Chin, S.; Evans, C. A.; Ferriera, S.; Fosler, C.; Glodek, A.; Gu, Z.; Jennings, D.; Kraft, C. L.; Nguyen, T.; Pfannkoch, C. M.; Sitter, C.; Sutton, G. G.; Venter, J. C.; Woodage, T.; Smith, D.; Lee, H. M.; Gustafson, E.; Cahill, P.; Kana, A.; Doucette-Stamm, L.; Weinstock, K.; Fechtel, K.; Weiss, R. B.; Dunn, D. M.; Green, E. D.; Blakesley, R. W.; Bouffard, G. G.; De Jong, P. J.; Osoegawa, K.; Zhu, B.; Marra, M.; Schein, J.; Bosdet, I.; Fjell, C.; Jones, S.; Krzywinski, M.; Mathewson, C.; Siddiqui, A.; Wye, N.; McPherson, J.; Zhao, S.; Fraser, C. M.; Shetty, J.; Shatsman, S.; Geer, K.; Chen, Y.; Abramzon, S.; Nierman, W. C.; Havlak, P. H.; Chen, R.; Durbin, K. J.; Egan, A.; Ren, Y.; Song, X. Z.; Li, B.; Liu, Y.; Qin, X.; Cawley, S.; Worley, K. C.; Cooney, A. J.; D'Souza, L. M.; Martin, K.; Wu, J. Q.; Gonzalez-Garay, M. L.; Jackson, A. R.; Kalafus, K. J.; McLeod, M. P.; Milosavljevic, A.; Virk, D.; Volkov, A.; Wheeler, D. A.; Zhang, Z.; Bailey, J. A.; Eichler, E. E.; Tuzun, E.; Birney, E.; Mongin, E.; Ureta-Vidal, A.; Woodwark, C.; Zdobnov, E.; Bork, P.; Suyama, M.; Torrents, D.; Alexandersson, M.; Trask, B. J.; Young, J. M.; Huang, H.; Wang, H.; Xing, H.; Daniels, S.; Gietzen, D.; Schmidt, J.; Stevens, K.; Vitt, U.; Wingrove, J.; Camara, F.; Mar Alba, M.; Abril, J. F.; Guigo, R.; Smit, A.; Dubchak, I.; Rubin, E. M.; Couronne, O.; Poliakov, A.; Hubner, N.; Ganten, D.; Goesele, C.; Hummel, O.; Kreitler, T.; Lee, Y. A.; Monti, J.; Schulz, H.; Zimdahl, H.; Himmelbauer, H.; Lehrach, H.; Jacob, H. J.; Bromberg, S.; Gullings-Handley, J.; Jensen-Seaman, M. I.; Kwitek, A. E.; Lazar, J.; Pasko, D.;

Tonellato, P. J.; Twigger, S.; Ponting, C. P.; Duarte, J. M.; Rice, S.; Goodstadt, L.; Beatson, S. A.; Emes, R. D.; Winter, E. E.; Webber, C.; Brandt, P.; Nyakatura, G.; Adetobi, M.; Chiaromonte, F.; Elnitski, L.; Eswara, P.; Hardison, R. C.; Hou, M.; Kolbe, D.; Makova, K.; Miller, W.; Nekrutenko, A.; Riemer, C.; Schwartz, S.; Taylor, J.; Yang, S.; Zhang, Y.; Lindpaintner, K.; Andrews, T. D.; Caccamo, M.; Clamp, M.; Clarke, L.; Curwen, V.; Durbin, R.; Eyras, E.; Searle, S. M.; Cooper, G. M.; Batzoglou, S.; Brudno, M.; Sidow, A.; Stone, E. A.; Venter, J. C.; Payseur, B. A.; Bourque, G.; Lopez-Otin, C.; Puente, X. S.; Chakrabarti, K.; Chatterji, S.; Dewey, C.; Pachter, L.; Bray, N.; Yap, V. B.; Caspi, A.; Tesler, G.; Pevzner, P. A.; Haussler, D.; Roskin, K. M.; Baertsch, R.; Clawson, H.; Furey, T. S.; Hinrichs, A. S.; Karolchik, D.; Kent, W. J.; Rosenbloom, K. R.; Trumbower, H.; Weirauch, M.; Cooper, D. N.; Stenson, P. D.; Ma, B.; Brent, M.; Arumugam, M.; Shteynberg, D.; Copley, R. R.; Taylor, M. S.; Riethman, H.; Mudunuri, U.; Peterson, J.; Guyer, M.; Felsenfeld, A.; Old, S.; Mockrin, S.; Collins, F., Genome sequence of the Brown Norway rat yields insights into mammalian evolution. *Nature* **2004,** *428* (6982), 493-521.

104. Kettleborough, R. N.; Busch-Nentwich, E. M.; Harvey, S. A.; Dooley, C. M.; de Bruijn, E.; van Eeden, F.; Sealy, I.; White, R. J.; Herd, C.; Nijman, I. J.; Fenyes, F.; Mehroke, S.; Scahill, C.; Gibbons, R.; Wali, N.; Carruthers, S.; Hall, A.; Yen, J.; Cuppen, E.; Stemple, D. L., A systematic genome-wide analysis of zebrafish protein-coding gene function. *Nature* **2013,** *496* (7446), 494-7.

105. Muller, B.; Grossniklaus, U., Model organisms--A historical perspective. *Journal of proteomics* **2010,** *73* (11), 2054-63.

106. Menalled, L. B.; Chesselet, M. F., Mouse models of Huntington's disease. *Trends Pharmacol Sci* **2002,** *23* (1), 32-9.

107. Streisinger, G.; Edgar, R. S.; Denhardt, G. H., CHROMOSOME STRUCTURE IN PHAGE T4. I. CIRCULARITY OF THE LINKAGE MAP. *Proc Natl Acad Sci U S A* **1964,** *51*, 775-9.

108. Grunwald, D. J.; Eisen, J. S., Headwaters of the zebrafish--emergence of a new model vertebrate. *Nature reviews. Genetics* **2002,** *3* (9), 717.

109. Phillips, J. B.; Westerfield, M., Zebrafish models in translational research: tipping the scales toward advancements in human health. *Dis Model Mech* **2014,** *7* (7), 739-43.

110. Hoon, M.; Okawa, H.; Della Santina, L.; Wong, R. O., Functional architecture of the retina: development and disease. *Progress in retinal and eye research* **2014,** *42*, 44-84.

2 SEROTONIN RELEASE MEASUREMENTS IN HUNTINGTON'S DISEASE MODEL MICE

2.1 ABSTRACT

Huntington's disease is an autosomal dominant movement disorder associated with depression and other mood disorders. Serotonin has been implicated in depression. Despite this, serotonin has not been extensively measured in Huntington's disease model rodents. In this work, we use fast-scan cyclic voltammetry to investigate how serotonin release in both the substantia nigra pars reticulata and the dorsal raphe nucleus, two brain regions densely innervated with serotonin-releasing terminals, are affected in Huntington's disease model mice.

2.2 INTRODUCTION

Huntington's disease is a fatal, progressive neurodegenerative movement disorder caused by a polymorphic trinucleotide CAG expansion on the *htt* gene, which encodes the protein huntingtin. The result of this expansion is an excess of polyglutamine repeats at the N-terminus leading to cellular toxicity[1]. Symptoms are typically onset between age 35-45 in humans, and death occurs 10-15 years afterward.[2] Huntington's disease affects about 30,000 Americans, and over 200,000 people in the United States are at risk. While its most obvious symptom is choreic movements, the tendency of patients with Huntington's disease toward cognitive and mood disorders, as well as a marked increase in suicide, has been observed.[3] Moreover, more recent studies have shown that patients with Huntington's Disease display a higher prevalence of both depression and aggression compared to the general population. Interestingly, the onset of these systems often occurs before the onset of the motor deficits characteristic of Huntington's disease and before patients are diagnosed; the prevalence of mood disorders has been found to be up to 69%, with the prevalence of major depression 29%.[4-8] Serotonin is thought to be involved in

depression both in the general population and in patients with Huntington's disease. Therefore, we wanted to determine whether serotonin release was affected in mice carrying a truncated version of the human Huntington gene. In this work, we use fast-scan cyclic voltammetry (FSCV) to measure serotonin release in rodent models of Huntington's.

2.2.1 Huntington's disease

Huntington's chorea was first described by George Huntington (April 9, 1850 – March 3, 1916) in 1872.[3] Huntington was a physician in East Hampton on Long Island, and treated many patients in one family who presented with a similar phenotype.[9] Huntington accurately described the adult-onset nature of the disease as well as the uncontrolled, choreic movements in his patients.[3] Despite the newness of the field of genetics (Gregor Mendel had only just proposed his initial work on "genes" six years before Huntington's paper in 1872),[10] through careful study, Huntington was able to determine the inheritance pattern of the disease. As George Huntington initially described, Huntington's Disease is a genetic disease passed down in an autosomal dominant pattern;[3] the Huntington gene (htt), which encodes the protein *huntingtin* is located on the short arm of chromosome 4p16.3 in the Huntingtin gene.[1, 11] The mutant htt gene includes a series of at least 36 CAG repeats, encoding a polyglutamine expansion on the huntingtin protein.[1, 11] Figure 2.2.1 shows a schematic of a typical pedigree for a family carrying the Huntington gene. Some key features are the autosomal (i.e. not sex-linked) and dominant nature of the inheritance pattern. Since chromosome 4p16.3 is not a sex-linked gene, males and females are both equally likely to inherit the disease, and equally likely to pass it on to their children. The dominant nature of its inheritance means that just one copy of the mutant htt allele causes full-blown Huntington's disease. Thus, in families with one parent with Huntington's, there is a 50% chance of passing the disease to each child, regardless of sex.

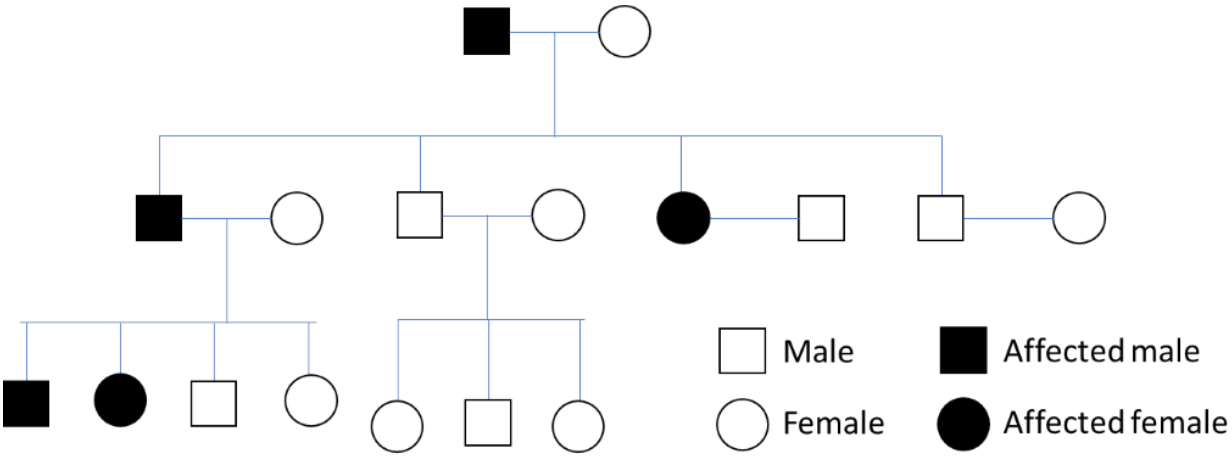

Figure 2.2.1. Huntington's disease is inherited in an autosomal dominant pattern.

2.2.2 The three stages of Huntington's disease

Huntington's disease can be broken down into three stages. In early stage Huntington's disease, patients experience slight changes in motor function, coordination, and mood.[12] At this stage, antidepressants are often prescribed to combat depression.[2] In the middle stage of the disease, choreic movements, control over speech, and difficulty swallowing become more pronounced. In late stage Huntington's disease, patients become unable to walk or speak, although their comprehension of surroundings does not diminish.[2, 11] At this stage, patients are at risk for pneumonia due to lack of control over esophageal muscles, which is the number one cause of death in patients with Huntington's disease.[2, 11]

2.2.3 Psychiatric aspects of Huntington's disease

Huntington's disease affects not just motor control, but also results in a variety of psychiatric symptoms. These include major depression,[13] anxiety and irritability, apathy, and obsessive compulsive disorder.[7] The prevalence of depressed mood in Huntington's disease patients was found to range from 33% to 69% by different studies.[4-5, 14] Suicide is the second leading cause of death in Huntington's patients, and the prevalence of suicide in Huntington's patients is four to

eight-fold greater than in the general population.[15] Similarly, anxiety ranged from 17-61% and irritability varied as well (35-73%).[5, 14, 16] Obsessive compulsive disorder and psychosis were less common; both are estimated to have a prevalence of less than 20 percent.[6, 17]

2.2.4 Prognosis and therapies for Huntington's patients

Thus far, therapies for Huntington's patients remain limited. There is no cure for Huntington's Disease. However, drugs such as tetrabenazine,[18] deutetrabenazine,[19] benzodiazapines,[20] and pridopidine[21] are given to ameliorate motor symptoms or delay their onset. In the case of the psychiatric aspects of the disease, selective serotonin reuptake inhibitors and antipsychotic drugs are given.[20, 22] Recent advances in surgical options such as stem cell implantation have also shown promise in treating chorea in Huntington's Disease patients.[23-24] In addition to pharmacological intervention, some success has been had with homeopathic medicine,[25] physical therapy,[26] music therapy,[27] diet, and exercise[8, 28-29] regimens in patients with Huntington's disease.

2.2.5 A summary of current Huntington's models

Before genetically manipulated models were readily available, researchers used chemicals, such as quinolinic acid,[30] 3-nitropropionic acid,[31] and malonate[32] to create legions in the striatal brain tissue in rats, mimicking the pathology of Huntington's Disease. These chemical models have a number of disadvantages, including the acute nature of the lesions. Furthermore, these models do not affect the other regions of the brain, where the Huntington protein is also expressed.[33]

Several mutant rodent models of Huntington's disease have been developed, including truncated N-terminal fragment models and full-length knock-in models. The truncated models typically have a fragment of the human *HTT* or a fragment of either rat or mouse *HTT*, including

the R6/1 and R6/2 mouse models[34] and the tgHD rat model.[35] Several knock-in models containing the full-length human *HTT* also exist, as well as several transgenic models containing the full-length human *HTT*, such as the YAC-18, YAC-46, and YAC-72 mouse models.[33-34]

2.2.6 R6/1 and R6/2 Huntington's Disease models

This work makes use of the R6/1 and R6/2 Huntington's disease model mice, both of which are truncated fragment models. Both models contain 67 amino acids of the human *HTT* on IT15 promoter. However, the R6/2 mouse contains 144 CAG repeats, whereas the R6/1 model only contains 116 repeats. In R6/2 mice, motor deficits can be observed as early as 5-6 weeks of age, while R6/1 model mice do not develop the overt motor phenotype until about 15 weeks of age. In mice displaying the overt motor phenotype, clasping, tremor, impaired gait, and choreic movements can be observed.[34]

2.2.7 Serotonin

Serotonin has been thought to be involved in depression because of the usefulness of serotonin reuptake inhibitors in treating this condition.[36] However, the initial monoamine hypothesis—that decreased levels of serotonin cause depression—has proven to be overly simplistic.[37] A newer theory suggests that the interplay between external factors and genetics may be a better predictor of depression. In this area, much attention has been given to the serotonin transporter gene; a polymorphism on this gene can cause increase sensitivity to stress. Therefore, external stressors could be more likely to lead to depression in individuals carrying the polymorphism on the serotonin transporter gene.[38]

In this work, serotonin release is measured in the dorsal raphe nucleus and the substantia nigra pars reticulata. The substantia nigra pars reticulata receives input from the dorsal raphe

nucleus, where serotonin is synthesized. The dorsal raphe nucleus contains about 50% serotonergic neurons, and has the highest concentration of serotonergic neurons in the brain.[39] The substantia nigra pars reticulata has been found to be involved in motor control and movement disorders,[40-45] while the dorsal raphe nucleus appears to be important in depression and neuroplasticity.[46-47]

2.2.8 Previous work in Huntington's disease model rodents

Alterations in the dopaminergic neurotransmission in multiple rodent models of Huntington's disease models have been found using electrophysiology,[48-49] voltammetry,[31, 50-52] and microdialysis.[53-54] With respect to serotonin, less work has been done in Huntington's disease models. However, inhibition of tryptophan hydroxylase, the rate-limiting enzyme in serotonin synthesis, was found in R6/2 model mice.[55] Another study showed that both overall tissue levels of serotonin and serotonin 5HT2A receptor function were decreased in R6/2 model mice.[56] Furthermore, one study found altered serotonin receptor expression to be correlated with depressive behavior in R6/1 model mice,[57] and another group successfully decreased depressive symptoms in R6/2 model mice with sertraline, a selective serotonin reuptake inhibitor.[58]

2.2.9 This work

Fast-scan cyclic voltammetry is an electrochemical technique with great selectivity, as well as spatial and temporal resolution. This allows for measurements in real-time in live tissues and for determination of serotonin release measurements in response to stimuli. In this work, serotonin release measurements in the substantia nigra in R6/2 and R6/1 Huntington's Disease model mice will be discussed.

2.3 EXPERIMENTAL PROCEDURES

2.3.1 Animals

R6/2 and R6/1 Huntington's Disease model mice, and their respective wild-type control mice were obtained from The Jackson Laboratory (Bar Harbor, ME). These mice were received at approximately 5 weeks old. For the initial study of serotonin release in the substantia nigra pars reticulata of R6/2 model mice, were aged to two experimental groups: 8 weeks and 12 weeks. For the study of serotonin release in the dorsal raphe of R6/2 model mice, mice were aged to 12 weeks. For the study of serotonin release in the dorsal raphe of R6/1 model mice, mice were aged to 18 weeks. Mice were housed in the University of Kansas Animal Care Unit (ACU). The temperature and humidity were regulated (70 ± 2ºC, and 50% ± 25%, respectively). Mice were kept in a 12 h light/dark cycle, with unrestricted access to food and water.

2.3.2 Brain slices

Substantia nigra brain slices were prepared as previously described.[50-52]. Immediately following anesthetization, mice were decapitated and the brain was removed. The extracted brain was then placed in an ice bath of artificial cerebrospinal fluid (aCSF) containing 95% O_2/5%CO_2, 126 mM NaCl, 22 mM HEPES, 1.6 mM NaH_2PO_4, 2.5 mM KCl, 25 mM $NaHCO_3$, 2.4 mM $CaCl_2$, 1.2 mM $MgCl_2$, and 11 mM D-glucose, adjusted to a pH of 7.4. After removal of the cerebellum with a razorblade, the brain was superglued with all purpose Krazy glue (Elmer's Products, Westerville, OH, USA) to the slice platform and supported by a 1 cm^3 block of agarose gel for slicing. The slice platform was then submerged in an ice bath of aCSF. A Leica VT1000 S vibrating-blade microtome (Leica Microsystems, Nussloch, Germany) was used to obtain coronal slices of 300 um thickness. Slices were placed in a perfusion chamber. Slices were

perfused with aCSF at a flow rate of 1 mL/min and kept at a temperature of 34° C. An equilibration time of 60 min was allowed before measurements were obtained.

2.3.3 Drug

In order to confirm the measurement of serotonin, fluoxetine, a selective serotonin reuptake inhibitor, was used. Fluoxetine was obtained from Sigma-Aldrich, St. Louis, MO, USA. Prior to drug application, a stable serotonin signal was established. Fluoxetine was dissolved in a stock solution of water. Then, the stock was added to the aCSF perfusing over the slice at a concentration of 2 µM.

2.3.4 Electrode fabrication

Carbon-fiber microelectrodes were fabricated as previously described.[50-52, 59] Glass capillaries (1.2 mm outer diameter, 4 inch-long A-M Systems, Inc. Carlsborg, WA, USA) were threaded with 7 µm diameter carbon fibers (Goodfellow, Huntingdon, UK). The capillaries were then heated and pulled with a PE-22 heated coil puller (Narishige Int. USA, East Meadow, NY),. The carbon fiber was cut to a length of 30 µm from the glass tip. Electrode tips were sealed with epoxy (EPON resin 815 C, EPIKURE 3234 curing agent, Miller-Stephenson, Danbury, CT, USA). Electrodes were cured for 1 h at 100 ºC.

Prior to serotonin measurements, the electrodes were coated with Nafion by electrodeposition using a method adapted from Robinson et al.[60] The electrode tips were soaked in isopropyl alcohol for 30 min. A 0.5 M potassium acetate solution was used to backfill electrodes in order to allow the carbon fiber to conduct to a silver wire inserted in the back of the electrode. The electrode was then lowered such that the tip was immersed in Nafion solution (Nafion perfluorinated ion-exchange resin, 5 wt. % solution in a mixture of lower aliphatic alcohols and

water, Sigma-Aldrich, St. Louis, MO, USA). A constant potential of +1.0 V vs. Ag/AgCl was then applied for 30 s, and the electrode was cured for 10 min at 70 ºC. Electrodes were stored for up to 1 week until use.

2.3.5 Electrochemistry

Electrodes were calibrated before and after experiments by collecting measurements for known concentrations of serotonin in a flow cell. Stimulation electrodes were fabricated by gluing two stainless steel electrodes (A-M Systems Inc., Carlsborg, WA, USA) and controlling the distance between them (200 um) with heat shrink (3 M Electronics, Austin, TX). Electrochemical measurements were obtained using a Dagan Chem-Clamp Voltammetric Amperometric Amplifier (Dagan Corporation, Minneapolis, MN, USA), which was interfaced with a computer by a breakout box. Software written by M. L. A. V. Heien and R. M. Wightman (Department of Chemistry, University of North Carolina, Chapel Hill, NC, USA) was used to analyze stimulated serotonin release plots.

Carbon fiber microelectrodes were inserted 100 µm into brain slices, directly between the two stimulating electrodes in the substantia nigra. Serotonin release was then evoked by the application of 20 biphasic electrical pulses (4 ms long, 350 µA current) at 50 Hz. In order to detect serotonin, a modified triangular waveform of +0.2 V to +1.0 V down to -0.1 V and back up to +0.2 V at a scan rate of 800 V/s was used.[61] A Ag/AgCl reference electrode was used. Peak currents after stimulation were background-subtracted, and cyclic voltammograms characteristic of serotonin were observed.

2.3.6 Statistical analyses

For the R6/2 SNr study, statistical analyses were performed using a two-way ANOVA in GraphPad Prism 6.0 ($p < 0.005$). Values were expressed as averages ± SEM; $n = 6$ to 9 mice. For the R6/2 dorsal raphe study, statistical analysis were performed using a t-test; n = 4 mice, $p < 0.05$. For the R6/1 dorsal raphe study, statistical analysis was performed using a t-test; n = 5 mice.

2.4 RESULTS AND DISCUSSION

2.4.1 Confirmation of serotonin release

Serotonin release in brain slices was confirmed by addition of fluoxetine, a selective serotonin reuptake inhibitor. Fluoxetine (10 µM) was added to the aCSF perfusate. Figure 2.4.1 shows representative data collected in the substantia nigra pars reticulata confirming serotonin release. On the left, a representative current vs. time plot, serotonin cyclic voltammogram, and color plot is shown for a file obtained before the addition of any drug to the perfusate. On the right is a current vs. time plot, cyclic voltammogram, and color plot obtained 15 min after the addition of 10 µM fluoxetine to the perfusate. In these color plots, which consist of a series of cyclic voltammograms unfolded, rotated, and stacked over time, potential is plotted on the *y*-axis, time is on the *x*-axis, and current is encoded in false color representing the *z*-axis. Horizontal dashed lines on the color plots indicate the potential from which the representative current vs. time plots were extracted, while vertical dashed lines indicate the times from which the representative cyclic voltammograms were extracted. Here, serotonin release was stimulated by 20 biphasic 4-ms 350µA electrical pulses at 50 Hz. Electrical stimulation occurred at 5 s. Immediately following electrical stimulation, a peak occurs on the representative current vs. time plots; the

extracted cyclic voltammogram at this time is characteristic of serotonin. After adding fluoxetine, a selective serotonin reuptake inhibitor, serotonin reuptake was inhibited, as evidenced by the current not returning to baseline and the increase in maximum current due to serotonin release.

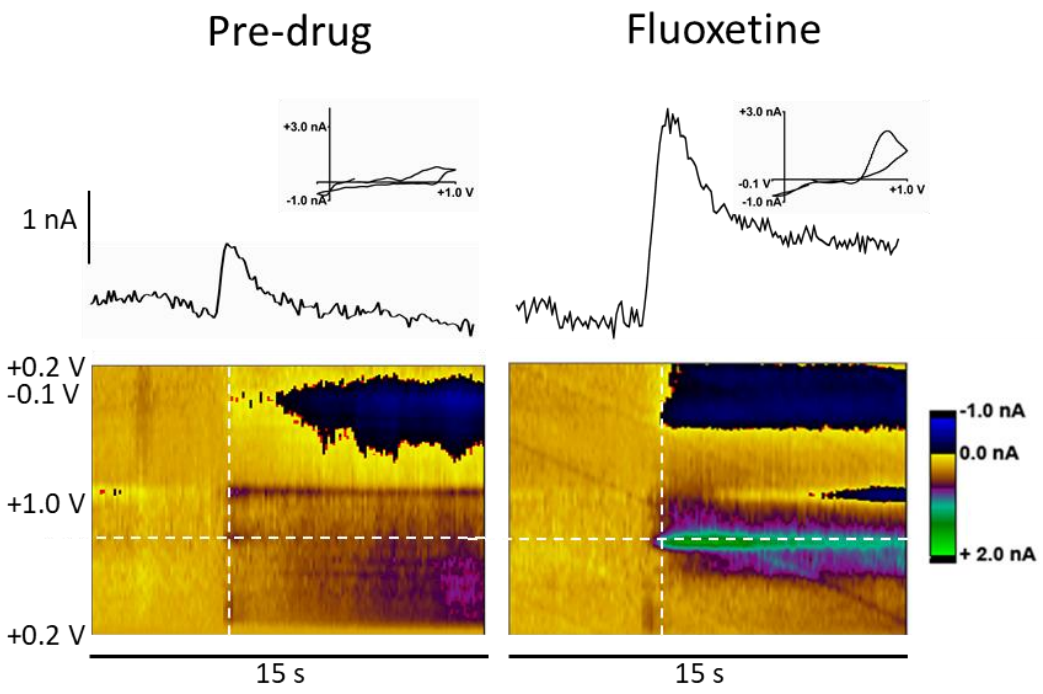

Figure 2.4.1. Serotonin release is confirmed by perfusing 10 µM fluoxetine over the brain slice. Left: current vs. time plot, representative serotonin cyclic voltammogram, and color plot obtained from substantia nigra pars reticulata brain slice before adding any drug to the perfusate. Right: current vs. time plot, serotonin cyclic voltammogram, and color plot after addition of 10 µM fluoxetine to the perfusate. Horizontal dashed lines represent potential from which each current vs. time plot was extracted; vertical dashed lines represent time from which each respective cyclic voltammogram was extracted.

2.4.2 Serotonin release is diminished in the substantia nigra pars reticulata in an age-dependent manner

For this study, serotonin release was measured in the substantia nigra, pars reticulata (SNr) in R6/2 model mice. A carbon fiber microelectrode was placed between two stimulating electrodes in a 350-µm thick brain slice containing SNr tissue at a depth of 100-µm. Serotonin release was evoked by applying 20 biphasic 350-µA electrical pulses at 50 Hz at the stimulating electrodes. Figure 2.4.2A shows representative data from both wild-type and R6/2 mice.

First, measurements were recorded in 8-week old R6/2 model mice and their age-matched wild-type controls. Serotonin release was diminished to 41.0±5.0% of the controls (two-way ANOVA; N=5 R6/2 and 5 wild-type; Sidak's multiple comparisons test, $p<0.01$). Considering the progressive nature of Huntington's disease, we sought to determine whether there was an age-dependent effect. Therefore, we obtained serotonin release measurements in 12-week old R6/2 model mice and their age matched controls. Our results, depicted in Figure 2.4.2B, show that serotonin release was further diminished at 12 weeks to 15.9±2.5% of the controls (two-way ANOVA; N=5 R6/2 and 5 wild-type; Sidak's multiple comparisons test, $p<0.001$), suggesting an age-dependent effect. Age was determined to have a significant effect on serotonin release (two-way ANOVA, $p<0.05$).

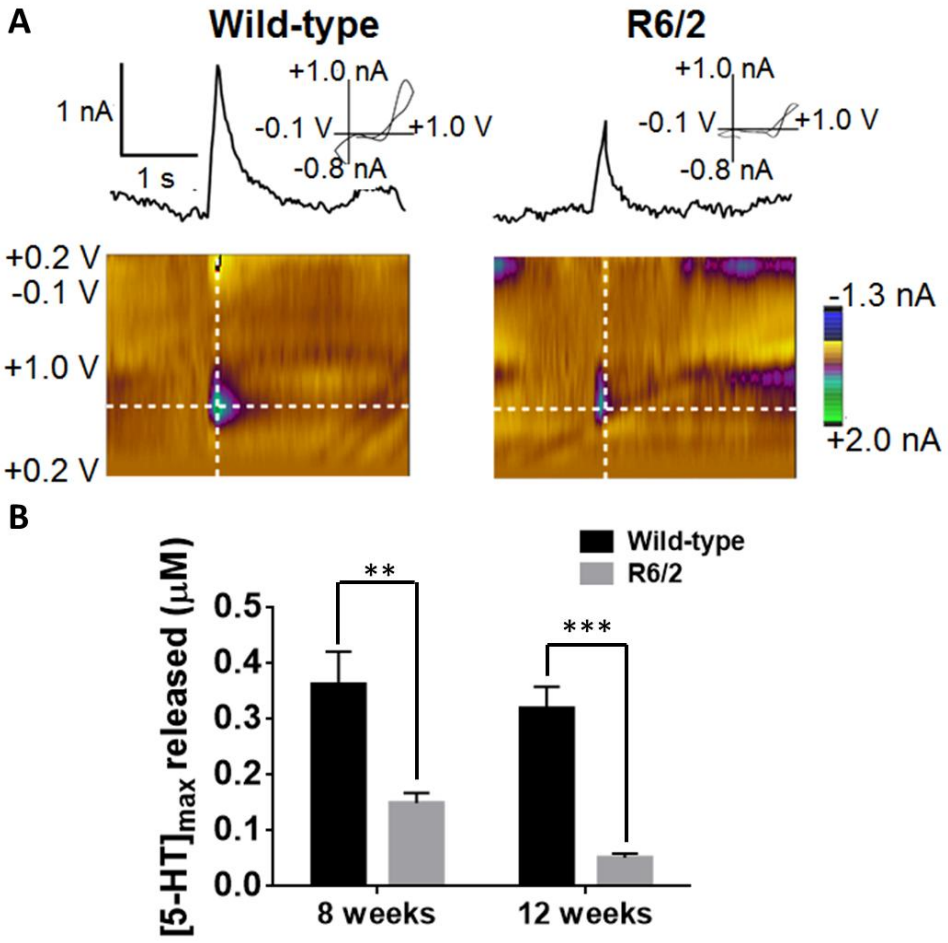

Figure 2.4.2. (A) Representative color plots, current traces, and CVs collected from the substantia nigra, pars reticulata in wild-type and R6/2 model mice, respectively. Horizontal dashed lines indicate the potential from which each current vs. time plot was extracted; vertical dashed lines show the time from which each cyclic voltammogram was obtained. Representative cyclic voltammograms are characteristic of serotonin, confirming serotonin release. (B) Average concentrations of maximum serotonin released shown at 8 and 12 weeks for both R6/2 and wild-type controls. Error bars are SEM. N = 5 R6/2 and 5 wild-type mice for both 8- and 12-week groups; two-way ANOVA, $p<0.01$ for 8 weeks, $p<0.001$ for 12 weeks.

2.4.3 Serotonin release is decreased in both the dorsal raphe and substantia nigra regions of the brain

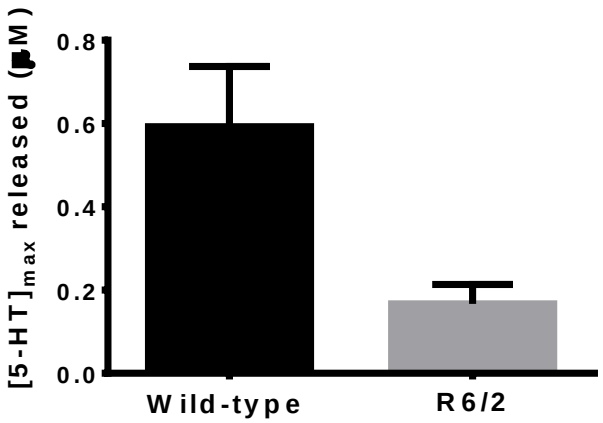

Figure 2.4.3. Average concentrations of maximum serotonin release in the dorsal raphe of WT and R6/2 mice. Mice were 12 weeks old. ($p<0.05$, paired t-test, N = 5 WT and 5 R^/2 mice)

After determining that serotonin release was decreased in the SNr of R6/2 model mice, we decided to perform further experiments to discern whether release was also decreased in the dorsal raphe (DR). Figure 2.4.3 shows the results of those experiments; serotonin release was found to be decreased by 28.2±7.9% in 12-week old R6/2 model mice compared to the age-matched wild-type controls. These data suggest that release impairments may be generalized throughout the entire brain. Furthermore, as the dorsal raphe is implicated in mood disorders, serotonin release dysfunction could play some role in depression and anxiety in Huntington's disease.

2.4.4 Decreased serotonin release in the dorsal raphe is conserved across multiple mouse models

Upon finding that serotonin release is decreased in multiple regions of the brain in R6/2 model mice, we performed further studies to determine if this effect was conserved across multiple models of Huntington's disease. Thus, we obtained measurements of serotonin release using the same methods in the DR of a different mouse model, the R6/1 Huntington's Disease model. Figure 2.4.3 shows that in 18-week old R6/1 model mice, serotonin release was decreased to 66.8±10.9% of release in the age-matched wild-type controls.

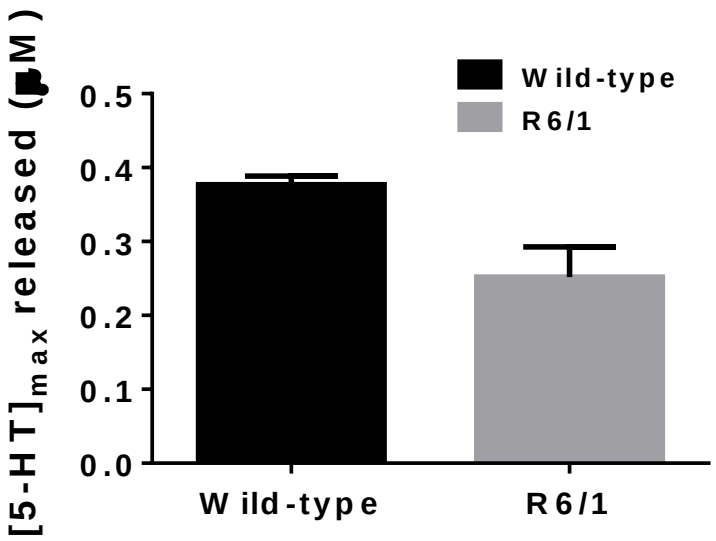

Figure 2.4.3. Average concentrations of serotonin released in the dorsal raphe of WT and R6/1 mice. These data were collected from current vs. time plots. Mice were 12 weeks old. ($p<0.05$, paired t test, N = 5 WT and 5 R6/1)

To our knowledge, this is the first time serotonin release has be measured in Huntington's disease model mice using fast-scan cyclic voltammetry. After confirming serotonin release, we

were able to quantify serotonin release in the substantia nigra pars reticulata and the dorsal raphe of R6/2 model mice, as well as the dorsal raphe of R6/1 model mice.

Previous work shows that dopamine release in brain slices is impaired in R6/2 and R6/1 model mice.[50-51] Our work builds on this and suggests that release impairments may be persistent throughout the entire brain. Moreover, it shows that release impairments throughout the brain are conserved across different mouse models of Huntington's disease. Furthermore, our results show that neurotransmitter release throughout the brain is affected in an age-dependent manner.

There is evidence that depressive symptoms in Huntington's disease model mice could be related to serotonin dysfunction.[56-58, 62] Our work here shows that serotonin release is diminished in the dorsal raphe of both R6/1 and R6/2 model mice. As this brain region is thought to be involved in mood disorders such as depression,[46] a decrease in serotonin release in the dorsal raphe could be a contributing factor to depression in Huntington's disease.

Interestingly, serotonin release was decreased in two different regions of the brain in R6/2 model mice. In the past, alterations in dopamine release have been found in the striatum.[50-52] Since release in multiple neurotransmitter systems is attenuated, it is possible that this decrease in release occurs due to similar mechanisms.

2.5 CONCLUSIONS

Taken together, this work suggests a global decrease in release and raises the possibility of a common mechanism. Additionally, a robust effect is conserved across multiple models. Furthermore, it implies that regions of the brain other than the striatum ought to be given more attention with respect to Huntington's disease, given the roles of the DR and SNr in both mood and motor control.

2.6 REFERENCES

1. Group, T. H. s. D. C. R., A novel gene containing a trinucleotide repeat that is expanded and unstable on Huntington's disease chromosomes. *Cell* **1993,** *72* (6), 971-83.

2. Walker, F. O., Huntington's disease. *The Lancet* **2007,** *369* (9557), 218-228.

3. Huntington, G., On Chorea. *Medical and Surgical Reporter* **1872**, 320-321.

4. Nehl, C.; Ready, R. E.; Hamilton, J.; Paulsen, J. S., Effects of depression on working memory in presymptomatic Huntington's disease. *J Neuropsychiatry Clin Neurosci* **2001,** *13* (3), 342-6.

5. Paulsen, J. S.; Ready, R. E.; Hamilton, J. M.; Mega, M. S.; Cummings, J. L., Neuropsychiatric aspects of Huntington's disease. *J Neurol Neurosurg Psychiatry* **2001,** *71* (3), 310-4.

6. Julien, C. L.; Thompson, J. C.; Wild, S.; Yardumian, P.; Snowden, J. S.; Turner, G.; Craufurd, D., Psychiatric disorders in preclinical Huntington's disease. *J Neurol Neurosurg Psychiatry* **2007,** *78* (9), 939-43.

7. van Duijn, E.; Kingma, E. M.; van der Mast, R. C., Psychopathology in verified Huntington's disease gene carriers. *J Neuropsychiatry Clin Neurosci* **2007,** *19* (4), 441-8.

8. Ho, A. K.; Gilbert, A. S.; Mason, S. L.; Goodman, A. O.; Barker, R. A., Health-related quality of life in Huntington's disease: Which factors matter most? *Mov Disord* **2009,** *24* (4), 574-8.

9. Lanska, D. J., George Huntington (1850-1916) and hereditary chorea. *Journal of the history of the neurosciences* **2000,** *9* (1), 76-89.

10. Mendel, G., Gregor Mendel's letters to Carl Nageli, 1866-1873. *Genetics* **1950,** *35* (5 2), 1-29.

11. Roos, R. A., Huntington's disease: a clinical review. *Orphanet journal of rare diseases* **2010,** *5*, 40.

12. Wyant, K. J.; Ridder, A. J.; Dayalu, P., Huntington's Disease-Update on Treatments. *Current neurology and neuroscience reports* **2017,** *17* (4), 33.

13. Leroi, I.; O'Hearn, E.; Marsh, L.; Lyketsos, C. G.; Rosenblatt, A.; Ross, C. A.; Brandt, J.; Margolis, R. L., Psychopathology in patients with degenerative cerebellar diseases: a comparison to Huntington's disease. *The American journal of psychiatry* **2002,** *159* (8), 1306-14.

14. Litvan, I.; Paulsen, J. S.; Mega, M. S.; Cummings, J. L., Neuropsychiatric assessment of patients with hyperkinetic and hypokinetic movement disorders. *Arch Neurol* **1998,** *55* (10), 1313-9.

15. Hubers, A. A. M.; Reedeker, N.; Giltay, E. J.; Roos, R. A. C.; van Duijn, E.; van der Mast, R. C., Suicidality in Huntington's disease. *Journal of Affective Disorders* **2012,** *136* (3), 550-557.

16. Kulisevsky, J.; Litvan, I.; Berthier, M. L.; Pascual-Sedano, B.; Paulsen, J. S.; Cummings, J. L., Neuropsychiatric assessment of Gilles de la Tourette patients: comparative study with other hyperkinetic and hypokinetic movement disorders. *Mov Disord* **2001,** *16* (6), 1098-104.

17. Craufurd, D.; Thompson, J. C.; Snowden, J. S., Behavioral changes in Huntington Disease. *Neuropsychiatry Neuropsychol Behav Neurol* **2001,** *14* (4), 219-26.

18. Kegelmeyer, D. A.; Kloos, A. D.; Fritz, N. E.; Fiumedora, M. M.; White, S. E.; Kostyk, S. K., Impact of tetrabenazine on gait and functional mobility in individuals with Huntington's disease. *Journal of the neurological sciences* **2014,** *347* (1-2), 219-23.

19. Frank, S.; Testa, C. M.; Stamler, D.; Kayson, E.; Davis, C.; Edmondson, M. C.; Kinel, S.; Leavitt, B.; Oakes, D.; O'Neill, C.; Vaughan, C.; Goldstein, J.; Herzog, M.; Snively, V.; Whaley, J.; Wong, C.; Suter, G.; Jankovic, J.; Jimenez-Shahed, J.; Hunter, C.; Claassen, D. O.; Roman, O. C.; Sung, V.; Smith, J.; Janicki, S.; Clouse, R.; Saint-Hilaire, M.; Hohler, A.; Turpin, D.; James, R. C.; Rodriguez, R.; Rizer, K.; Anderson, K. E.; Heller, H.; Carlson, A.; Criswell, S.; Racette, B. A.; Revilla, F. J.; Nucifora, F., Jr.; Margolis, R. L.; Ong, M.; Mendis, T.; Mendis, N.; Singer, C.; Quesada, M.; Paulsen, J. S.; Brashers-Krug, T.; Miller, A.; Kerr, J.; Dubinsky, R. M.; Gray, C.; Factor, S. A.; Sperin, E.; Molho, E.; Eglow, M.; Evans, S.; Kumar, R.; Reeves, C.; Samii, A.; Chouinard, S.; Beland, M.; Scott, B. L.; Hickey, P. T.; Esmail, S.; Fung, W. L.; Gibbons, C.; Qi, L.; Colcher, A.; Hackmyer, C.; McGarry, A.; Klos, K.; Gudesblatt, M.; Fafard, L.; Graffitti, L.; Schneider, D. P.; Dhall, R.; Wojcieszek, J. M.; LaFaver, K.; Duker, A.; Neefus, E.; Wilson-Perez, H.; Shprecher, D.; Wall, P.; Blindauer, K. A.; Wheeler, L.; Boyd, J. T.; Houston, E.; Farbman, E. S.; Agarwal, P.; Eberly, S. W.; Watts, A.; Tariot, P. N.; Feigin, A.; Evans, S.; Beck, C.; Orme, C.; Edicola, J.; Christopher, E., Effect of Deutetrabenazine on Chorea Among Patients With Huntington Disease: A Randomized Clinical Trial. *Jama* **2016,** *316* (1), 40-50.

20. Burgunder, J.-M.; Guttman, M.; Perlman, S.; Goodman, N.; van Kammen, D. P.; Goodman, L., An International Survey-based Algorithm for the Pharmacologic Treatment of Chorea in Huntington's Disease. *PLoS Currents* **2011,** *3,* RRN1260.

21. Lundin, A.; Dietrichs, E.; Haghighi, S.; Goller, M. L.; Heiberg, A.; Loutfi, G.; Widner, H.; Wiktorin, K.; Wiklund, L.; Svenningsson, A.; Sonesson, C.; Waters, N.; Waters, S.; Tedroff, J., Efficacy and safety of the dopaminergic stabilizer Pridopidine (ACR16) in patients with Huntington's disease. *Clinical neuropharmacology* **2010,** *33* (5), 260-4.

22. Zielonka, D.; Mielcarek, M.; Landwehrmeyer, G. B., Update on Huntington's disease: advances in care and emerging therapeutic options. *Parkinsonism & related disorders* **2015,** *21* (3), 169-178.

23. McBride, J. L.; Behrstock, S. P.; Chen, E. Y.; Jakel, R. J.; Siegel, I.; Svendsen, C. N.; Kordower, J. H., Human neural stem cell transplants improve motor function in a rat model of Huntington's disease. *J Comp Neurol* **2004,** *475* (2), 211-9.

24. Dunnett, S. B.; Rosser, A. E., Stem cell transplantation for Huntington's disease. *Exp Neurol* **2007,** *203* (2), 279-92.

25. Law, B. Y.; Wu, A. G.; Wang, M.; Zhu, Y. Z., Chinese Medicine: A Hope for Neurodegenerative Diseases? *Journal of Alzheimer's disease : JAD* **2017**.

26. Quinn, L.; Busse, M.; Carrier, J.; Fritz, N.; Harden, J.; Hartel, L.; Kegelmeyer, D.; Kloos, A.; Rao, A., Physical therapy and exercise interventions in Huntington's disease: a mixed methods systematic review protocol. *JBI database of systematic reviews and implementation reports* **2017,** *15* (7), 1783-1799.

27. van Bruggen-Rufi, M.; Vink, A.; Achterberg, W.; Roos, R., Music therapy in Huntington's disease: a protocol for a multi-center randomized controlled trial. *BMC psychology* **2016,** *4* (1), 38.

28. Frese, S.; Petersen, J. A.; Ligon-Auer, M.; Mueller, S. M.; Mihaylova, V.; Gehrig, S. M.; Kana, V.; Rushing, E. J.; Unterburger, E.; Kagi, G.; Burgunder, J. M.; Toigo, M.; Jung, H. H., Exercise effects in Huntington disease. *J Neurol* **2017,** *264* (1), 32-39.

29. Quinn, L.; Trubey, R.; Gobat, N.; Dawes, H.; Edwards, R. T.; Jones, C.; Townson, J.; Drew, C.; Kelson, M.; Poile, V.; Rosser, A.; Hood, K.; Busse, M., Development and Delivery of

a Physical Activity Intervention for People With Huntington Disease: Facilitating Translation to Clinical Practice. *Journal of neurologic physical therapy : JNPT* **2016,** *40* (2), 71-80.

30. Gianfriddo, M.; Corsi, C.; Melani, A.; Pèzzola, A.; Reggio, R.; Popoli, P.; Pedata, F., Adenosine A2A antagonism increases striatal glutamate outflow in the quinolinic acid rat model of Huntington's disease. *Brain Research* **2003,** *979* (1-2), 225-229.

31. Kraft, J. C.; Osterhaus, G. L.; Ortiz, A. N.; Garris, P. A.; Johnson, M. A., In vivo dopamine release and uptake impairments in rats treated with 3-nitropropionic acid. *Neuroscience* **2009,** *161* (3), 940-9.

32. Valdeolivas, S.; Satta, V.; Pertwee, R. G.; Fernandez-Ruiz, J.; Sagredo, O., Sativex-like combination of phytocannabinoids is neuroprotective in malonate-lesioned rats, an inflammatory model of Huntington's disease: role of CB1 and CB2 receptors. *ACS chemical neuroscience* **2012,** *3* (5), 400-6.

33. Pouladi, M. A.; Morton, A. J.; Hayden, M. R., Choosing an animal model for the study of Huntington's disease. *Nat Rev Neurosci* **2013,** *14* (10), 708-721.

34. Menalled, L. B.; Chesselet, M. F., Mouse models of Huntington's disease. *Trends Pharmacol Sci* **2002,** *23* (1), 32-9.

35. von Horsten, S.; Schmitt, I.; Nguyen, H. P.; Holzmann, C.; Schmidt, T.; Walther, T.; Bader, M.; Pabst, R.; Kobbe, P.; Krotova, J.; Stiller, D.; Kask, A.; Vaarmann, A.; Rathke-Hartlieb, S.; Schulz, J. B.; Grasshoff, U.; Bauer, I.; Vieira-Saecker, A. M. M.; Paul, M.; Jones, L.; Lindenberg, K. S.; Landwehrmeyer, B.; Bauer, A.; Li, X. J.; Riess, O., Transgenic rat model of Huntington's disease. *Human Molecular Genetics* **2003,** *12* (6), 617-624.

36. aan het Rot, M.; Mathew, S. J.; Charney, D. S., Neurobiological mechanisms in major depressive disorder. *Can. Med. Assoc. J.* **2009,** *180* (3), 305-313.

37. Hirschfeld, R. M., History and evolution of the monoamine hypothesis of depression. *The Journal of clinical psychiatry* **2000,** *61 Suppl 6*, 4-6.

38. Charney, D. S.; Manji, H. K., Life stress, genes, and depression: multiple pathways lead to increased risk and new opportunities for intervention. *Science's STKE : signal transduction knowledge environment* **2004,** *2004* (225), re5.

39. Frazer, A.; Hensler, J., Serotonin. In *Basic Neurochemistry: Molecular, Cellular and Medical Aspects.* , 6th ed.; Siegel, G.; Agranoff, B.; Albers, R., Eds. Lippincott-Raven: Philadelphia, 1999.

40. Castro, M. E.; Pascual, J.; Romon, T.; Berciano, J.; Figols, J.; Pazos, A., 5-HT1B receptor binding in degenerative movement disorders. *Brain Res* **1998,** *790* (1-2), 323-8.

41. Threlfell, S.; Greenfield, S. A.; Cragg, S. J., 5-HT(1B) receptor regulation of serotonin (5-HT) release by endogenous 5-HT in the substantia nigra. *Neuroscience* **2010,** *165* (1), 212-20.

42. Lehericy, S.; Bardinet, E.; Poupon, C.; Vidailhet, M.; Francois, C., 7 Tesla magnetic resonance imaging: a closer look at substantia nigra anatomy in Parkinson's disease. *Movement disorders : official journal of the Movement Disorder Society* **2014,** *29* (13), 1574-81.

43. Broadstock, M.; Austin, P. J.; Betts, M. J.; Duty, S., Antiparkinsonian potential of targeting group III metabotropic glutamate receptor subtypes in the rodent substantia nigra pars reticulata. *British journal of pharmacology* **2012,** *165* (4b), 1034-45.

44. Lobb, C. J.; Jaeger, D., Bursting activity of substantia nigra pars reticulata neurons in mouse parkinsonism in awake and anesthetized states. *Neurobiol Dis* **2015,** *75*, 177-85.

45. Jahanshahi, A.; Vlamings, R.; van Roon-Mom, W. M. C.; Faull, R. L. M.; Waldvogel, H. J.; Janssen, M. L. F.; Yakkioui, Y.; Zeef, D. H.; Kocabicak, E.; Steinbusch, H. W. M.; Temel, Y.,

Changes in brainstem serotonergic and dopaminergic cell populations in experimental and clinical Huntington's disease. *Neuroscience* **2013,** *238*, 71-81.

46. Michelsen, K. A.; Prickaerts, J.; Steinbusch, H. W., The dorsal raphe nucleus and serotonin: implications for neuroplasticity linked to major depression and Alzheimer's disease. *Progress in brain research* **2008,** *172*, 233-64.

47. Hendricksen, M.; Thomas, A. J.; Ferrier, I. N.; Ince, P.; O'Brien, J. T., Neuropathological study of the dorsal raphe nuclei in late-life depression and Alzheimer's disease with and without depression. *The American journal of psychiatry* **2004,** *161* (6), 1096-102.

48. Dallerac, G. M.; Vatsavayai, S. C.; Cummings, D. M.; Milnerwood, A. J.; Peddie, C. J.; Evans, K. A.; Walters, S. W.; Rezaie, P.; Hirst, M. C.; Murphy, K. P., Impaired long-term potentiation in the prefrontal cortex of Huntington's disease mouse models: rescue by D1 dopamine receptor activation. *Neuro-degenerative diseases* **2011,** *8* (4), 230-9.

49. Holley, S. M.; Joshi, P. R.; Parievsky, A.; Galvan, L.; Chen, J. Y.; Fisher, Y. E.; Huynh, M. N.; Cepeda, C.; Levine, M. S., Enhanced GABAergic Inputs Contribute to Functional Alterations of Cholinergic Interneurons in the R6/2 Mouse Model of Huntington's Disease. *eNeuro* **2015,** *2* (1).

50. Johnson, M. A.; Rajan, V.; Miller, C. E.; Wightman, R. M., Dopamine release is severely compromised in the R6/2 mouse model of Huntington's disease. *J Neurochem* **2006,** *97* (3), 737-46.

51. Ortiz, A. N.; Kurth, B. J.; Osterhaus, G. L.; Johnson, M. A., Impaired dopamine release and uptake in R6/1 Huntington's disease model mice. *Neuroscience letters* **2011,** *492* (1), 11-4.

52. Ortiz, A. N.; Kurth, B. J.; Osterhaus, G. L.; Johnson, M. A., Dysregulation of intracellular dopamine stores revealed in the R6/2 mouse striatum. *J Neurochem* **2010,** *112* (3), 755-61.

53. Callahan, J. W.; Abercrombie, E. D., In vivo Dopamine Efflux is Decreased in Striatum of both Fragment (R6/2) and Full-Length (YAC128) Transgenic Mouse Models of Huntington's Disease. *Front Syst Neurosci* **2011,** *5*, 61.

54. Petersén, Å.; Puschban, Z.; Lotharius, J.; NicNiocaill, B.; Wiekop, P.; O'Connor, W. T.; Brundin, P., Evidence for Dysfunction of the Nigrostriatal Pathway in the R6/1 Line of Transgenic Huntington's Disease Mice. *Neurobiology of Disease* **2002,** *11* (1), 134-146.

55. Yohrling, I. G.; Jiang, G. C.; DeJohn, M. M.; Robertson, D. J.; Vrana, K. E.; Cha, J. H., Inhibition of tryptophan hydroxylase activity and decreased 5-HT1A receptor binding in a mouse model of Huntington's disease. *J Neurochem* **2002,** *82* (6), 1416-23.

56. Renoir, T.; Zajac, M. S.; Du, X.; Pang, T. Y.; Leang, L.; Chevarin, C.; Lanfumey, L.; Hannan, A. J., Sexually dimorphic serotonergic dysfunction in a mouse model of Huntington's disease and depression. *PLoS One* **2011,** *6* (7), e22133.

57. Pang, T. Y.; Du, X.; Zajac, M. S.; Howard, M. L.; Hannan, A. J., Altered serotonin receptor expression is associated with depression-related behavior in the R6/1 transgenic mouse model of Huntington's disease. *Hum Mol Genet* **2009,** *18* (4), 753-66.

58. Renoir, T.; Pang, T. Y.; Zajac, M. S.; Chan, G.; Du, X.; Leang, L.; Chevarin, C.; Lanfumey, L.; Hannan, A. J., Treatment of depressive-like behaviour in Huntington's disease mice by chronic sertraline and exercise. *Br J Pharmacol* **2012,** *165* (5), 1375-89.

59. Ortiz, A. N.; Osterhaus, G. L.; Lauderdale, K.; Mahoney, L.; Fowler, S. C.; von Horsten, S.; Riess, O.; Johnson, M. A., Motor function and dopamine release measurements in transgenic Huntington's disease model rats. *Brain Res* **2012,** *1450*, 148-56.

60. Robinson, D. L.; Venton, B. J.; Heien, M. L.; Wightman, R. M., Detecting subsecond dopamine release with fast-scan cyclic voltammetry in vivo. *Clin Chem* **2003,** *49* (10), 1763-73.

61. Hashemi, P.; Dankoski, E. C.; Petrovic, J.; Keithley, R. B.; Wightman, R. M., Voltammetric detection of 5-hydroxytryptamine release in the rat brain. *Anal Chem* **2009,** *81* (22), 9462-71.

62. Gill, J. S.; Jamwal, S.; Kumar, P.; Deshmukh, R., Sertraline and venlafaxine improves motor performance and neurobehavioral deficit in quinolinic acid induced Huntington's like symptoms in rats: Possible neurotransmitters modulation. *Pharmacol Rep* **2017,** *69* (2), 306-313.

3 NEUROTRANSMITTER RELEASE AND BEHAVIORAL MEASUREMENTS IN CHEMOTHERAPY-TREATED RATS

3.1 ABSTRACT

Chemobrain is a condition affecting as many of 75% of patients who have received chemotherapy treatments for cancer. As cancer survival rates improve and the population of cancer survivors grows, it is becoming more important to consider the quality of life of this population. In this work, we investigate the effect of two chemotherapeutic agents, 5-fluorouracil (5-FU) and carboplatin, on neurotransmitter release in rat brain. We also investigate a potential therapy, a heat shock protein inhibitor developed at the University of Kansas by Dr. Brian Blagg's group, KU-32. In addition to this, we have collaborated with Dr. David Jarmolowicz's group to study the effect of these treatments on cognitive behavior. We found that in rats treated with 5-FU, dopamine release was impaired, but was recovered after a recovery time of three weeks. 5-FU-treated rats also showed cognitive behavior deficits; their performance on a paradigm testing attention was decreased. Interestingly, KU-32 treatments were able to prevent this effect. We also found that in rats treated with carboplatin, serotonin release was decreased in the substantia nigra pars reticulata and the dorsal raphe nucleus. Our collaborator found that carboplatin-treated rats showed decreased performance on paradigms testing both inhibition and spatial learning. This work suggests that multiple neurotransmitter systems are affected across multiple chemotherapeutic drugs, and that these neurotransmitter measurements can be correlated with cognitive deficits. Furthermore, work suggest a potential therapy in KU-32.

3.2 INTRODUCTION

3.2.1 Chemobrain

As outcomes for cancer patients continue to improve, new challenges have arisen. Over the course of the past half-century, cancer mortality rates have decreased globally.[1] Figure 3.2.1A shows the decline in cancer mortality with the United States and Canada since 1975. A growing population of cancer survivors creates a growing need to improve the quality of life of cancer survivors post-chemotherapy. In 2013, depending on the stage of diagnosis, 55-82% of breast cancer patients received chemotherapy as part of their treatment,[2] and yet, the toxicity of chemotherapeutic agents can cause a slew of complications for patients, including severe nausea and vomiting, anemia, infertility, hair loss, fatigue, depression, and cognitive impairment.[3] Figure 3.2.1B shows the increase in interest in chemotherapy-induced cognitive impairment within the scientific community. The focus of this work is chemotherapy-induced cognitive impairment, or "chemobrain."

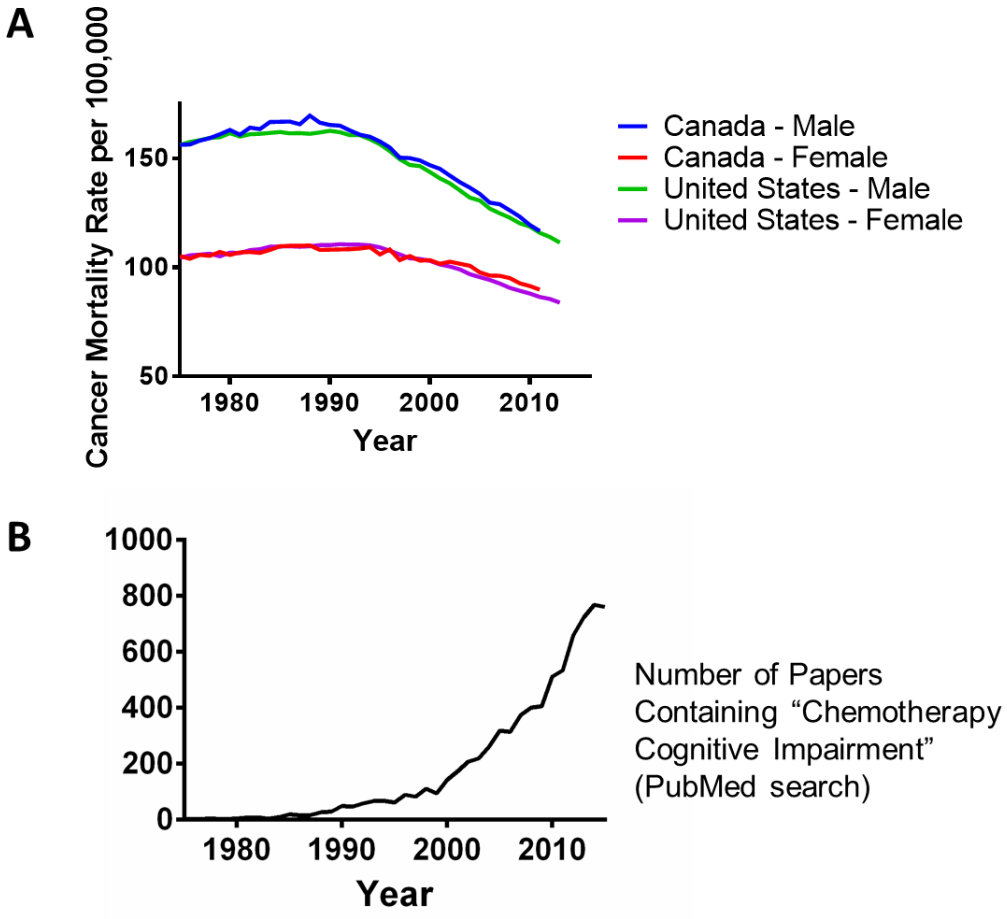

Figure 3.2.1. (A) The cancer mortality rates in the United States and Canada in the past 40 years. (World Health Organization, Department of Information, Evidence and Research, mortality database (accessed on July 20 2017)).[1] (B) Publications on cognitive impairment and chemotherapy within the same time frame (Search performed July 20 2017).

Chemobrain has been described clinically as a decline in executive function, including memory, learning, and attention span. Patients describe their symptoms as forgetfulness and lack of focus.[4] Furthermore, patients with chemobrain also experience an increased prevalence of mood disorders, including anxiety[4] and depression.[5] Estimates vary, but chemobrain may affect as many as many as 75% of patients receiving chemotherapy treatment. Due to the implications

of quality of life in a growing population, it is important to study the underlying neurological mechanisms of chemobrain as well as quantifying cognitive behavior effects associated with chemotherapy treatment.

3.2.2 5-FU

5-FU is a chemotherapy drug that has been used to treat several cancers including gastrointestinal cancer,[6] head and neck cancer,[7] colorectal cancer,[8] pancreatic cancer,[9] and breast cancer.[10-11]

5-FU acts as a thymidylate synthase inhibitor. Thymidilate synthase is an enzyme that normally methylates deoxyuridine monophosphate, forming thymidine monophosphate. Thymidine monophosphate is essential for DNA replication; therefore, 5-FU halts DNA replication and causes cell death. Figure 3.2.2 shows the structures of 5-FU and deoxyuridine monophosphate (dUMP).[12]

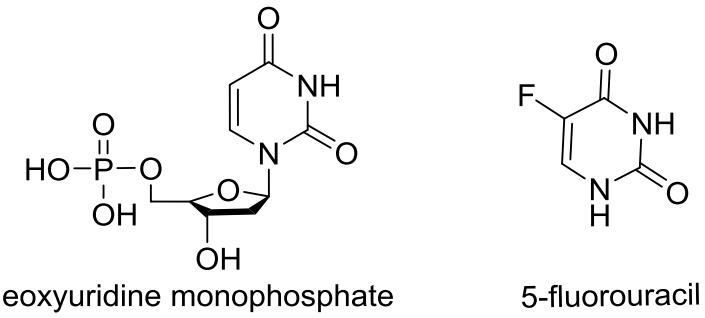

Figure 3.2.2. Structures of 5-FU and dUMP.

There is mixed evidence regarding 5-FU and chemobrain. Andreis et al. found a lack of chemobrain effect with oxaliplatin, 5-FU, and leucovorin combination treatment in colon cancer patients.[13] On the other hand, Mustafa et al. found that 5-FU affected spatial and working

memory and neurons in the adult rat hippocampus,[14] and Fardell et al. found that 5-FU and oxaliplatin treatment impaired novel object recognition and spatial reference memory.[15] Moreover, 5-FU has been shown to cross the blood brain barrier and cause destruction of myelin.[16] In this work, we investigate the effect of 5-FU treatment on dopamine release in the striatum, combined with behavioral measurements of attention and inhibition.

3.2.3 KU-32

KU-32 was used in this work as a potential therapy for chemobrain and was given to rats via oral gavage along with their 5-FU injections. KU-32 is a novel novobiocin-based heat shock protein 90 inhibitor developed at The University of Kansas by Dr. Brian Blagg's group[17] and has shown promise as a therapy for diabetic neuropathy.[18] KU-32 works by binding to heat shock protein 90, releasing heat shock factor 1, and inducing the heat shock response; heat shock proteins maintain protein homeostasis through proper folding.[19] Figure 3.2.3 shows the structure of KU-32.

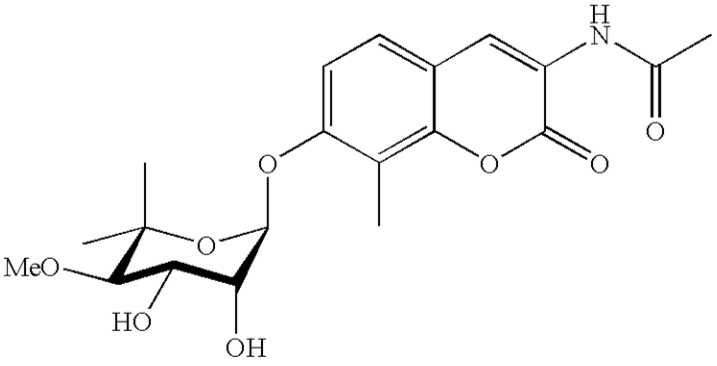

Figure 3.2.3. KU-32.

As KU-32 has shown promise in treating degeneration in the peripheral nervous system, it could prove effective in treating toxicity in the central nervous system as well. Here, we

investigate the potential of KU-32 as a therapy for chemobrain by co-administering KU-32 with 5-FU treatment.

3.2.4 Carboplatin

Carboplatin is a chemotherapeutic agent that has been used to treat a variety of cancers, including esophageal cancer,[20] neuroblastoma,[21] small-cell lung cancer,[22] cervical cancer,[23] and triple negative breast cancer.[24] In cancer patients receiving carboplatin as a single agent (i.e. not in combination with other drugs), carboplatin is typically administered by intravenous infusion once every 21 days for about six months.[25] It works by covalently binding to DNA, forming reactive platinum complexes, and causing cell death.[26-27] **Figure 3.2.4** shows the chemical structure of carboplatin.

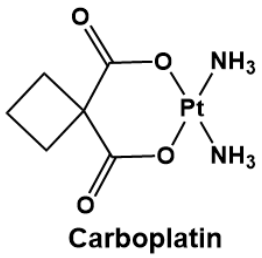

Figure 3.2.4. Carboplatin.

In humans, carboplatin has been found to cause cognitive impairment in elderly patients;[28] a combination of cyclophosphamide, methotrexate, and 5-FU has also been shown to cause cognitive impairment.[29] We wanted to investigate further the effect of carboplatin on working memory and to combine behavioral measurements with neurotransmitter release measurements. In this work, rats were treated with carboplatin by i.v. tail vein injection to study these effects.

3.2.5 Neurotransmitter release measurements in this work

Previous work has been done to elucidate mechanisms of chemobrain and investigate possible therapies.[30-31] For instance, Sara Thomas used microdialysis to measure glutamate and GABA in rats treated with 5-FU, carboplatin, or doxorubicin.[32] Biosensors have also been used to examine dopamine uptake in mice treated with doxorubicin.[33] In our lab, Kaplan et al. used fast-scan cyclic voltammetry to measure dopamine release and uptake.[34] Fast-scan cyclic voltammetry (FSCV) at carbon fiber microelectrodes is an electrochemical technique that allows measurements of neurotransmitter release to be obtained with low limits of detection and high spatial and temporal resolution. In this work, we use FSCV to investigate whether 5-FU affects dopamine release and whether changes in dopamine release caused by chemotherapy treatment correspond with cognitive deficits measured by behavioral paradigms for attention shifting, inhibition, and spatial learning. We then determine whether KU-32 could be a possible therapy for chemobrain. We also investigated whether dopamine release recovers in rats treated with 5-FU are given time to recover from treatments. Finally, we determine whether serotonin release is affected by carboplatin treatments and correlate those measurements to cognitive behavioral measurements.

3.3 MATERIALS AND METHODS

3.3.1 Animals

All animal procedures were approved by the Institutional Animal Care and Use Committee at the University of Kansas. Wistar rats were obtained from Charles River (Raleigh, NC) and housed and fed in pairs in the Animal Care Unit at the University of Kansas. Rats were maintained on 22-h food restriction. on a 24-hour light-dark cycle. Rats who underwent

behavioral testing were kept on 22-hour food restriction. During 1-h behavioral experiment sessions, rats received food pellets (45 mg, Bio-Serv, Frenchtwon, NJ) followed by ad libitum food for the remainder of the 2-h access period. Cages were kept on a 12-h:12-h light-dark cycle, with experimental sessions occurring in the light phase.

3.3.2 Treatments

3.3.2.1 5-FU and KU-32 study

Wistar rats were treated with either a 20 mg/kg dose of 5-FU or an equivalent volume of saline vehicle once per week for two weeks via i.v. tail vein injection. Half of the rats receiving 5-FU also received KU-32 via oral gavage. KU-32 oral gavage treatments were administered immediately following 5-FU injections.

3.3.2.2 5-FU recovery study

Wistar rats were treated with either a 20 mg/kg dose of 5-FU or an equivalent volume of saline vehicle once per week for two weeks via i.v. tail vein injection. Half of the rats receiving 5FU treatments were euthanized for electrochemical measurements one week following the final injection, and the other half were euthanized three weeks after receiving their final injection. Vehicle-treated rats were euthanized one week after receiving their final injections.

3.3.2.3 Carboplatin study

Male Wistar rats received one injection (i.v., tail vein) of carboplatin once a week for four consecutive weeks. For this round of treatment, there were two experimental groups consisting of treatment with 0.9% biological saline or a 20 mg/kg dose of pharmaceutical grade carboplatin (10 mg/mL, Hospira, Inc.). Both dosage and treatment regimen were chosen to mimic clinical dosing regimens and to allow the drug effects to stabilize.

3.3.3 Brain Slices

Rats under isoflurane anesthesia were decapitated and the brain was removed. Next, 350-µm thick slices containing the striatum were obtained using a vibratome. Striatal slices were placed on a perfusion chamber, and artificial cerebrospinal fluid (aCSF) was perfused over the slices. The aCSF (126 mM NaCl, 22 mM HEPES, 1.6 mM NaH_2PO_4, 2.5 mM KCl, 25 mM $NaHCO_3$, 2.4 mM $CaCl_2$, 1.2 mM $MgCl_2$, and 11 mM D-glucose, adjusted to a pH of 7.4) was oxygenated with 95/5% O_2/CO_2 and kept at physiological temperature using a heater (manufacturer) in order to keep the slices viable for the duration of the experiment. Once placed on the perfusion chamber, slices were allowed to equilibrate for 1 hour prior to electrochemical measurements.

3.3.4 Carbon fiber microelectrode fabrication

FSCV at carbon fiber microelectrodes was used to measure neurotransmitter release. Electrodes were fabricated in-house as previously described.[35] First, a 7-µm in diameter carbon fiber (Goodfellow, Huntingdon, UK) was threaded through a glass capillary (0.6 mm I.d., 1.2 mm o.d., 4-in long, A-M systems, Inc. Carlsborg, WA, USA) using a vacuum pump. Then, the glass capillary was pulled to a point encasing the carbon fiber using a heated-coil puller. Next, the carbon fiber tip was cut to 30 µm in length using a scalpel. The electrodes were dipped in epoxy resin (815 C, EPIKURE 3234 curing agent, Miller-Stephenson, Danbury, CT, USA). Excess epoxy was removed by dipping electrodes in toluene. Finally, electrodes were cured in an oven for 1 hour at 100°C.

In addition to these steps, electrodes used for serotonin release measurements were coated with Nafion, a cation exchange polymer, in order to increase sensitivity to serotonin and decrease sensitivity to 5-hydroxyindoleacetic acid, a serotonin metabolite that could interfere with serotonin measurements. Electrodes were soaked in isopropyl alcohol to remove any

impurities from the electrode surface. Then, they were backfilled with a 0.5 M potassium acetate solution to make a connection with the silver wire in the back of the electrode and the carbon fiber. Electrodes were manipulated so they were immersed in Nafion (Nafion perfluorinated ion-exchange resin, 5 wt. % solution in a mixture of lower aliphatic alcohols and water, Sigma-Aldrich, St. Louis, MO, USA), and Nafion was electrodeposited on the carbon fiber surface by applying a constant potential of 1.0V for 30 seconds. After electrodeposition, electrodes were dried in an oven at 70°C for 10 minutes and stored in a cool, dry place. Electrodes with Nafion coatings were used within 1 week in order to avoid any issues with Nafion degradation.

3.3.5 Dopamine measurements in the striatum of 5-FU-treated rats

After equilibration, dopamine release measurements were made by FSCV. Four measurements were made in each of four quadrants (dorsal lateral, dorsal medial, ventral lateral, and ventral medial) of the striatum, to account for the heterogeneity of the striatum. Dopamine release was evoked using a single biphasic 4-ms 350-µA pulse applied at the stimulating electrodes. FSCV measurements were made using carbon fiber microelectrodes. Microelectrodes were 7-µm in diameter and cut to 30-µm long. A waveform of -0.4V up to +1.0V and back down to a holding potential of -0.4V was applied at 300 V/s. Characteristic dopamine cyclic voltammograms were obtained, and the corresponding current vs. time plots were compared to flow cell calibrations in order to obtain concentration data. Measurements were made vs. a Ag/AgCl reference electrode.

3.3.6 Serotonin measurements in the dorsal raphe of carboplatin-treated rats

Serotonin measurements were collected similarly to dopamine measurements. However, a different electrical stimulation paradigm was used: 20 4-ms biphasic 350 µA pulses at a

frequency of 50 Hz. A serotonin-optimized waveform was applied at the working electrode: 0.2 V scanning up to 1.0 V, down to –0.1 V, and back up to 0.2 V at a scan rate of 800 V/s.

3.3.7 Behavioral experiments

3.3.7.1 Apparatus

Behavioral sessions were conducted in standard MedPC operant chambers (30.5 cm long, 24.1 cm wide, 29.2 cm high; Med Associates, Inc., St. Albans, VT) illuminated by 28-V houselights centered on the back wall (26.7 cm from the floor). Centered on the front wall, 1 cm above the floor grid was a pellet receptacle (3 cm × 4 cm) into which a pellet dispenser dispensed pellets. On the curved, rear wall were five side-by-side nose-poke access openings (2.54 cm × 2.54 cm), each illuminated by a cue light and featuring infrared response recording. Nose-poke openings were 2.54 cm apart and 2 cm from the floor. Chambers were housed in sound attenuating cabinets with white noise fans.

3.3.7.2 5-choice serial reaction time paradigm

Sessions occurred 6 days a week at approximately the same time each day and lasted for 1 h. A nose poke into the pellet receptacle was required to trigger the start of the task. Then, 5 s after the initial nose poke into the receptacle, a stimulus light turned on above the active target. Triggering the active target within 5 s of the light turning on resulted in the delivery of one 45 mg pellet.

3.3.7.3 Differential reinforcement of low rates paradigm

The rats were 5 months old at the beginning of the experiment. Behavioral testing was performed a minimum of six out of every seven days, at approximately the same time each day, for four weeks. There was no pre-training performed because rats had previous experience with schedules of reinforcement. All rats experienced 12–14 sessions prior to the experimental phase and twice received saline intravenous (i.v.) and saline oral gavage administrations immediately following behavioral sessions. For the experimental phase, rats were randomly placed into one of two groups (KU32 + 5-FU or SAL + 5FU). The experimental phase for each rat began following the first administration of 5-FU and KU32/SAL. A second administration occurred one week later. Behavioral data were collected up to one week following the second administration

Rats began behavioral sessions on differential reinforcement of low-rate 20-s schedules of reinforcement (DRL20). Food pellets were contingent on successive nose-poke responses in the center nose-poke opening (NP3) with inter-response times (IRTs) greater than or equal to 20 s. An NP3 response with an IRT less than 20-s reset the interval, such that the IRT between the resetting response and the subsequent response needed to be 20 s in order to earn a reinforcer. Nose-poke responses on the other four nose-poke openings were recorded but did not reset the interval or earn reinforcement. DRL20 schedules moved to DRL40 schedules prior to the experimental phase for all but two rats.

3.3.7.4 Spatial learning paradigm

Sessions occurred 6 days a week at approximately the same time each day and ended either after the rats earned 100 reinforcers or 1 h had passed. At the beginning of each session, the house light and the stimulus lights in each of the five nose poke receptacles were turned on. In each session, one of the five nose pokes was made active. Specifically, triggering the infrared

sensor in that receptacle resulted in a brief tone (0.1 s), the extinguishing of all nose poke cue lights for 5 s, the lighting of the pellet receptacle, and the delivery of one 45 mg pellet. Responding on the other four nose poke receptacles was recorded but did not result in any differential consequences. The target nose poke remained constant for each session, with the order of conditions varying quasi-randomly.

3.4 RESULTS AND DISCUSSION

3.4.1 Dopamine release impairment in rats treated with 5-FU

As previously mentioned, dopaminergic transmission is involved in a host of neurological functions, including memory,[36] attention,[37-38] inhibition,[39-41] and mood control.[42-44] In chemobrain, multiple studies have shown that dopamine may be involved.[45-49] Therefore, we chose to investigate the potential role of dopamine release in 5-FU-treated rats.

The striatum was divided into four quadrants in each coronal slice, and electrically stimulated dopamine release was quantified in the quadrants. Measurements were taken in the four quadrants to account for the heterogeneity of innervation in the striatum.[50] Figure 3.4.1A shows the division of a coronal brain slice into dorsal lateral (DL), dorsal medial (DM), ventral medial (VM), and ventral lateral (VL) quadrants.

Electrically stimulated DA release in each quadrant of the striatum was measured with FSCV in 350 µm-thick coronal brain slices. Here, a single, biphasic 4-ms 350 µA electrical pulse was applied at the stimulating electrodes at 5 seconds. In response to electrical stimulation, dopamine release and uptake was observed. Figure 3.4.1B shows representative color plots, current vs time, and cyclic voltammograms for vehicle- and 5-FU-treated rats, respectively. The cyclic voltammograms are characteristic of dopamine, confirming dopamine release. The color

plots consist of cyclic voltammograms that have been unfolded, rotated, and stacked over time. Current is represented in false color on the z-axis. No other faradaic currents are apparent, suggesting that other electroactive species do not contribute to the dopamine signal.

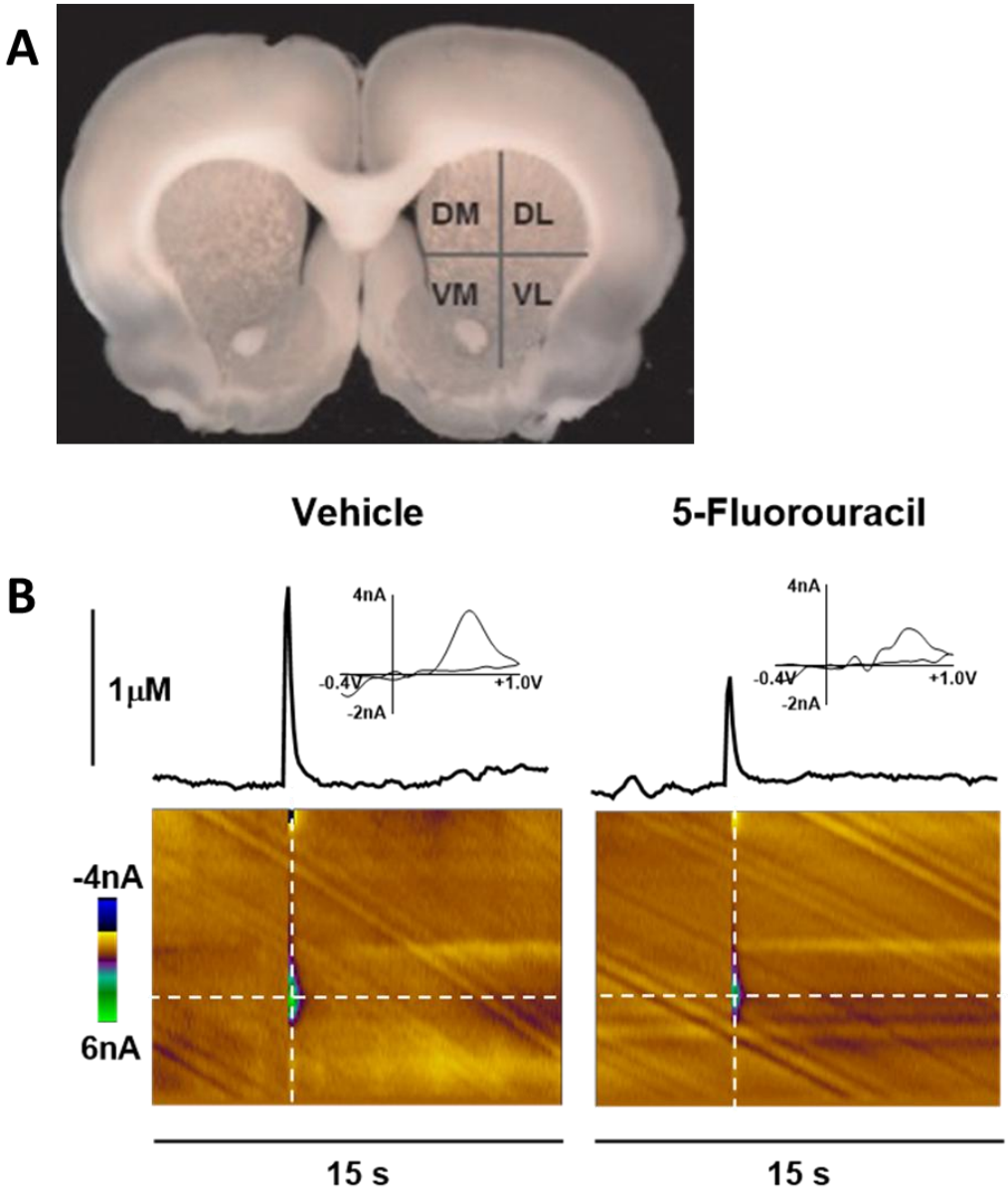

Figure 3.4.1. (A) Four quadrants of the striatum in coronal slices. DL = dorsal lateral, DM = dorsal medial, VM = ventral medial, and VL = ventral lateral. (B) Representative data collected in the striatum of vehicle- and 5-FU-treated rats, respectively.

Figure 3.4.2 shows the overall results for dopamine release in 5-FU treated rats and the saline vehicle-treated controls. Wistar rats were treated with either a 20 mg/kg dose of 5-FU via i.v. tail vein injection or the equivalent volume of saline vehicle. A two-way ANOVA revealed no significant interaction between treatment group and region of the striatum ($p=0.94$), so there did not appear to be a region-dependent difference in effect of 5-FU. Therefore, dopamine release was averaged across all four quadrants; in rats treated with 20 mg/kg 5-FU, dopamine release in the striatum was decreased to 63.3±9.5% of the vehicle-treated controls (two-way ANOVA, $p<0.05$, N = 5 vehicle and 9 5-FU treated rats). Chemobrain symptom include learning and memory deficits, as well as lack of attention span and inhibition;[46, 51-54] dopamine has been shown to influence each of these.[36-39, 41, 44, 55] Thus, it is possible that dopamine release attenuation throughout the striatum in response to 5-FU treatment could be a contributing factor in chemobrain.

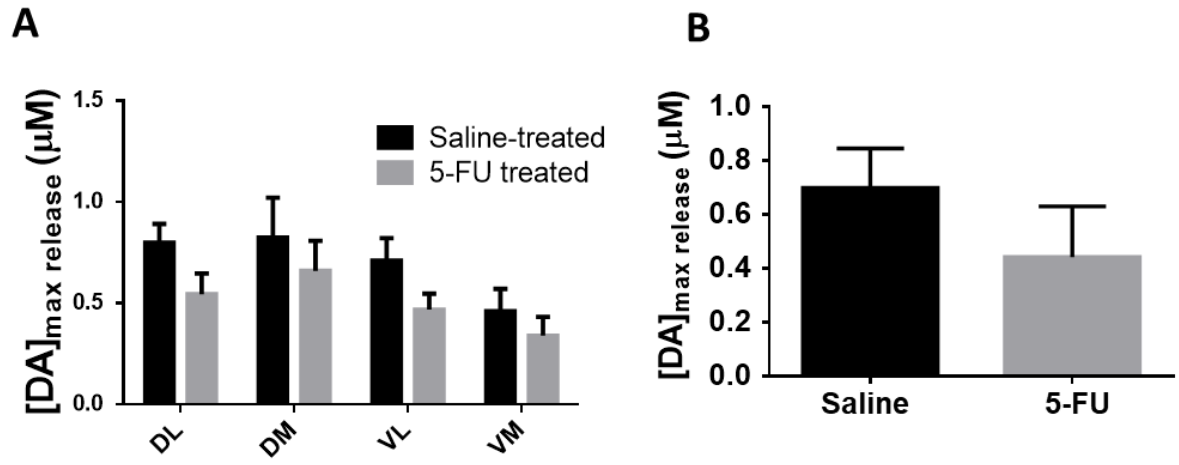

Figure 3.4.2. Dopamine release is impaired in 5-FU treated rats compared to saline-treated controls. (n = 5; two-way ANOVA, $p < 0.05$)

3.4.2 Dopamine release recovery study

Clinical studies have shown mixed results on the lasting effects of chemobrain. Some find that chemobrain symptoms are transient. Whitney et al. found that in patients who received cisplatin for non-small cell lung cancer, 62% of patients in the study showed cognitive decline after treatments, but the effect dissipated after 7 months.[56] Others have found a longer-lasting effect. Wefel et al. found both acute and long-term cognitive effects in breast cancer patients receiving 5-fluorouracil, doxorubicin, and cyclophosphamide.[57] Therefore, we wanted to investigate further whether 5-FU-induced depression of dopamine release in the striatum was a transient or lasting effect.

Figure 3.4.3 shows the overall dopamine release data for the 5-FU recovery study. For this study, rats were given either one week or three weeks to recover from 20 mg/kg 5-FU treatments (i.v. tail vein) before dopamine release measurements were made. Our results show that dopamine release impairment was not significantly different in different quadrants of the striatum; therefore, release measurements were averaged across all four quadrants. Dopamine

release was found to be significantly impaired in the one-week recovery group (50.4±8.7% of vehicle-treated control), and the three week recovery group (66.0±9.7% of vehicle-treated control). These results suggest that dopamine release impairment is a lasting effect in rats treated with 5-FU. Thus, lasting cognitive changes in patients treated with 5-FU may be related to dysfunction in the dopamine system; more work ought to be done to further study the lasting cognitive changes.

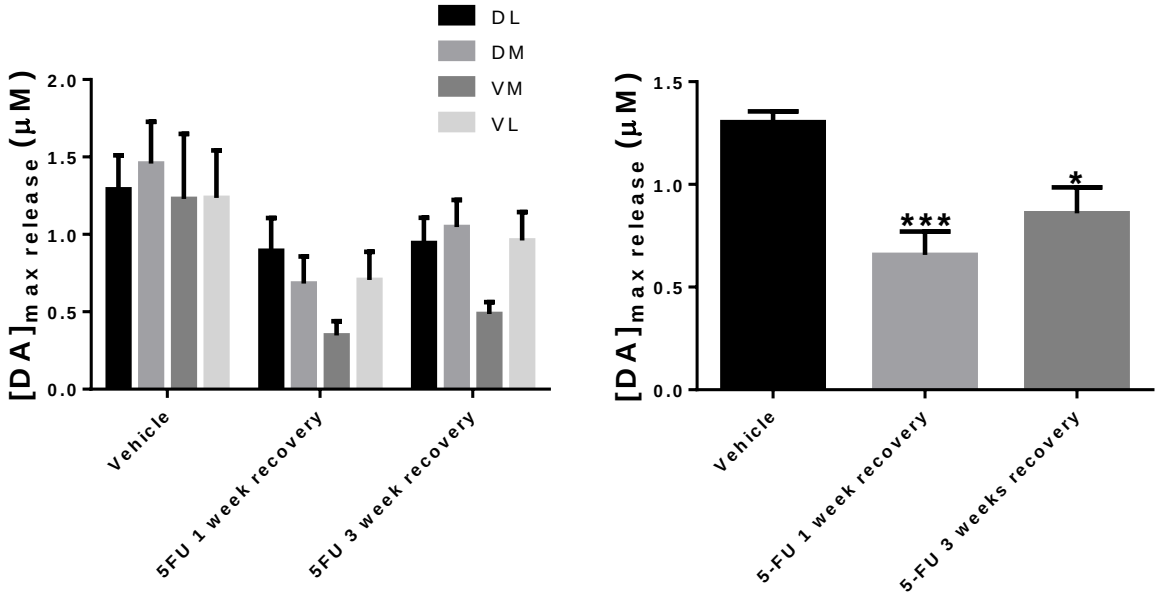

Figure 3.4.3. Striatal dopamine release in 5-FU-treated rats was attenuated in both 5-FU groups: 1 week and 3 week recovery. (N = 4 vehicle, 5 5-FU 1 week recovery, and 6 5-FU 3 week recovery rats; *$p < 0.05$, ***$p < 0.001$, two-way ANOVA Tukey's multiple comparisons test)

3.4.3 5-FU impairs performance on 5-choice serial reaction time test

Figure 3.4.4 shows the performance of rats treated with 20 mg/kg 5-FU compared to saline vehicle-treated controls on the 5-choice serial reaction time paradigm. After just one injection of 5-FU, the percent change from baseline in number of reinforcers earned was significantly lower than rats who received saline injections. The effect remained after a second injection.

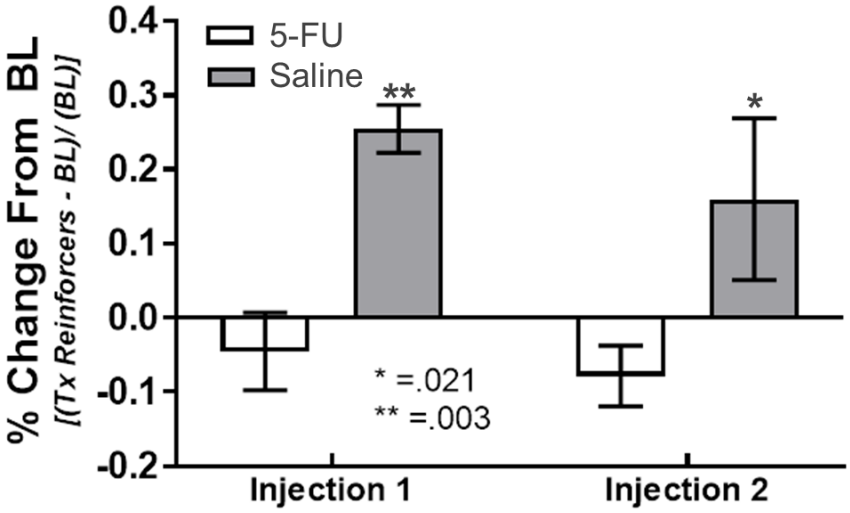

Figure 3.4.4. Rats treated with 5-FU (20 mg/kg, i.v. tail vein injection) showed a significantly lower % change from baseline compared to saline-treated controls. (n = 10 5-FU rats and 6 saline rats)

3.4.4 KU-32 treatment prevents 5-FU-induced inhibition deficits

Figure 3.4.5 shows mean reinforcers earned across D1, D7, and D14 for rats in the 5-FU + KU32 group (squares) and 5-FU + Saline (circles). A Two-way ANOVA revealed significant main effects of group ($F = 10.5$, $p = 0.003$) and non-significant effects for time point ($F = 0.286$, $p = 0.75$). A significant interaction effect ($F = 3.92$, $p = 0.029$), however, was found between group and time point. Post hoc comparisons revealed that the 5-FU + KU32 group earned significantly

more reinforcers than the 5-FU + Saline group at the second (p = 0.033) and third (p = 0.031) treatment (i.e. three time points).

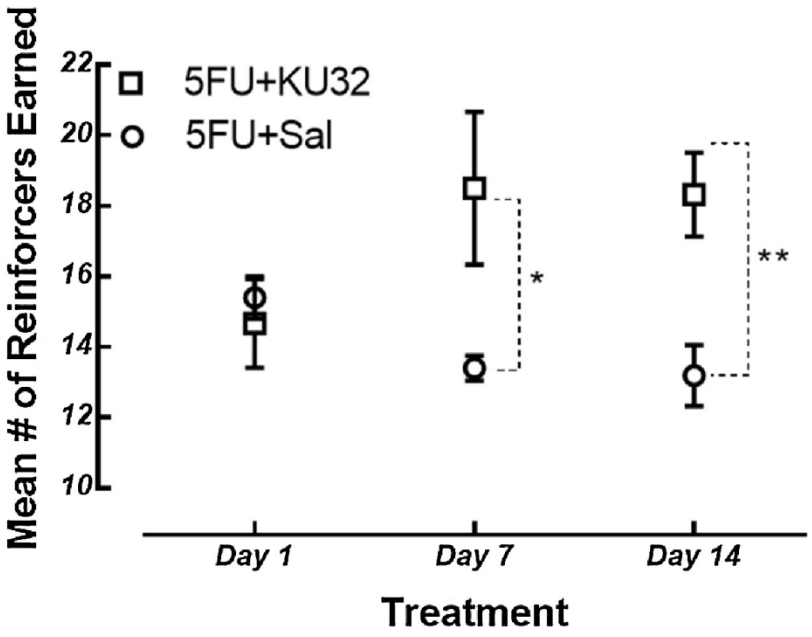

Figure 3.4.5. Mean number of reinforcers earned (y-axis) for the 5-FU + Saline group (circles) and 5-FU + KU32 group (squares) across D1, D7, and D14 (x-axis).

The top panel of Figure 3.4.6 shows mean reinforcers earned divided by total NP3 responses across D1, D7, D14 for rats in the 5-FU + KU32 (squares) and 5-FU + Saline (circles) groups. There were significant main effects of group (F = 13.3, p = 0.001), time point (F = 3.5, p = 0.046), and the interaction of group and time point (F = 5.9, p = 0.008). Post hoc comparisons revealed that those rats in the KU32 + 5-FU group were significantly more efficient in their reinforcers/total NP3 responses than those in the Saline + 5-FU group at D14 (p = 0.0001). Within groups, there were no significant differences across time points within the 5-FU group, however, those rats in the 5-FU + KU32 group were significantly more efficient in their reinforcers/NP3 responding at D14 compared to D1 (p = 0.002) or D7 (p = 0.002).

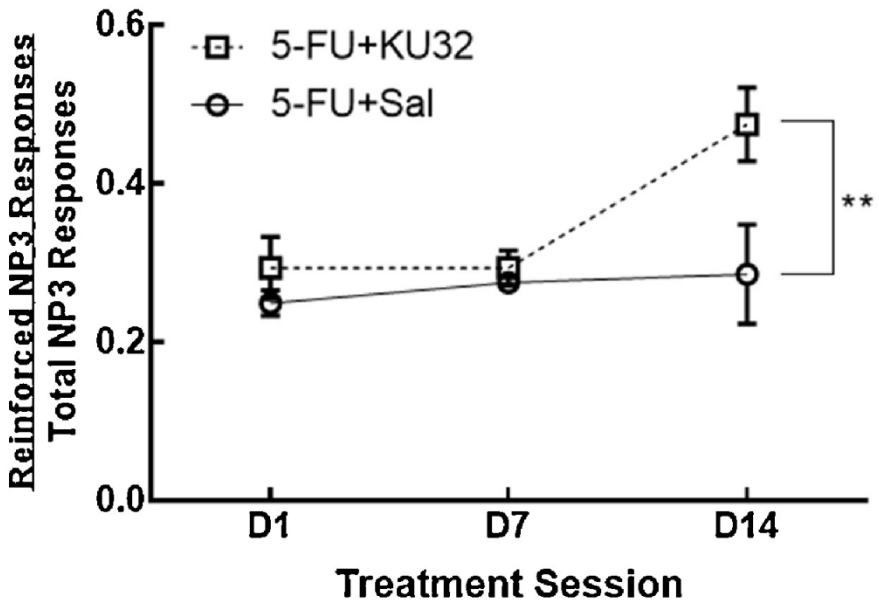

Figure 3.4.6. Mean reinforcers earned divided by total NP3 responses (y-axis) across D1, D7, and D14 (x-axis) for rats in the 5-FU + KU32 (squares) and 5-FU + Saline (circles) groups.

Figure 3.4.7 shows mean nose-poke responses (y-axis) per nose-poke target (x-axis) for both 5-FU + Saline (open squares) and 5-FU + KU32 rats (open circles) for D1 (top panel), D7 (middle panel), and D14 (bottommost panel). Gaussian curves are fit to each group's mean responses across each target at a given time point (i.e. D1, D7, and D14). To determine level differences in responses between the two groups, two-way ANOVAs comparing mean responses across nose-poke targets were used. Significant differences were only observed between the groups on D14 such that the 5-FU + Saline group exhibited more responses than the 5-FU + KU32 group. A post hoc comparison revealed that the only significant difference in mean responses between the groups on D14 was at NP3 ($p = 0.006$). An index of the Gaussian gradient (FWHM) was derived for each group at each time point. A two-way ANOVA revealed non-significant findings for group ($p = 0.23$) and time point ($p = 0.26$) suggesting no differences in spatial discrimination across the two groups.

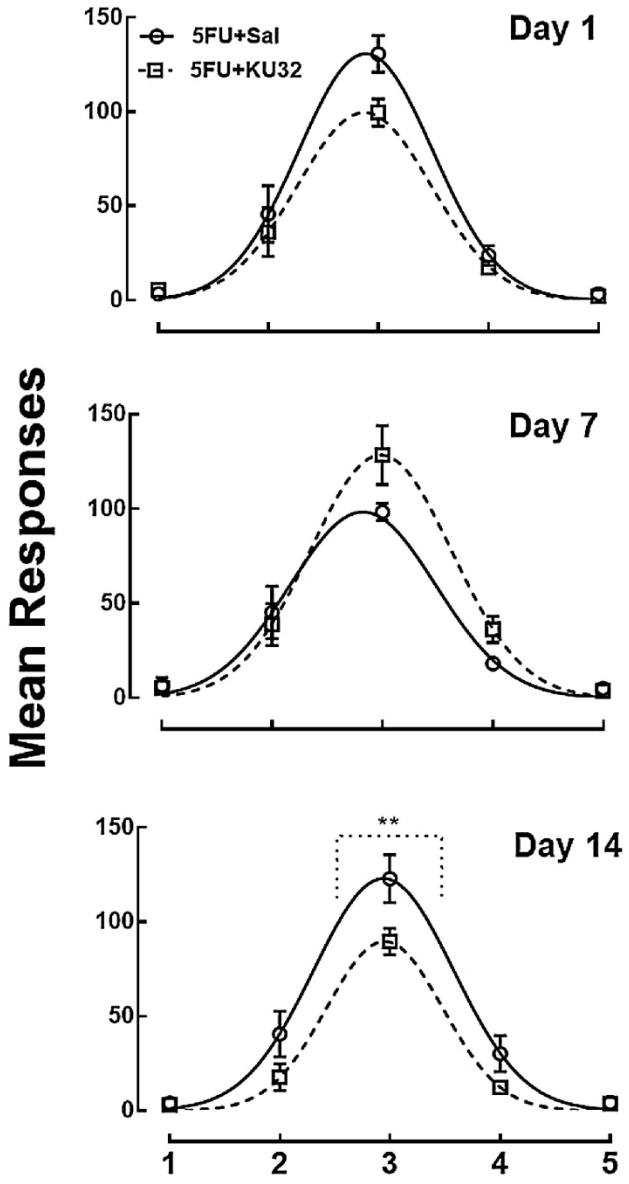

Figure 3.4.7. Top, middle, and bottom panels represent D1, D7, and D14 respectively. Mean responses (y-axis) per nose-poke target (axis) are plotted for 5-FU + KU32 rats (squares and dotted gradient) and 5-FU + Saline (circles and non-dotted gradient).

3.4.5 Serotonin release in carboplatin-treated rats

To examine further the mechanism underlying chemobrain, we also measured the stimulated release of 5-HT within the dorsal raphe nucleus. Serotonin plays a vital role in

cognition, including memory and learning processes[58-59] and synaptic plasticity.[60] Furthermore, the interplay between 5-HT and other neurotransmitter systems, including DA, has been shown.[61-62] Due to the specific involvement in cognition and interplay with the DA system, we chose to study electrically stimulated 5-HT release in the dorsal raphe nucleus by FSCV. Five measurements were taken within the dorsal raphe from each brain slice and averaged. Representative data from the 0 and 20 mg/kg carboplatin treatment groups are shown in Figure 3.4.8A. The representative cyclic voltammograms indicate that the analyte measured is 5-HT. As shown in Figure 3.4.8B, the peak concentration of serotonin released following electrical stimulation was significantly diminished in 20 mg/kg carboplatin-treated rats compared to saline-treated rats (45 ± 9% of saline control, $n = 5$ carboplatin-treated and 5 vehicle-treated rats, $p < 0.05$, unpaired t test). Our results suggest that impaired 5-HT release may contribute to the cognitive deficits experienced by patients who have undergone chemotherapy treatment. Taken together with DA release impairments, these results indicate that chemotherapy may induce a general effect upon the mechanism of neurotransmitter release. Thus, it is likely that the release of other neurotransmitters, such as glutamate and GABA, is impaired; consequently, the impact of these deficits on cognitive function should also be considered.

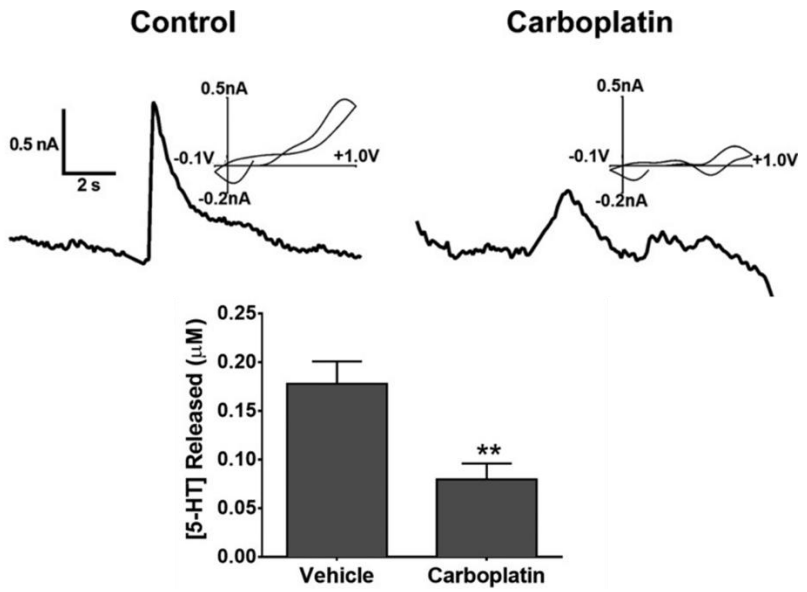

Figure 3.4.8. Serotonin release in the dorsal raphe nucleus is attenuated in carboplatin-treated rats.

3.4.6 Carboplatin treatment causes decreased performance on a spatial learning paradigm

To test for carboplatin related deficits in spatial learning, rats were evaluated on a spatial learning paradigm in which five response options (i.e., nose-pokes detected by infrared beam) were presented in a horizontal row. When the rats poked their noses to a target preselected by the investigator, a food reward was delivered. This paradigm consistently results in Gaussian response distributions centered on the target location, with steeper Gaussian functions indicating more robust spatial learning.[63] Figure 3.4.9 shows the spread of responses to nontarget nose pokes (A), responses at the nontarget positions, 2 and 4 (B), overall rates of nose pokes (C), and rats' weights during the testing phase (D). As can be seen, the responses to nontarget nose poke locations (expressed as a proportion of the rate of nose pokes on the target location) fit well into a Gaussian function for rats treated with saline (r^2= 0.99) and 20 mg/kg carboplatin (r 2 = 0.96).

The parameters for these Gaussian functions significantly differed between groups ($F[2,64] = 4.339$, $p < 0.05$). Moreover, t test of responding at individual targets found that the proportion of target responses on nose poke location 2 ($t[60] = 2.0651$, $p < 0.05$) and 4 ($t[60] = 2.41287$, $p < 0.05$) differed significantly between carboplatin and vehicle-treated rats (Figure 3.4.9B). No significant differences were obtained for overall rate of nose pokes (Figure 3.4.9C; $p = 0.65$) or rats' weights during the testing phase (Figure 3.4.9D; $p = 0.29$). Consistent with the neurochemical data, a treatment course of carboplatin resulted in altered cognitive function. Here, carboplatin resulted in small but significant alterations in spatial learning/memory that resulted in increased responding to nontarget nose poke locations on a spatial learning paradigm. The degree of cognitive impairment observed following carboplatin treatment is consistent with chemotherapy patients' symptoms, which often present as subtle impairments in parameters such as learning, concentration, reasoning, and executive function.[64] An important aspect of these cognitive measurements is that the overall rates of responding did not significantly differ between carboplatin- and vehicle-treated groups ($p > 0.05$). Additionally, rats did not lose weight during or after treatment, suggesting that food consumption and general feeling of well-being was not impacted. Taken together, these results strongly suggest that the decreased responding of carboplatin-treated rats on locations 2 and 4 was not due merely to a detriment of overall health, but rather to the more specific effect of cognitive impairment.

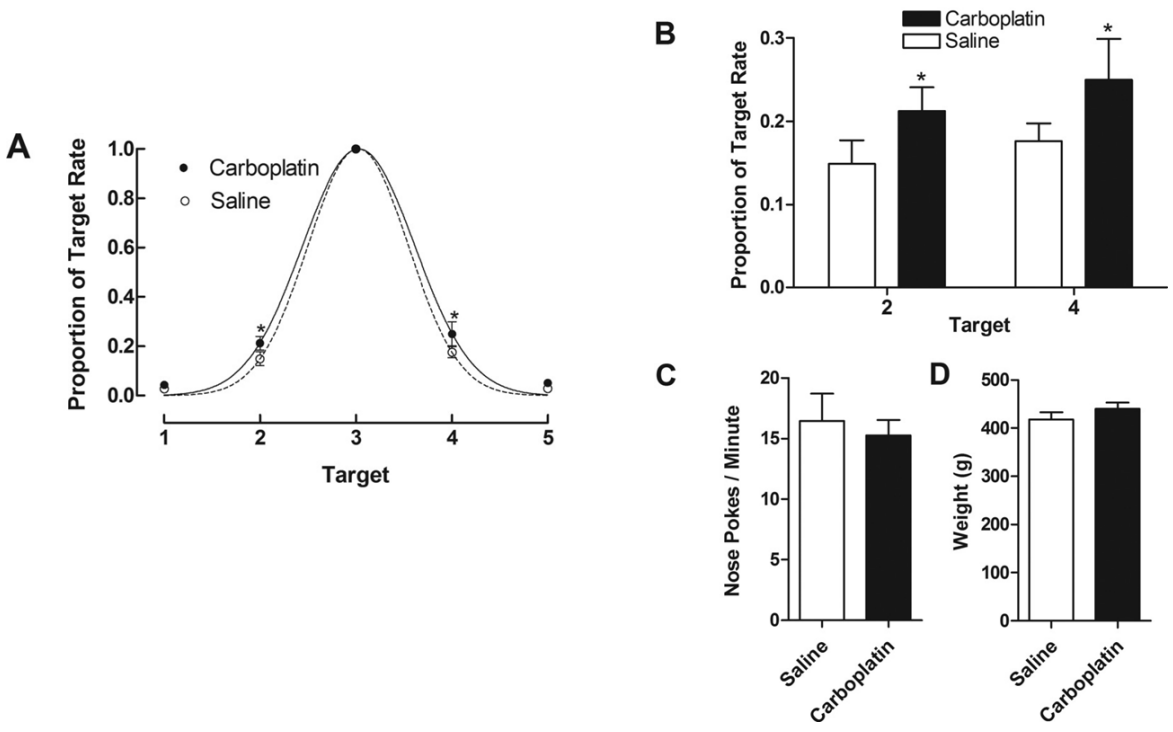

Figure 3.4.9. Spatial learning measurements obtained using operant conditioning chambers. The spread of responses (A) is expressed as a proportion of the rates of nose pokes at each location and is fit to a Gaussian function for both the vehicle-treated (r 2 = 0.99) and carboplatin-treated (r 2 = 0.96) rats (F [2,64] = 4.339, $p < 0.05$, n = 7, vehicle versus carboplatin). The responses at the nontarget positions, 2 and 4 (B), overall rates of nose pokes (C), and rats' weights during the testing phase (D) are also shown (*$p < 0.05$, n = 7 rats per group).

3.5 CONCLUSIONS

The particular mechanisms underlying neurotransmitter release impairments following chemotherapeutic treatment have not yet been identified. However, it is possible that multiple factors contribute, including influences by other neurotransmitters and neuromodulators that have become dysregulated due to carboplatin treatment, damage to proteins that mediate exocytosis, and morphological degradation of neuronal terminals. In future studies, it will be

important to address these issues to identify specific cellular mechanisms that contribute to release impairment. Additionally, it will be critical to design behavioral and neurochemical experiments so that we can determine the relevance of neurotransmitter release alterations in specific brain regions, such as the striatum and dorsal raphe nucleus, to cognitive ability.

In summary, our 5-choice serial reaction time, differential reinforcement of low rates, and spatial learning paradigm results indicate a decrease in cognitive performance; thus, it is possible that diminished neurotransmitter release capability negatively impacts cognitive ability. Collectively, these findings (1) suggest neurotransmitter release impairment as a possible mechanism of cognitive dysfunction in patients treated with chemotherapeutic agents and (2) support the need for more refined behavioral and neurochemical analyses to elucidate how release is impaired and which neurotransmitter systems are affected.

3.6 REFERENCES

1. Organization, W. H. World Health Organization Cancer Mortality Database. http://www-dep.iarc.fr/WHOdb/WHOdb.htm (accessed July 20).

2. Miller, K. D.; Siegel, R. L.; Lin, C. C.; Mariotto, A. B.; Kramer, J. L.; Rowland, J. H.; Stein, K. D.; Alteri, R.; Jemal, A., Cancer treatment and survivorship statistics, 2016. *CA: A Cancer Journal for Clinicians* **2016,** *66* (4), 271-289.

3. Society, A. C. *Cancer Treatment & Survivorship Facts & Figures 2016-2017.* ; American Cancer Society: Atlanta, 2016.

4. Myers, J. S., Chemotherapy-related cognitive impairment. *Clin J Oncol Nurs* **2009,** *13* (4), 413-21.

5. Cheung, Y. T.; Ong, Y. Y.; Ng, T.; Tan, Y. P.; Fan, G.; Chan, C. W.; Molassiotis, A.; Chan, A., Assessment of mental health literacy in patients with breast cancer. *J Oncol Pharm Pract* **2016,** *22* (3), 437-47.

6. Moertel, C.; Frytak, S.; Hahn, R.; O'Connell, M.; Reitemeier, R.; Rubin, J.; Schutt, A.; Weiland, L.; Childs, D.; Holbrook, M., Therapy of locally unresectable pancreatic carcinoma: A randomized comparison of high dose (6000 rads) radiation alone, moderate dose radiation (4000 rads+ 5- fluorouracil), and high dose radiation+ 5- fluorouracil. The gastrointestinal tumor study group. *Cancer* **1981,** *48* (8), 1705-1710.

7. Khuri, F. R.; Nemunaitis, J.; Ganly, I.; Arseneau, J.; Tannock, I. F.; Romel, L.; Gore, M.; Ironside, J.; MacDougall, R.; Heise, C., A controlled trial of intratumoral ONYX-015, a selectively-replicating adenovirus, in combination with cisplatin and 5-fluorouracil in patients with recurrent head and neck cancer. *Nature medicine* **2000,** *6* (8), 879.

8. Douillard, J.; Cunningham, D.; Roth, A.; Navarro, M.; James, R.; Karasek, P.; Jandik, P.; Iveson, T.; Carmichael, J.; Alakl, M., Irinotecan combined with fluorouracil compared with fluorouracil alone as first-line treatment for metastatic colorectal cancer: a multicentre randomised trial. *The Lancet* **2000,** *355* (9209), 1041-1047.

9. Klinkenbijl, J. H.; Jeekel, J.; Sahmoud, T.; van Pel, R.; Couvreur, M. L.; Veenhof, C. H.; Arnaud, J. P.; Gonzalez, D. G.; de Wit, L. T.; Hennipman, A., Adjuvant radiotherapy and 5-fluorouracil after curative resection of cancer of the pancreas and periampullary region: phase III trial of the EORTC gastrointestinal tract cancer cooperative group. *Annals of surgery* **1999,** *230* (6), 776.

10. Creech, R. H.; Catalano, R. B.; Mastrangelo, M. J.; Engstrom, P. F., An effective low- dose intermittent cyclophosphamide, methotrexate, and 5- fluorouracil treatment regimen for metastatic breast cancer. *Cancer* **1975,** *35* (4), 1101-1107.

11. Buzdar, A. U.; Valero, V.; Ibrahim, N. K.; Francis, D.; Broglio, K. R.; Theriault, R. L.; Pusztai, L.; Green, M. C.; Singletary, S. E.; Hunt, K. K., Neoadjuvant therapy with paclitaxel followed by 5-fluorouracil, epirubicin, and cyclophosphamide chemotherapy and concurrent trastuzumab in human epidermal growth factor receptor 2–positive operable breast cancer: an update of the initial randomized study population and data of additional patients treated with the same regimen. *Clinical Cancer Research* **2007,** *13* (1), 228-233.

12. Longley, D. B.; Harkin, D. P.; Johnston, P. G., 5-fluorouracil: mechanisms of action and clinical strategies. *Nature reviews. Cancer* **2003,** *3* (5), 330-8.

13. Andreis, F.; Ferri, M.; Mazzocchi, M.; Meriggi, F.; Rizzi, A.; Rota, L.; Di Biasi, B.; Abeni, C.; Codignola, C.; Rozzini, R.; Zaniboni, A., Lack of a chemobrain effect for adjuvant FOLFOX chemotherapy in colon cancer patients. A pilot study. *Support Care Cancer* **2013,** *21* (2), 583-90.

14. Mustafa, S.; Walker, A.; Bennett, G.; Wigmore, P. M., 5-Fluorouracil chemotherapy affects spatial working memory and newborn neurons in the adult rat hippocampus. *Eur J Neurosci* **2008,** *28* (2), 323-30.

15. Fardell, J. E.; Vardy, J.; Shah, J. D.; Johnston, I. N., Cognitive impairments caused by oxaliplatin and 5-fluorouracil chemotherapy are ameliorated by physical activity. *Psychopharmacology* **2012,** *220* (1), 183-93.

16. Han, R.; Yang, Y. M.; Dietrich, J.; Luebke, A.; Mayer-Proschel, M.; Noble, M., Systemic 5-fluorouracil treatment causes a syndrome of delayed myelin destruction in the central nervous system. *Journal of biology* **2008,** *7* (4), 12.

17. Anyika, M.; McMullen, M.; Forsberg, L. K.; Dobrowsky, R. T.; Blagg, B. S., Development of Noviomimetics as C-Terminal Hsp90 Inhibitors. *ACS medicinal chemistry letters* **2016,** *7* (1), 67-71.

18. Farmer, K.; Williams, S. J.; Novikova, L.; Ramachandran, K.; Rawal, S.; Blagg, B. S.; Dobrowsky, R.; Stehno-Bittel, L., KU-32, a novel drug for diabetic neuropathy, is safe for human islets and improves in vitro insulin secretion and viability. *Experimental diabetes research* **2012,** *2012*, 671673.

19. Ma, J.; Farmer, K. L.; Pan, P.; Urban, M. J.; Zhao, H.; Blagg, B. S.; Dobrowsky, R. T., Heat shock protein 70 is necessary to improve mitochondrial bioenergetics and reverse diabetic sensory neuropathy following KU-32 therapy. *The Journal of pharmacology and experimental therapeutics* **2014,** *348* (2), 281-92.

20. Gao, R.; Zhang, Y.; Wen, X. P.; Fu, J.; Zhang, G. J., Chemotherapy with cisplatin or carboplatin in combination with etoposide for small-cell esophageal cancer: a systemic analysis of case series. *Diseases of the esophagus : official journal of the International Society for Diseases of the Esophagus* **2014,** *27* (8), 764-9.

21. Kushner, B. H.; Modak, S.; Kramer, K.; Basu, E. M.; Roberts, S. S.; Cheung, N. K., Ifosfamide, carboplatin, and etoposide for neuroblastoma: a high-dose salvage regimen and review of the literature. *Cancer* **2013,** *119* (3), 665-71.

22. de Castria, T. B.; da Silva, E. M.; Gois, A. F.; Riera, R., Cisplatin versus carboplatin in combination with third-generation drugs for advanced non-small cell lung cancer. *The Cochrane database of systematic reviews* **2013,** (8), Cd009256.

23. Lorusso, D.; Petrelli, F.; Coinu, A.; Raspagliesi, F.; Barni, S., A systematic review comparing cisplatin and carboplatin plus paclitaxel-based chemotherapy for recurrent or metastatic cervical cancer. *Gynecologic oncology* **2014,** *133* (1), 117-23.

24. Valsecchi, M. E.; Kimmey, G.; Bir, A.; Silbermins, D., Role of Carboplatin in the Treatment of Triple Negative Early- Stage Breast Cancer. *Reviews on recent clinical trials* **2015,** *10* (2), 101-10.

25. Trimbos, J. B.; Parmar, M.; Vergote, I.; Guthrie, D.; Bolis, G.; Colombo, N.; Vermorken, J. B.; Torri, V.; Mangioni, C.; Pecorelli, S.; Lissoni, A.; Swart, A. M., International Collaborative Ovarian Neoplasm trial 1 and Adjuvant ChemoTherapy In Ovarian Neoplasm trial: two parallel randomized phase III trials of adjuvant chemotherapy in patients with early-stage ovarian carcinoma. *Journal of the National Cancer Institute* **2003,** *95* (2), 105-12.

26. Ando, Y.; Shimokata, T.; Yasuda, Y.; Hasegawa, Y., Carboplatin dosing for adult Japanese patients. *Nagoya journal of medical science* **2014,** *76* (1-2), 1-9.

27. Hah, S. S.; Stivers, K. M.; de Vere White, R. W.; Henderson, P. T., Kinetics of carboplatin-DNA binding in genomic DNA and bladder cancer cells as determined by accelerator mass spectrometry. *Chemical research in toxicology* **2006,** *19* (5), 622-6.

28. Mandilaras, V.; Wan-Chow-Wah, D.; Monette, J.; Gaba, F.; Monette, M.; Alfonso, L., The impact of cancer therapy on cognition in the elderly. *Frontiers in pharmacology* **2013,** *4*, 48.

29. Schagen, S. B.; Muller, M. J.; Boogerd, W.; Rosenbrand, R. M.; van Rhijn, D.; Rodenhuis, S.; van Dam, F. S., Late effects of adjuvant chemotherapy on cognitive function: a

follow-up study in breast cancer patients. *Annals of oncology : official journal of the European Society for Medical Oncology* **2002,** *13* (9), 1387-97.

30. Iarkov, A.; Appunn, D.; Echeverria, V., Post-treatment with cotinine improved memory and decreased depressive-like behavior after chemotherapy in rats. *Cancer Chemother Pharmacol* **2016,** *78* (5), 1033-1039.

31. Ramalingayya, G. V.; Nampoothiri, M.; Nayak, P. G.; Kishore, A.; Shenoy, R. R.; Mallikarjuna Rao, C.; Nandakumar, K., Naringin and Rutin Alleviates Episodic Memory Deficits in Two Differentially Challenged Object Recognition Tasks. *Pharmacognosy magazine* **2016,** *12* (Suppl 1), S63-70.

32. Thomas, S. R. Investigation of microdialysis sampling to monitor pharmacodynamics The University of Kansas, Lawrence, KS, 2014.

33. Thomas, T. C.; Beitchman, J. A.; Pomerleau, F.; Noel, T.; Jungsuwadee, P.; Allan Butterfield, D.; Clair, D. K. S.; Vore, M.; Gerhardt, G. A., Acute Treatment with Doxorubicin Affects Glutamate Neurotransmission in the Mouse Frontal Cortex and Hippocampus. *Brain research* **2017**.

34. Kaplan, S. V.; Limbocker, R. A.; Gehringer, R. C.; Divis, J. L.; Osterhaus, G. L.; Newby, M. D.; Sofis, M. J.; Jarmolowicz, D. P.; Newman, B. D.; Mathews, T. A.; Johnson, M. A., Impaired Brain Dopamine and Serotonin Release and Uptake in Wistar Rats Following Treatment with Carboplatin. *ACS chemical neuroscience* **2016,** *7* (6), 689-99.

35. Ortiz, A. N.; Kurth, B. J.; Osterhaus, G. L.; Johnson, M. A., Dysregulation of intracellular dopamine stores revealed in the R6/2 mouse striatum. *J Neurochem* **2010,** *112* (3), 755-61.

36. Puig, M. V.; Rose, J.; Schmidt, R.; Freund, N., Dopamine modulation of learning and memory in the prefrontal cortex: insights from studies in primates, rodents, and birds. *Frontiers in neural circuits* **2014,** *8*, 93.

37. Gurvich, C.; Rossell, S. L., Dopamine and cognitive control: sex-by-genotype interactions influence the capacity to switch attention. *Behavioural brain research* **2015,** *281*, 96-101.

38. Dang, L. C.; O'Neil, J. P.; Jagust, W. J., Dopamine supports coupling of attention-related networks. *The Journal of neuroscience : the official journal of the Society for Neuroscience* **2012,** *32* (28), 9582-7.

39. Albrecht, D. S.; Kareken, D. A.; Christian, B. T.; Dzemidzic, M.; Yoder, K. K., Cortical dopamine release during a behavioral response inhibition task. *Synapse* **2014,** *68* (6), 266-74.

40. Saez, I.; Zhu, L.; Set, E.; Kayser, A.; Hsu, M., Dopamine modulates egalitarian behavior in humans. *Current biology : CB* **2015,** *25* (7), 912-9.

41. Bari, A.; Robbins, T. W., Inhibition and impulsivity: behavioral and neural basis of response control. *Progress in neurobiology* **2013,** *108*, 44-79.

42. Cawley, E. I.; Park, S.; aan het Rot, M.; Sancton, K.; Benkelfat, C.; Young, S. N.; Boivin, D. B.; Leyton, M., Dopamine and light: dissecting effects on mood and motivational states in women with subsyndromal seasonal affective disorder. *Journal of psychiatry & neuroscience : JPN* **2013,** *38* (6), 388-97.

43. Ruhe, H. G.; Mason, N. S.; Schene, A. H., Mood is indirectly related to serotonin, norepinephrine and dopamine levels in humans: a meta-analysis of monoamine depletion studies. *Molecular psychiatry* **2007,** *12* (4), 331-59.

44. Goschke, T.; Bolte, A., Emotional modulation of control dilemmas: the role of positive affect, reward, and dopamine in cognitive stability and flexibility. *Neuropsychologia* **2014,** *62*, 403-23.

45. Ahles, T. A.; Saykin, A. J., Candidate mechanisms for chemotherapy-induced cognitive changes. *Nature reviews. Cancer* **2007,** *7* (3), 192-201.

46. Staat, K.; Segatore, M., The phenomenon of chemo brain. *Clinical journal of oncology nursing* **2005,** *9* (6), 713-21.

47. Merriman, J. D.; Von Ah, D.; Miaskowski, C.; Aouizerat, B. E., Proposed mechanisms for cancer- and treatment-related cognitive changes. *Seminars in oncology nursing* **2013,** *29* (4), 260-9.

48. Seigers, R.; Fardell, J. E., Neurobiological basis of chemotherapy-induced cognitive impairment: a review of rodent research. *Neurosci Biobehav Rev* **2011,** *35* (3), 729-41.

49. Madhyastha, S.; Somayaji, S. N.; Rao, M. S.; Nalini, K.; Bairy, K. L., Hippocampal brain amines in methotrexate-induced learning and memory deficit. *Canadian journal of physiology and pharmacology* **2002,** *80* (11), 1076-84.

50. Calipari, E. S.; Huggins, K. N.; Mathews, T. A.; Jones, S. R., Conserved dorsal-ventral gradient of dopamine release and uptake rate in mice, rats and rhesus macaques. *Neurochem Int* **2012,** *61* (7), 986-91.

51. Asher, A., Cognitive dysfunction among cancer survivors. *Am J Phys Med Rehabil* **2011,** *90* (5 Suppl 1), S16-26.

52. Boykoff, N.; Moieni, M.; Subramanian, S. K., Confronting chemobrain: an in-depth look at survivors' reports of impact on work, social networks, and health care response. *J Cancer Surviv* **2009,** *3* (4), 223-32.

53. Castellino, S. M.; Ullrich, N. J.; Whelen, M. J.; Lange, B. J., Developing interventions for cancer-related cognitive dysfunction in childhood cancer survivors. *Journal of the National Cancer Institute* **2014,** *106* (8).

54. Morean, D. F.; O'Dwyer, L.; Cherney, L. R., Therapies for Cognitive Deficits Associated With Chemotherapy for Breast Cancer: A Systematic Review of Objective Outcomes. *Arch Phys Med Rehabil* **2015,** *96* (10), 1880-97.

55. Nestler, E. J.; Carlezon, W. A., Jr., The mesolimbic dopamine reward circuit in depression. *Biol Psychiatry* **2006,** *59* (12), 1151-9.

56. Whitney, K. A.; Lysaker, P. H.; Steiner, A. R.; Hook, J. N.; Estes, D. D.; Hanna, N. H., Is"chemobrain" a transient state? A prospective pilot study among persons with non-small cell lung cancer. *The journal of supportive oncology* **2008,** *6* (7), 313-21.

57. Wefel, J. S.; Saleeba, A. K.; Buzdar, A. U.; Meyers, C. A., Acute and late onset cognitive dysfunction associated with chemotherapy in women with breast cancer. *Cancer* **2010,** *116* (14), 3348-3356.

58. Seyedabadi, M.; Fakhfouri, G.; Ramezani, V.; Mehr, S. E.; Rahimian, R., The role of serotonin in memory: interactions with neurotransmitters and downstream signaling. *Experimental brain research* **2014,** *232* (3), 723-38.

59. Nic Dhonnchadha, B. A.; Cunningham, K. A., Serotonergic mechanisms in addiction-related memories. *Behav Brain Res* **2008,** *195* (1), 39-53.

60. Lesch, K. P.; Waider, J., Serotonin in the modulation of neural plasticity and networks: implications for neurodevelopmental disorders. *Neuron* **2012,** *76* (1), 175-91.

61. Howell, L. L.; Cunningham, K. A., Serotonin 5-HT2 receptor interactions with dopamine function: implications for therapeutics in cocaine use disorder. *Pharmacological reviews* **2015,** *67* (1), 176-97.

62. Hall, F. S.; Sora, I.; Hen, R.; Uhl, G. R., Serotonin/dopamine interactions in a hyperactive mouse: reduced serotonin receptor 1B activity reverses effects of dopamine transporter knockout. *PLoS One* **2014,** *9* (12), e115009.

63. Jarmolowicz, D. P.; Hudnall, J. L.; Darden, A. C.; Lemley, S. M.; Sofis, M. J., On the time course of rapid and repeatable response induction. *Behavioural processes* **2015,** *120*, 116-9.

64. Argyriou, A. A.; Assimakopoulos, K.; Iconomou, G.; Giannakopoulou, F.; Kalofonos, H. P., Either called "chemobrain" or "chemofog," the long-term chemotherapy-induced cognitive decline in cancer survivors is real. *J Pain Symptom Manage* **2011,** *41* (1), 126-39.

4 NEUROTRANSMITTER RELEASE MEASUREMENTS IN ADULT ZEBRAFISH WHOLE MOUNT RETINA

4.1 ABSTRACT

As the population in the United States ages, the prevalence of retinal disease has increased. However, the mechanisms of retinal disease are not well-understood. Here, we attempt to develop a new model for studying neurotransmitter release in adult zebrafish whole mount retina using fast-scan cyclic voltammetry at carbon fiber microelectrodes, a sensitive electrochemical technique that allows for high spatial and temporal resolution. In this work, we were able to confirm Ca^{2+}-mediated neurotransmitter release in response to light stimulation with a 470-nm wavelength fiber-optic-coupled LED system by titrating Ca^{2+} into the artificial cerebrospinal fluid; when Ca^{2+} was titrated into the solution, neurotransmitter release appeared. We also conducted experiments perfusing alpha-methyl-p-tyrosine, a tyrosine hydroxylase inhibitor, and quinpirole, a dopamine D2 receptor agonist. Our alpha-methyl-p-tyrosine experiments showed that dopamine release was diminished by 84.6±9.3% compared to the maximum signal obtained, supporting our hypothesis that the neurotransmitter release was a catecholamine. Our quinpirole experiments showed that dopamine release was decreased to 38.3±15.2% of the signal, suggesting that the catecholamine released was dopamine. Overall, dopamine release in the retina was found to be 0.27±.05 µM.

4.2 INTRODUCTION

As the population both in the United States and worldwide ages, diseases of the retina have become more important to study. Retinal degeneration will affect over 5 percent of the population at some time during their lives and is the leading cause of blindness in the developed

world.[1-2] Age-related macular degeneration (AMD) affects more than 8,000,000 Americans, with the prevalence of AMD projected to increase by 50% by 2020.[3] Since AMD is primarily a degeneration of cones,[4] it is important that a model organism used to study AMD should have a cone-rich retina. Therefore, zebrafish are an ideal model organism in which to study the retina, because their retinas are very rich in cones compared to other models such as rodents.[5]

Much work has been done mapping the retina with immunohistochemistry,[6-10] and Hirasawa et al. have measured dopamine and GABA released from amacrine cells cultured from mouse retina using a combination of patch-clamp and amperometry.[11-15] However, to our knowledge, real-time measurements of neurotransmitter release have not been recorded in whole-mount retinas. In this work, we have developed a method to use fast-scan cyclic voltammetry (FSCV) to measure real-time dopamine release in adult zebrafish whole-mount retinas.

4.2.1 Relevant ocular anatomy

This work is focused on development of a method to study neurotransmitter release in whole-mount retinas. Therefore, it is important to understand the role the retina plays in sight. Light enters the eye through the cornea, which is the transparent covering of the front of the eye, and passes through the aqueous anterior chamber.[16-18] The iris, which is the colored part of the eye, acts as a shutter on the pupil, the aperture through which light passes.[16-20] Then, light focused by the lens passes through the vitreous humor and forms an image on the retina, which transmits the image to the brain through the optic nerve.[16-18, 21] Figure 4.2.1 shows a schematic diagram of a human eye.

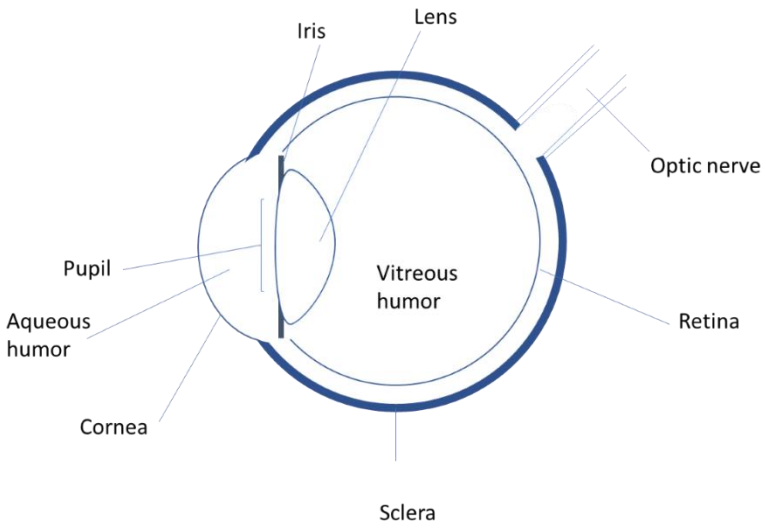

Fig 4.2.1. A schematic of the human eye. (Figure adapted from Kels et al.[17] with permission. ©Elsevier 2015)

As this work is concerned with the retina, it is important to understand the relevant retinal anatomy. Figure 4.2.2 shows a schematic of the layered structure of the retina, which is conserved across vertebrates. The outer nuclear level consists of photoreceptors, which can be divided into rods and cones; rods and cones are responsible for dim-light vision and color vision, respectively. Both types of photoreceptors are glutamatergic and synapse with bipolar cells at the outer plexiform layer; communication between bipolar cells and photoreceptors is modulated by horizontal cells. Bipolar cells can be either rod or cone-bipolar cells and receive input from those respective photoreceptor types. Additionally, bipolar cells can be divided into ON- and OFF-bipolar cells. ON bipolar cells depolarize in response to increments of light, whereas OFF bipolar cells hyperpolarize in response to increments of light.

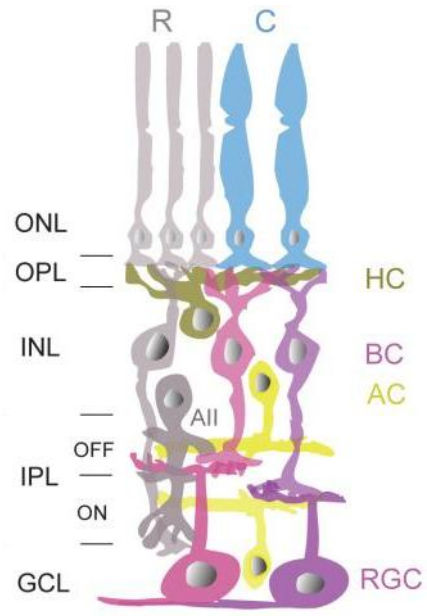

Figure 4.2.2. A schematic diagram of the layered structure of the vertebrate retina. ONL = Outer nuclear layer, OPL = Outer plexiform layer, INL = Inner nuclear layer, IPL = Inner plexiform layer (containing both OFF and ON sublamina), GCL = ganglion cell layer, R = rods, C = cones, HC = Horizontal cells, BC = Bipolar cells, AC = Amacrine cells, RGC = Retinal ganglion cells. Figure reproduced with permission from Hoon et al. ©Elsevier 2014.[22]

In this work, we sought to measure dopamine release in the retina. Contini and Raviola showed that dopaminergic amacrine cells in the retina synapse with cell bodies of AII amacrine cells.[23] Furthermore, Hirasawa et al. used electrophysiology to determine that dopamine and GABA were coreleased from dopaminergic amacrine cells and that dopamine acted on both nearby and distant retinal cells by volume transmission.[12]

4.2.2 Zebrafish as a model organism

In this work, we develop a method for using FSCV to measure dopamine release in zebrafish whole mount retina. Zebrafish (*danio rerio*) present some unique advantages for use as a model organism, and yet, they are a relatively young animal model in research. Zebrafish were

initially used as a model organism in the 1960s.[24] Their relatively large, external embryos and fast life cycle make them an ideal model organism for studying development.[25-26] The genome of zebrafish has been fully sequenced; thus, they are easily genetically manipulatable. As vertebrates, zebrafish have the added benefit of being relatively genetically similar to humans compared to invertebrate models such as fruit flies and c. elegans.[25] Specifically, the functional architecture retina is well-conserved across vertebrates.[22] However, there are a few differences between the structure of zebrafish retinas and human retinas, which we will discuss here. Humans have three major classes of cones with sensitivity to red, green, and blue wavelengths, respectively; zebrafish, on the other hand, have a fourth class of cones which are sensitive to ultraviolet wavelengths.[22] Moreover, there are differences between humans and zebrafish in cellular distribution and connectivity. Zebrafish have more types of horizontal cells, and their cone bipolar cells are more interconnected than human bipolar cells;[22] zebrafish retina is also less densely populated with ganglion cells.[27] Furthermore, the zebrafish retina is thinner than human retina (180 µm and 280 µm, respectively).[28-29] Nevertheless, the zebrafish retina is a better model of the human retina compared to other animals such as mice, as mice have rod-dominated vision instead of cone-dominant vision (i.e., zebrafish see in color while rodents do not).[30] This is essential for the study of diseases such as age-related macular degeneration, which is associated with cone degeneration.[5]

FSCV is a sensitive electrochemical technique with high temporal and spatial resolution when coupled with carbon fiber microelectrodes. In this work, we develop a method to study real-time neurotransmitter release in adult zebrafish whole mount retina at carbon fiber microelectrodes.

4.3 METHODS

4.3.1 Zebrafish

All animal procedures were approved by the University of Kansas Institutional Animal Care and Use Committee. Zebrafish were housed in the Molecular Probes Core of the Center for Molecular Analysis of Disease Pathways at the University of Kansas.

4.3.2 Retina removal

Zebrafish retinas were removed using a procedure adapted from Zou et al.[10] Briefly, zebrafish were euthanized by rapid chilling and decapitated. Zebrafish retina removal was performed under a dissection stereoscope (Leica Microsystem, Bannockburn, IL). The zebrafish head was immobilized on agarose for dissection using a 19-gauge syringe needle (Figure 4.3.1A). Two incisions were made on the top of the eye using SuperFine Vannas Scissors (8cm, curved, 3mm blades) and the lens was removed using Dumont #5 forceps (Figure 4.3.1B). The eye was removed and the optic nerve was severed using the same forceps and scissors (Figure 4.3.1 C). Finally, the sclera and whole mount retina were separated using the same forceps (Figure 4.3.1 D).

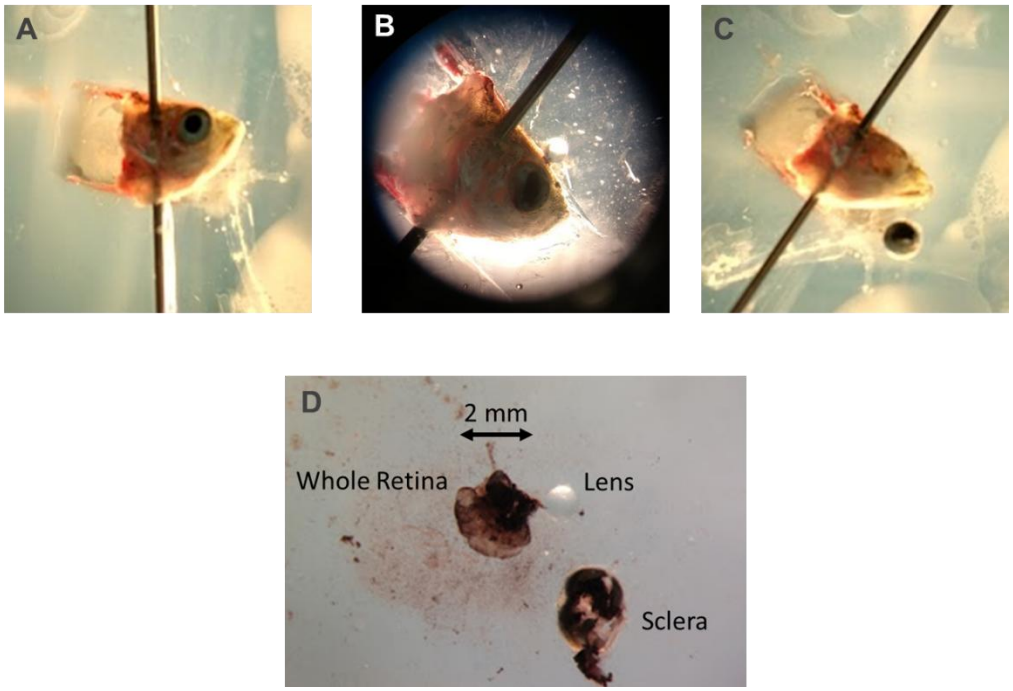

Figure 4.3.1. Retina removal. (A) After decapitation, the zebrafish head is immobilized on agarose using a 19-gauge syringe needle. (B) Small incisions in the front of the eye allow for removal of the lens. (C) The eye cup is removed and optic nerve severed. (D) The removed sclera, retina, and lens.

4.3.3 Electrochemistry

Once removed, retinas were placed in a perfusion chamber, and artificial cerebrospinal fluid (aCSF) was perfused over the retina. The aCSF was composed of 126 mM NaCl, 22 mM HEPES, 1.6 mM NaH_2PO_4, 2.5 mM KCl, 25 mM $NaHCO_3$, 2.4 mM $CaCl_2$, 1.2 mM $MgCl_2$, and 11 mM D-glucose, adjusted to a pH of 7.4. aCSF was maintained at a temperature of 27°C, the same temperature as the zebrafish tank system water, and oxygenated using 95/5% O_2/CO_2. The perfusion chamber was protected from light and retinas were equilibrated in darkness for 1-h prior to data collection. To stimulate neurotransmitter release, a 2-s, 850 mA light pulse was applied using a 470-nm fiber optic coupled LED (Thorlabs, Newton, New Jersey).

4.3.4 Pharmacological studies

Dopamine, α-methyl-p-tyrosine methyl ester (AMPT), nomifensine, and quinpirole, were purchased from Sigma-Aldrich (St. Louis, MO).

4.4 Results & Discussion

4.4.1 Initial neurotransmitter release data collected in the retina

Initially, we sought to measure dopamine release in adult zebrafish whole mount retinas. Figure 4.4.1 shows the very first representative data we obtained. A retina was removed from an adult zebrafish and placed in a perfusion chamber, which was perfused with oxygenated aCSF at 27°C. After placement on the perfusion chamber, the retina was equilibrated in darkness for one hour. These data were obtained by placing a carbon fiber microelectrode 100 µm deep in the center of the retina and stimulating the retina with white light. Figure 4.4.1 shows (A) placement of a carbon fiber microelectrode in zebrafish retina tissue and (B) placement of a fiber optic coupled LED such that light stimulus shines directly on the retina tissue. Here, a 2-s 850-mA light stimulus was applied using a 470-nm fiber optic coupled LED to obtain neurotransmitter release.

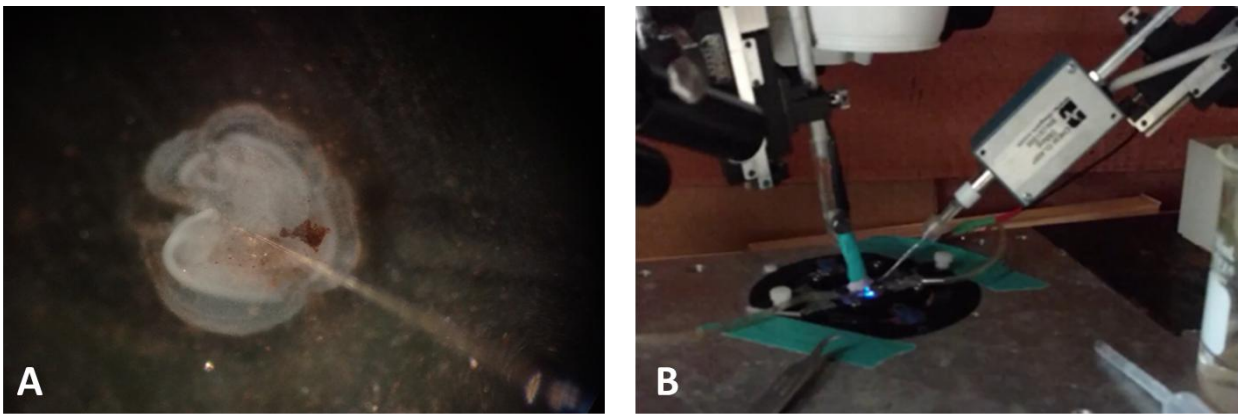

Figure 4.4.1. (A) A carbon fiber microelectrode is place 100 µm deep in the center of a zebrafish whole mount retina. (B) A fiber-optic coupled 470-nm LED is shone directly onto the retina in order to stimulate neurotransmitter release.

Figure 4.4.2 shows the initial representative data collected in the retina for an experiment in which nomifensine, a dopamine reuptake inhibitor, was perfused over the retina. The left panel shows a color plot, representative current vs time plot, and representative cyclic voltammogram before the addition of drug. The color plot consists of a series of cyclic voltammograms (i.e. current vs potential plots) unfolded, rotated, and stacked over time. These plots show potential on the *y*-axis, time on the *x*-axis, and current is encoded in false color, representing the *z*-axis. Horizontal dashed lines represent the potential at which current vs time plots were extracted, while vertical dashed lines show the time from which representative cyclic voltammograms were extracted. A 2-s light stimulation was applied 5-s into data collection. At 5 s, a current peak occurs on the current vs time plot, indicating stimulated neurotransmitter release. The peak returns to baseline, indicating reuptake into the cell. Since representative cyclic voltammogram resembled a dopamine cyclic voltammogram, we perfused 2 µM nomifensine over the retina to determine whether the neurotransmitter released was dopamine. The middle panel shows a representative color plot 20 min after addition of nomifensine to the perfusate. These data show that after addition of nomifensine, the current measured did not return to baseline as it did before the addition of drug, suggesting that reuptake was inhibited and that the neurotransmitter released could be dopamine. The panel on the right shows representative data collected 20 min after washing nomifensine out of the perfusate. Here, the current returned to slightly below the

pre-drug level, suggesting that the inhibition of uptake observed in the center panel was due to nomifensine addition.

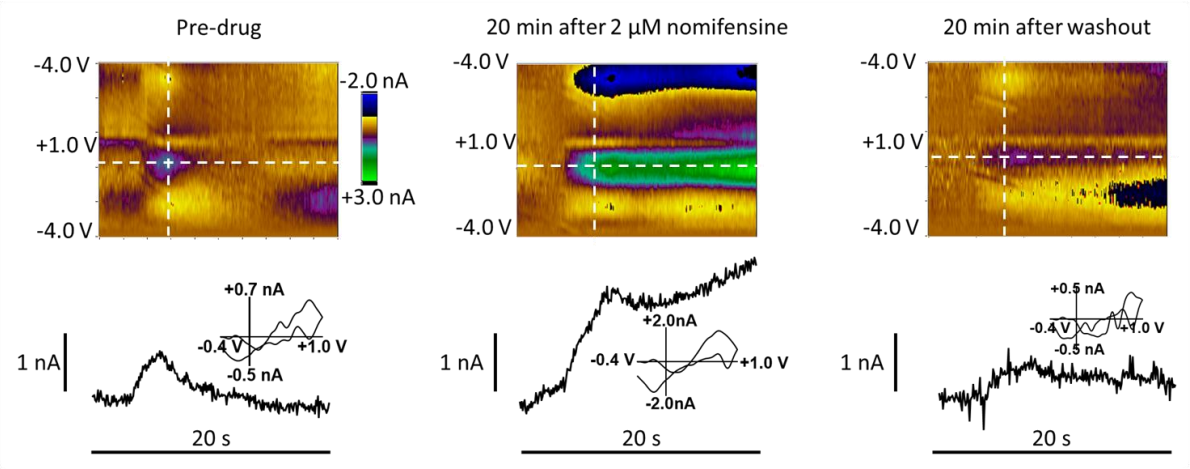

Figure 4.4.2. Initial experiments revealed potential dopamine release in response to light stimulation. Right: pre-drug; center: 20 min after adding 2 µM nomifensine to perfusate; right: 20 min after washing nomifensine out of perfusate.

4.4.2 Light-stimulated neurotransmitter release is Ca^{2+}-dependent

After our initial experiments, we decided to characterize further the release we observed by determining whether it was calcium-dependent. Exocytotic neurotransmitter release depends on the availability of calcium in cells.[31] Here, we performed our experiment in the same way as before, but without adding calcium to the aCSF. The carbon fiber microelectrode was placed 100 µm deep, directly in the center of the retina and not moved for the duration of the experiment. The retina was stimulated with a 2-s, 850 mA, 470-nm light pulse. Figure 4.4.3 shows (A) representative current vs time plots and (B) overall results for this set of experiments. The representative current vs time plots show that before addition of calcium, there was no significant current obtained in response to the light stimulus. After titration of calcium to 100% of the normal calcium concentration in aCSF (2.5 mM), release occurred in response to the light

stimulus. The amount of neurotransmitter released increased by 13.6-fold compared to the pre-calcium amount ($p<0.05$, one-tailed paired t test, N = 4 retinas). These results suggest calcium-dependent exocytosis is occurring in response to light stimulation.

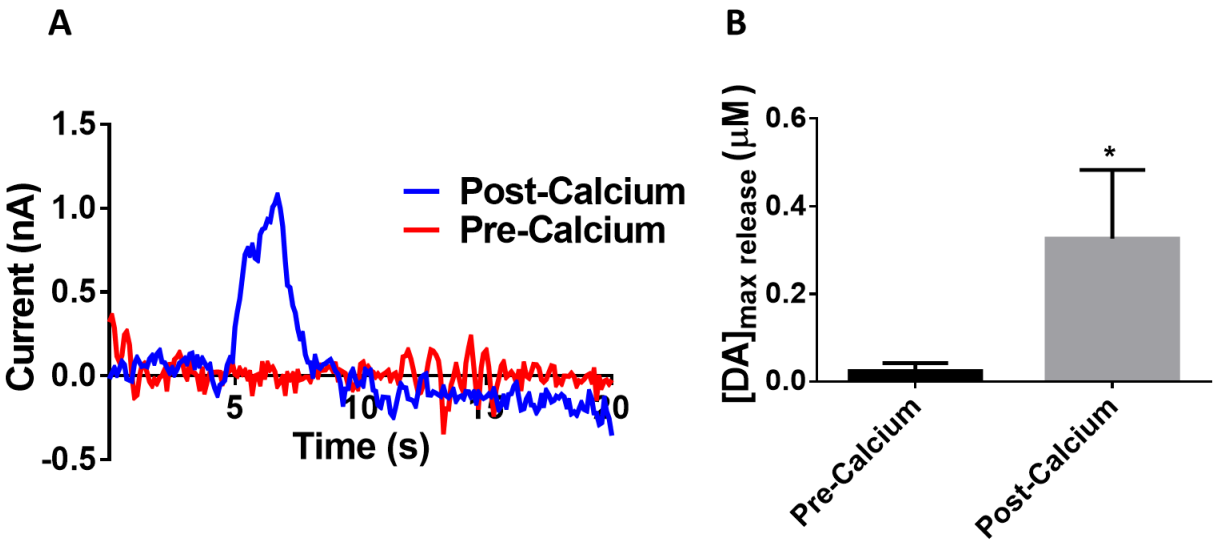

Figure 4.4.3. (A) Representative data; calcium-dependent neurotransmitter release in the retina. (B) Average maximum concentrations of dopamine released before and after addition of calcium to the aCSF (*$p<0.05$, one-tailed paired t test, N = 4 retinas.)

4.4.3 Alpha-methyl-*p*-tyrosine causes disappearance of light-stimulated neurotransmitter release

In order to determine whether any part of the signal was attributable to dopamine or norepinephrine, a pharmacological experiment was performed using the drug α-methyl-p-tyrosine (AMPT). Tyrosine hydroxylase (TH) is the rate-limiting enzyme in catecholaminesynthesis, and AMPT blocks TH. Therefore, one would expect a disappearance of catecholamine release after AMPT blocks synthesis. After a stable electrochemical signal was obtained, AMPT (50 μM) was added to the perfusate. Release was evoked every 10 minutes

using the same light stimulation paradigm. After 180 minutes, the signal diminished by 84.6±9.3% ($p<0.05$, one-way ANOVA, Sidak's multiple comparisons test, N = 4 retinas). After the signal reached a minimum, AMPT was washed out of the perfusate, and the retina was allowed to recover for one hour before another stimulation was applied. After one hour, when light stimulation was applied again, the signal returned to 58.9±18.0% of the maximum. There was no significant difference between the signal obtained after washout and the original maximum dopamine release. Figure 4.4.4 shows (A) a scheme depicting the action of AMPT inhibiting dopamine synthesis, (B) representative current vs time plots collected at various times after perfusion of AMPT over the retina, and (C) overall average maximum dopamine release concentrations before AMPT, 180 min after addition of AMPT, and 1 h after washout of AMPT. Our results suggest that the species released in response to light stimulation depends on the activity of AMPT. Therefore, the signal could be attributable to dopamine or norepinephrine. As previously mentioned, more work has been done measuring dopamine release[11-12, 15] than norepinephrine release in retinal cells. However, N. N. Osborne found by autoradiography that norepinephrine might be released in very small amounts in the inner nuclear layer of bovine retina.[32] Therefore, future studies are necessary to determine which catecholamine is responsible for the signal obtained here.

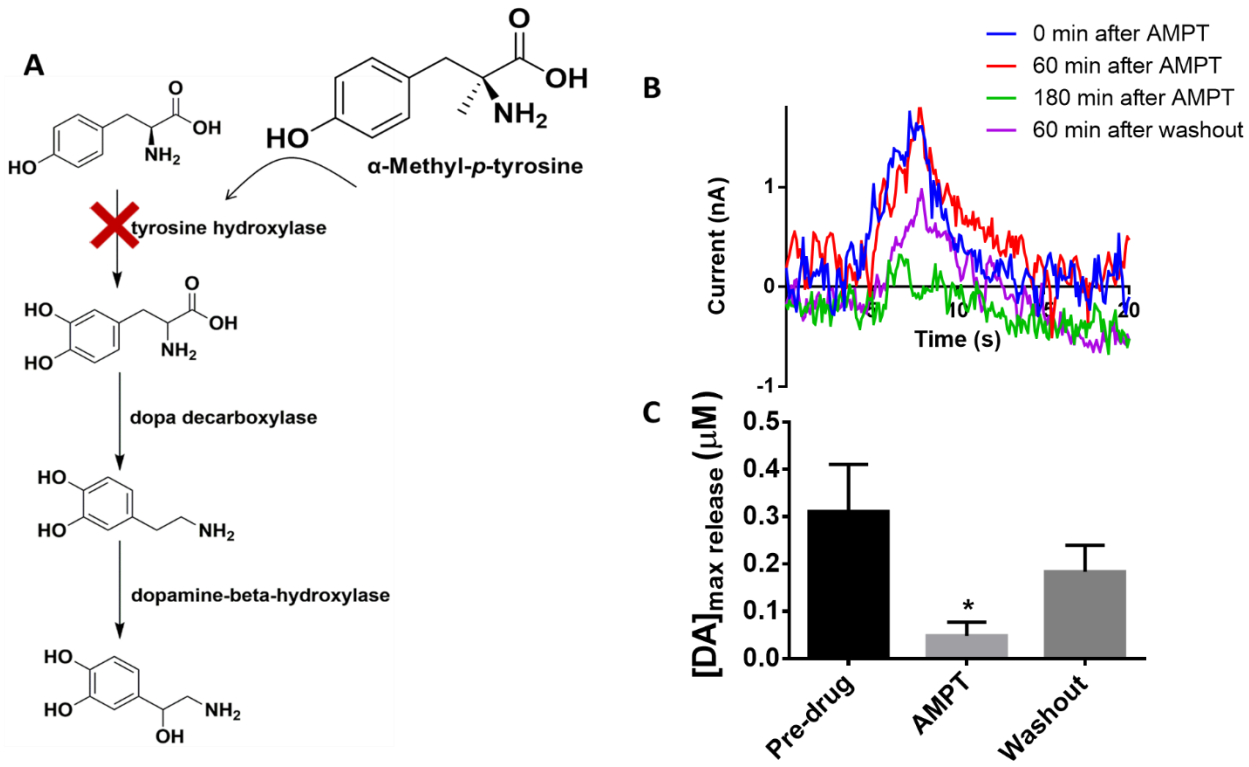

Figure 4.4.4. (A) A scheme depicting the inhibition of catecholamine synthesis, by AMPT. (B) Representative current vs time plots collected in zebrafish whole mount retina 0, 60, and 180 min after addition of AMPT, and 60 min after AMPT washout. (C) Average release pre-AMPT, 180 min after AMPT, and 60 min after AMPT washout (one-way ANOVA, Sidak's multiple comparisons test, *$p<0.05$, N = 4 retinas).

4.4.4 Quinpirole causes a significant decrease in the maximum concentration of dopamine released

To determine whether the signal we observed was due to dopamine or norepinephrine, we performed experiments using quinpirole, a selective D2 receptor agonist.[33] D2 dopamine autoreceptors are present in the retinal inner nuclear layer.[34] When an agonist binds a D2 autoreceptor, it activates the a negative feedback loop, inhibiting release of dopamine from

cells.[35] Therefore, a decrease in release due to addition of quinpirole would support the conclusion that the observed signal is dopamine. Here, 10 µM quinpirole was added to the aCSF perfusate. Figure 4.4.5 shows (A) representative current vs time plots before and after the addition of quinpirole, and after washing quinpirole out of the perfusate and (B) average maximum dopamine release concentrations before adding quinpirole, after adding quinpirole, and after a washout of the drug. After the addition of quinpirole, the dopamine signal decreased to 38.3±15.2% of the original signal ($p<0.05$, one-way ANOVA, Sidak's multiple comparisons test, N = 4 retinas). When quinpirole was washed out, the signal recovered to 78.5±25.3% of the original signal; there was no significant difference between the signal obtained after the washout and the original signal. These results suggest that at least some portion of the signal is due to release of dopamine in response to light stimulation.

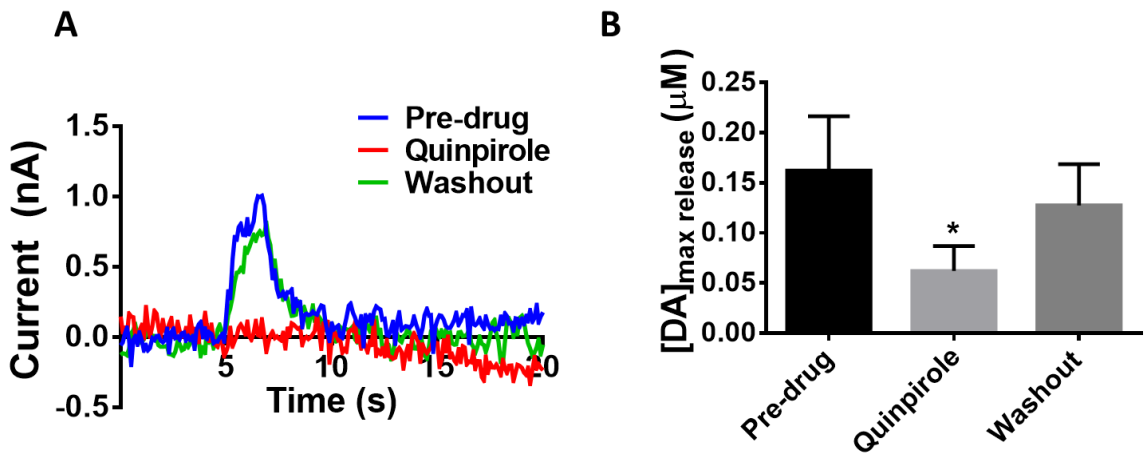

Figure 4.4.5. (A) Representative current vs time plots collected in adult zebrafish whole mount retina before the addition of 20 µM quinpirole, 20 min after the addition of quinpirole, and 20 min after a quinpirole washout. (B) Average dopamine release data for pre-quinpirole, after quinpirole, and after a quinpirole washout (one-way ANOVA, Sidak's multiple comparisons test, *$p<0.05$, N = 4 retinas).

Overall, data pooled from multiple retinas showed that dopamine release was 0.23 ± 0.05 µM. To our knowledge, these measurements are the first of their kind; therefore, we are unable to compare these data to previous results. However, Shin et al. found that dopamine release in response to electrical stimulation in zebrafish whole brain was 0.41 ± 0.07 µM.[36]

4.5 CONCLUSIONS

We have shown that dopamine release can be measured using FSCV in adult zebrafish whole mount retina. To our knowledge, these measurements are the first of their kind. The only other similar study by Witkovsky et al. found steady-state vitreal concentrations of dopamine in clawed frog eyes using a combination of FSCV and HPLC.[37] However, for their FSCV measurements, they did not stimulate release but simply lowered the working electrode into the eyecup during data collection to obtain a measurement of dopamine within the vitreous humor of the eye compared to the buffer in the perfusion chamber. Moreover, they did not perform any pharmacological studies to confirm dopamine release. We took their approach a step further by measuring light-stimulated dopamine release in the retina. In summary, our work represents an important step in the development of zebrafish as a model organism to study retinal function and disease.

4.6 REFERENCES

1. Congdon, N.; O'Colmain, B.; Klaver, C. C. W.; Klein, R.; Munoz, B.; Friedman, D. S.; Kempen, J.; Taylor, H. R.; Mitchell, P.; Hyman, L.; Eye Dis Prevalence Res, G., Causes and

prevalence of visual impairment among adults in the United States. *Arch. Ophthalmol.* **2004,** *122* (4), 477-485.

2. Pascolini, D.; Mariotti, S. P.; Pokharel, G. P.; Pararajasegaram, R.; Etya'ale, D.; Negrel, A. D.; Resnikoff, S., 2002 global update of available data on visual impairment: a compilation of population-based prevalence studies. *Ophthalmic Epidemiol.* **2004,** *11* (2), 67-115.

3. Friedman, D. S.; O'Colmain, B.; Tomany, S. C.; McCarty, C.; de Jong, P.; Nemesure, B.; Mitchell, P.; Kempen, J.; Congdon, N.; Eye Dis Prevalence Res, G., Prevalence of age-related macular degeneration in the United States. *Arch. Ophthalmol.* **2004,** *122* (4), 564-572.

4. Wood, A.; Margrain, T.; Binns, A. M., Detection of early age-related macular degeneration using novel functional parameters of the focal cone electroretinogram. *PloS one* **2014,** *9* (5), e96742.

5. Goldsmith, P.; Harris, W. A., The zebrafish as a tool for understanding the biology of visual disorders. *Seminars in cell & developmental biology* **2003,** *14* (1), 11-8.

6. Avanesov, A.; Malicki, J., Analysis of the retina in the zebrafish model. *Methods Cell Biol* **2010,** *100*, 153-204.

7. Williams, P. R.; Morgan, J. L.; Kerschensteiner, D.; Wong, R. O., In vivo imaging of zebrafish retina. *Cold Spring Harb Protoc* **2013,** *2013* (1).

8. Marc, R. E.; Cameron, D., A molecular phenotype atlas of the zebrafish retina. *Journal of neurocytology* **2001,** *30* (7), 593-654.

9. Yazulla, S.; Studholme, K. M., Neurochemical anatomy of the zebrafish retina as determined by immunocytochemistry. *Journal of neurocytology* **2001,** *30* (7), 551-92.

10. Zou, S.-Q.; Tian, C.; Du, S.-T.; Hu, B., Retrograde Labeling of Retinal Ganglion Cells in Adult Zebrafish with Fluorescent Dyes. **2014,** (87), e50987.

11. Hirasawa, H.; Betensky, R. A.; Raviola, E., Corelease of dopamine and GABA by a retinal dopaminergic neuron. *J Neurosci* **2012,** *32* (38), 13281-91.

12. Hirasawa, H.; Contini, M.; Raviola, E., Extrasynaptic release of GABA and dopamine by retinal dopaminergic neurons. *Philos Trans R Soc Lond B Biol Sci* **2015,** *370* (1672).

13. Hirasawa, H.; Puopolo, M.; Raviola, E., Extrasynaptic release of GABA by retinal dopaminergic neurons. *J Neurophysiol* **2009,** *102* (1), 146-58.

14. Hochstetler, S. E.; Puopolo, M.; Gustincich, S.; Raviola, E.; Wightman, R. M., Real-time amperometric measurements of zeptomole quantities of dopamine released from neurons. *Analytical chemistry* **2000,** *72* (3), 489-96.

15. Puopolo, M.; Hochstetler, S. E.; Gustincich, S.; Wightman, R. M.; Raviola, E., Extrasynaptic release of dopamine in a retinal neuron: activity dependence and transmitter modulation. *Neuron* **2001,** *30* (1), 211-25.

16. Snell, R. S.; Lemp, M. A.; Snell, R. S.; Lemp, M. A., The Eyeball. In *Clinical Anatomy of the Eye*, Blackwell Science Ltd,. 1997; pp 132-213.

17. Kels, B. D.; Grzybowski, A.; Grant-Kels, J. M., Human ocular anatomy. *Clin Dermatol* **2015,** *33* (2), 140-6.

18. Grant-Kels, J. M.; Kels, B. D., Human ocular anatomy. *Dermatologic clinics* **1992,** *10* (3), 473-82.

19. McCaa, C. S., The eye and visual nervous system: anatomy, physiology and toxicology. *Environmental health perspectives* **1982,** *44*, 1-8.

20. Hermsen, V. M.; Dreyer, R. F., Ophthalmic anatomy. *Primary care* **1982,** *9* (4), 627-45.

21. Snell, R. S.; Lemp, M. A.; Snell, R. S.; Lemp, M. A., The Anatomy of the Eyeball as Seen with the Ophthalmoscope, Slit Lamp, and Gonioscope. In *Clinical Anatomy of the Eye*, Blackwell Science Ltd,. 1997; pp 214-230.

22. Hoon, M.; Okawa, H.; Della Santina, L.; Wong, R. O., Functional architecture of the retina: development and disease. *Progress in retinal and eye research* **2014,** *42*, 44-84.

23. Contini, M.; Raviola, E., GABAergic synapses made by a retinal dopaminergic neuron. *Proceedings of the National Academy of Sciences of the United States of America* **2003,** *100* (3), 1358-63.

24. Streisinger, G.; Edgar, R. S.; Denhardt, G. H., CHROMOSOME STRUCTURE IN PHAGE T4. I. CIRCULARITY OF THE LINKAGE MAP. *Proc Natl Acad Sci U S A* **1964,** *51*, 775-9.

25. Grunwald, D. J.; Eisen, J. S., Headwaters of the zebrafish--emergence of a new model vertebrate. *Nature reviews. Genetics* **2002,** *3* (9), 717.

26. Phillips, J. B.; Westerfield, M., Zebrafish models in translational research: tipping the scales toward advancements in human health. *Dis Model Mech* **2014,** *7* (7), 739-43.

27. Curcio, C. A.; Allen, K. A., Topography of ganglion cells in human retina. *J Comp Neurol* **1990,** *300* (1), 5-25.

28. Chhetri, J.; Jacobson, G.; Gueven, N., Zebrafish--on the move towards ophthalmological research. *Eye (London, England)* **2014,** *28* (4), 367-80.

29. Yousef, Y. A.; Finger, P. T., Optical coherence tomography of radiation optic neuropathy. *Ophthalmic surgery, lasers & imaging : the official journal of the International Society for Imaging in the Eye* **2012,** *43* (1), 6-12.

30. Bibliowicz, J.; Tittle, R. K.; Gross, J. M., Toward a better understanding of human eye disease insights from the zebrafish, Danio rerio. *Progress in molecular biology and translational science* **2011,** *100*, 287-330.

31. Shin, O. H., Exocytosis and synaptic vesicle function. *Comprehensive Physiology* **2014,** *4* (1), 149-75.

32. Osborne, N. N., Noradrenaline, a Transmitter Candidate in the Retina. *Journal of Neurochemistry* **1981,** *36* (1), 17-27.

33. Levant, B., Novel drug interactions at D(2) dopamine receptors: modulation of [3H]quinpirole binding by monoamine oxidase inhibitors. *Life sciences* **2002,** *71* (23), 2691-700.

34. Schorderet, M.; Nowak, J. Z., Retinal dopamine D1 and D2 receptors: characterization by binding or pharmacological studies and physiological functions. *Cellular and molecular neurobiology* **1990,** *10* (3), 303-25.

35. Ford, C. P., The role of D2-autoreceptors in regulating dopamine neuron activity and transmission. *Neuroscience* **2014,** *282*, 13-22.

36. Shin, M.; Field, T. M.; Stucky, C. S.; Furgurson, M. N.; Johnson, M. A., Ex Vivo Measurement of Electrically Evoked Dopamine Release in Zebrafish Whole Brain. *ACS Chemical Neuroscience* **2017**.

37. Witkovsky, P.; Nicholson, C.; Rice, M. E.; Bohmaker, K.; Meller, E., Extracellular dopamine concentration in the retina of the clawed frog, Xenopus laevis. *Proceedings of the National Academy of Sciences of the United States of America* **1993,** *90* (12), 5667-71.

5 CONCLUSIONS AND FUTURE DIRECTIONS

In this work, we have used electroanalytical techniques to address biological problems in multiple model organisms. Specifically, we applied FSCV measurements in Huntington's disease model mice, rats treated with chemotherapy, and zebrafish retinas. Here, we discuss the overall conclusions from this work as well as future directions.

5.1 SEROTONIN MEASUREMENTS IN HUNTINGTON'S DISEASE MODEL MICE

In this work, we aimed to understand further the underlying neurochemical changes in Huntington's disease (HD). Therefore, we measured serotonin release in the substantia nigra and dorsal raphe nucleus of R6/2 HD model mice using fast scan cyclic voltammetry. We also measured serotonin release in the dorsal raphe nucleus of R6/1 model mice. Our results showed that serotonin release was impaired in both the substantia nigra, pars reticulata and dorsal raphe of R6/2 model mice. Additionally, we found that serotonin release in the substantia nigra, pars reticulata was progressively impaired as R6/2 mice aged. Our results in R6/1 model mice showed that serotonin release was impaired in the dorsal raphe. This work demonstrates that neurotransmitter release throughout the brain could be affected by HD and represents a key step in understanding the neurochemistry of HD.

5.2 SEROTONIN AND DOPAMINE RELEASE MEASUREMENTS IN CHEMOTHERAPY-TREATED RATS

Another aim of this work was to understand better the underlying neurochemical abnormalities of post-chemotherapy cognitive impairment, or "chemobrain." These alterations may contribute to cognitive changes including memory loss, attention deficits, and mood disorders such as depression.

Carboplatin is a platinum-based chemotherapeutic agent that works by binding DNA, forming reactive platinum complexes, and causing apoptosis.[1] Previously, Kaplan et al. found that dopamine release was impaired in the striatum in Wistar rats that were treated with carboplatin.[2] Here, we wanted to determine whether neurotransmitter release was generalized throughout the brain. Furthermore, since symptoms of chemobrain include depression and other mood disorders, we decided to measure serotonin release due to serotonin's involvement involvement in mood control.

In this work, rats were treated with either 25 mg/kg carboplatin (i.v. tail vein) or an equivalent volume of saline vehicle once per week for four weeks. One week after the final injection, we used FSCV to measure serotonin release in brain slices obtained from the dorsal raphe, which is a serotonin-rich region of the brain known to be involved in mood. We also collaborated with Dr. David Jarmolowicz's lab to measure spatial learning in the same rats throughout the course of the chemotherapeutic treatment regimen. Together, our results showed that rats treated with carboplatin had impairments in both dopamine and serotonin release, and these neurochemical changes corresponded with impairments in spatial learning and memory.

Next, we sought to determine whether dopamine release impairments occur after treatment with other chemotherapeutic agents. Here, we treated rats with the chemotherapy drug 5-fluorouracil (5-FU), which works by blocking thymidylate synthase, an enzyme required for DNA synthesis, thereby causing apoptosis.[3] One week after the final treatments, dopamine release was measured in striatal brain slices. In addition to our dopamine release measurements, our collaborator measured inhibition throughout the chemotherapeutic treatments. We found that dopamine release was impaired throughout the striatum.

We also wanted to investigate a potential therapy for chemobrain, so we co-administered KU-32, a heat shock protein inhibitor that has shown promise in treating neuropathy developed by Dr. Brian Blagg's group.[4] Rats received one injection of either 5-FU (20 mg/kg, i.v. tail vein) or an equivalent volume of saline vehicle, once per week for two weeks. Half of the rats who received 5-FU were also treated with KU-32 (25 mg/kg, oral gavage). Our collaborator used a 5-choice serial reaction time test to demonstrate that KU-32 prevented 5-FU-induced impairment of attention shifting. Another student in our lab, Anuranga Bandara, measured peroxide transients in striatal brain slices obtained from these rats; preliminary data showed that KU-32 normalized hydrogen peroxide transients. However, more work needs to be done to characterize peroxide transients further.

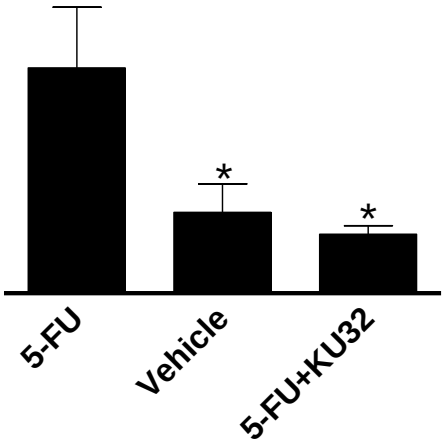

Figure 5.2.1. KU-32 normalized hydrogen peroxide transients. One-way ANOVA, $p<0.05$, N = 3 to 5 rats.

There is some disagreement among clinicians as to whether chemobrain is a transient or long-lasting disorder.[5-6] Therefore, we wanted to determine whether the changes in dopamine release that we observed were recovered after rats were allowed to recover from treatments for

longer than one week. Here, we repeated the 5-FU treatment regimen (20 mg/kg i.v. tail vein, once per week for two weeks). Then, we measured dopamine release in striatal brain slices at two different times after the final injection: one week and three weeks. Our results demonstrated that dopamine release impairments did not recover after a slightly prolonged recovery time. In the future, it will be important to measure neurotransmitter release at even longer recovery times.

This work is useful because it provides a framework for future studies. Recently, students in the Johnson and Jarmolowicz groups have been training to perform in vivo FSCV measurements in combination with behavioral measurements. This will allow our groups to combine in vivo measurements with simultaneous cognitive behavior measurements in the future. Furthermore, in vivo measurements have the advantage of allowing researchers to collect data at multiple time points, which will allow our groups to track the cognitive behavior and neurotransmitter release measurements of individual rats over time.

5.3 DEVELOPMENT OF A METHOD TO MEASURE DOPAMINE RELEASE WITH FSCV IN ZEBRAFISH WHOLE MOUNT RETINA

As the population in the United States with age-related macular degeneration (AMD) is set to increase to 20 million by 2020,[7] it has become increasingly important to study the retina. Here, we developed a method to use FSCV to measure dopamine release in adult zebrafish whole mount retinas. Preliminary data suggested that dopamine release could be occurring in response to stimulation with a 470-nm LED, so we chose to investigate further. Our results showed that the signal was dependent on calcium, suggesting that exocytotic release was occurring. Then, we wanted to determine whether the neurotransmitter released was a catecholamine, so we perfused α-methyl-*p*-tyrosine (AMPT), a tyrosine hydroxylase inhibitor, over the retina. These experiments revealed that the signal disappeared after 180 min of perfusing AMPT and returned

60 min after washing AMPT out of the perfusate. Finally, we sought to determine whether the catecholamine signal could be attributed to dopamine, which has been shown to be present in the retina. Therefore, we performed experiments in which we added quinpirole, a selective D2 dopamine receptor agonist, to the perfusate. After 20 min of perfusing quinpirole over the retina, the signal was significantly decreased. Thus, we concluded that at least a portion of the signal was due to dopamine release.

This work represents a crucial step toward understanding neurotransmission in the whole retina. Previously published work has drawn a link between dopamine receptor activation and the ability of retinal pigmented epithelium cells to break down waste products, which is a crucial function for retinal health.[8-9] Therefore, a longer term goal of this work is to identify alteration in dopamine release and uptake properties in the retina, especially in genetically altered zebrafish, to identify possible mechanisms of AMD. Keeping the retina intact instead of measuring neurotransmitter release in retina cells creates many possibilities. For example, we will be able to measure the effects of different retinal cell types on each other. In the future, we will be able to use the methods developed here to study the effects of retinal disease on neurotransmitter release in whole mount retinas. Here, we have developed a very promising tool for understanding mechanisms of retinal disease, such as AMD.

5.4 REFERENCES

1. Hah, S. S.; Stivers, K. M.; de Vere White, R. W.; Henderson, P. T., Kinetics of carboplatin-DNA binding in genomic DNA and bladder cancer cells as determined by accelerator mass spectrometry. *Chemical research in toxicology* **2006,** *19* (5), 622-6.

2. Kaplan, S. V.; Limbocker, R. A.; Gehringer, R. C.; Divis, J. L.; Osterhaus, G. L.; Newby, M. D.; Sofis, M. J.; Jarmolowicz, D. P.; Newman, B. D.; Mathews, T. A.; Johnson, M. A., Impaired Brain Dopamine and Serotonin Release and Uptake in Wistar Rats Following Treatment with Carboplatin. *ACS chemical neuroscience* **2016,** *7* (6), 689-99.

3. Longley, D. B.; Harkin, D. P.; Johnston, P. G., 5-fluorouracil: mechanisms of action and clinical strategies. *Nature reviews. Cancer* **2003,** *3* (5), 330-8.

4. Farmer, K.; Williams, S. J.; Novikova, L.; Ramachandran, K.; Rawal, S.; Blagg, B. S.; Dobrowsky, R.; Stehno-Bittel, L., KU-32, a novel drug for diabetic neuropathy, is safe for human islets and improves in vitro insulin secretion and viability. *Experimental diabetes research* **2012,** *2012*, 671673.

5. Whitney, K. A.; Lysaker, P. H.; Steiner, A. R.; Hook, J. N.; Estes, D. D.; Hanna, N. H., Is"chemobrain" a transient state? A prospective pilot study among persons with non-small cell lung cancer. *The journal of supportive oncology* **2008,** *6* (7), 313-21.

6. Argyriou, A. A.; Assimakopoulos, K.; Iconomou, G.; Giannakopoulou, F.; Kalofonos, H. P., Either called "chemobrain" or "chemofog," the long-term chemotherapy-induced cognitive decline in cancer survivors is real. *J Pain Symptom Manage* **2011,** *41* (1), 126-39.

7. Congdon, N.; O'Colmain, B.; Klaver, C. C. W.; Klein, R.; Munoz, B.; Friedman, D. S.; Kempen, J.; Taylor, H. R.; Mitchell, P.; Hyman, L.; Eye Dis Prevalence Res, G., Causes and prevalence of visual impairment among adults in the United States. *Arch. Ophthalmol.* **2004,** *122* (4), 477-485.

8. Shibagaki, K.; Okamoto, K.; Katsuta, O.; Nakamura, M., Beneficial protective effect of pramipexole on light-induced retinal damage in mice. *Experimental eye research* **2015,** *139*, 64-72.

9. Guha, S.; Baltazar, G. C.; Tu, L. A.; Liu, J.; Lim, J. C.; Lu, W.; Argall, A.; Boesze-Battaglia, K.; Laties, A. M.; Mitchell, C. H., Stimulation of the D5 dopamine receptor acidifies the lysosomal pH of retinal pigmented epithelial cells and decreases accumulation of autofluorescent photoreceptor debris. *J Neurochem* **2012,** *122* (4), 823-33.